Utah State University

DigitalCommons@USU

5-2009

Analysis of Total Electron Content (TEC) Variations in the Low- and Middle-Latitude Ionosphere

Ja Soon Shim
Utah State University

Follow this and additional works at: https://digitalcommons.usu.edu/etd

Part of the Fluid Dynamics Commons

UtahState University
MERRILL-CAZIER LIBRARY

ANALYSIS OF TOTAL ELECTRON CONTENT (TEC) VARIATIONS

IN THE LOW- AND MIDDLE-LATITUDE IONOSPHERE

by

Ja Soon Shim

A dissertation submitted in partial fulfillment
of the requirements for the degree

of

DOCTOR OF PHILOSOPHY

in

Physics

Approved:

_____   _____
Ludger Scherliess   Robert W. Schunk
Major Professor   Committee Member

_____   _____
W. Farrell Edwards   Lie Zhu
Committee Member   Committee Member

_____   _____
Todd Moon   Byron R. Burnham
Committee Member   Dean of Graduate Studies

UTAH STATE UNIVERSITY
Logan, Utah

2009

ABSTRACT

Analysis of Total Electron Content (TEC) Variations

in the Low- and Middle-Latitude Ionosphere

by

Ja Soon Shim, Doctor of Philosophy

Utah State University, 2009

Major Professor: Dr. Ludger Scherliess
Department: Physics

Detailed study of the spatial correlations of day-to-day ionospheric TEC variations on a global scale was performed for four 30-day-long periods in 2004 (January, March/April, June/July, September/October) using observations from more than 1000 ground-based GPS receivers. In order to obtain the spatial correlations, initially, the day-to-day variability was calculated by first mapping the observed slant TEC values for each 5-minute GPS ground receiver-satellite pair to the vertical and then differencing it with its corresponding value from the previous day. This resulted in more than 150 million values of day-to-day change in TEC (ΔTEC). Next, statistics were performed on the ΔTEC values. The study indicates strong correlations between geomagnetic conjugate points, and these correlations are larger at low latitudes than at middle latitudes. Typical correlation lengths, defined as the angular separation at which the correlation coefficient drops to 0.7, were found to be larger at middle latitudes than at low latitudes. The correlation lengths are larger during daytime than during nighttime. The results indicate that the spatial correlation is largely independent of season. These spatial correlations are important for understanding the physical mechanisms that cause ionospheric weather variability and are also relevant to data assimilation. In an effort to better understand the effects of

neutral wind and electric field on the TEC variability, a physics-based numerical Ionosphere/Plasmasphere Model (IPM) was used. The model solves the transport equations for the six ions, $O^+, NO^+, O_2^+, N_2^+, H^+,$ and He^+, on convecting flux tubes that realistically follow the geomagnetic field. Two of the inputs required by the IPM are the thermospheric neutral wind and the low-latitude electric field, which can be given by existing empirical model or externally specified by the user. To study the relative importance of the neutral wind and the electric field for the TEC variations, these two model inputs were externally modified and the resulting variations in TEC were compared. Neutral wind and electric field modifications were introduced at three different local times in order to investigate the effect of different start times of the imposed perturbations on TEC. This study focused on modeled low- and middle-latitude TEC variations in the afternoon and post-sunset at three different longitude sectors for medium solar activity and low geomagnetic activity. The largest changes in TEC were found predominantly in the equatorial anomaly, and a significant longitudinal dependence was observed. The results indicate that the perturbation effect on the TEC at 2100 LT varied nonlinearly with the elapsed time after the imposed neutral wind and electric field perturbations. An important outcome of this study is that daytime neutral wind and/or electric field modifications will lead to essentially identical TEC changes in the 2100 local time sector.

(113 pages)

CONTENTS

LIST OF TABLES

LIST OF FIGURES

CHAPTER 1

INTRODUCTION

1.1 The Ionosphere of the Earth

The ionosphere is the partially ionized region of the Earth's upper atmosphere. It extends from about 60 km to 1000 km. The main source of the ionization in the ionosphere is the solar radiations such as extreme ultra violate (EUV) and X-ray radiations. In addition to photoionization, collisional ionization due to particle precipitation from the magnetosphere is another source of ionization, in particular in the high latitude region. Once the plasma is produced by these processes, it undergoes chemical reactions with neutrals, diffuses due to the gravitational force and plasma pressure gradients, and is transported via neutral winds and electric fields under the influence of the Earth's magnetic field.

Due to the altitude variations in the atmospheric neutral composition and the production rate with altitude, the plasma density in the ionosphere has a vertical layered structure, denoted by the D, E, and F layers (Figure 1.1). Each layer is controlled by different physical processes and has different main ions. In the D and E regions, the main ions are O_2^+, N_2^+, NO^+, and photochemistry is dominant. The F layer is usually divided into three sub-layers. The lowest layer, where photochemistry is dominant, is called the F_1. Here the ionization is produced through the photoionization process and disappears through recombination processes with the electrons. The next sub-layer where the transition from chemical to diffusion occurs is called the F_2 layer. Here the maximum electron density usually occurs. The uppermost part of the ionosphere, above the F_2 layer is termed the topside of the ionosphere. Here diffusion dominates [*Schunk and Nagy*, 2000].

In addition to the variation of the plasma density with altitude, the iono-
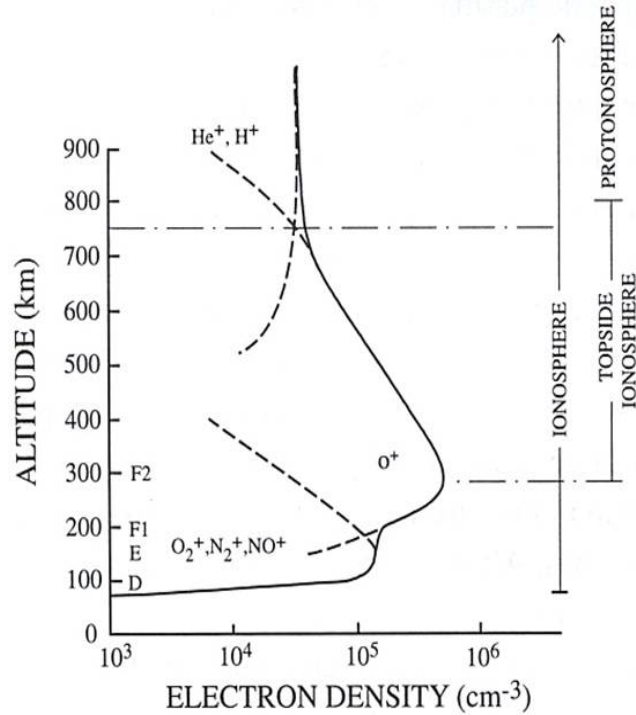
Figure 1.1. Representative ion density profiles for the daytime middle-latitude ionosphere showing the layered structure (D, E, F_1, and F_2) [*Banks et al.*, 1976].

sphere also shows significant variations with time of day, latitude, longitude, season, solar activity, and geomagnetic activity. A distinctive latitudinal characteristic in the ionosphere is created owing to the geometry of the Earth's dipolar magnetic field lines. The ionosphere, therefore, is classified into three latitude regions, low- (equatorial), middle-, and high- (auroral) latitude regions, which are controlled by different physical processes. In the following sections, the discussion will be limited to the low and middle latitudes, since my dissertation research focuses on these regions.

1.2   The Low-Latitude Ionosphere

At low latitudes, during the day, one of the most prominent features in the ionosphere is the equatorial anomaly, which is also often called the Appleton anomaly

[*Appleton*, 1946]. This feature is distinguished by higher plasma density on both sides of the equator, rather than at the equator itself. The equatorial anomaly is formed as a consequence of $\mathbf{E} \times \mathbf{B}$ upward plasma drifts associated with an eastward $\mathbf{E}$ field and a northward horizontal $\mathbf{B}$ field. The lifted plasma then diffuses downward along the geomagnetic field lines due to the gravitational force and the plasma pressure gradient, and this results in ionization enhancements on both sides of the magnetic equator (at about $\pm 10° \sim \pm 15°$ in the latitude). This physical mechanism phenomenon is called the fountain effects (Figure 1.2).

Often, asymmetry is found between the northern and southern anomaly. Due to an interhemispheric wind blowing from the summer to the winter hemisphere, in the summer hemisphere, plasma moves upward along the geomagnetic field lines, while plasma moves downward in the winter hemisphere. Therefore, the transport of the lifted plasma toward the winter hemisphere is enhanced, and the plasma transport toward the summer hemisphere is decreased. As a result, the equatorial anomaly in the winter hemisphere is generally larger than in the summer hemisphere (Figure 1.2) [*Anderson and Roble*, 1981].

The Equatorial anomaly morphology is often disturbed due to magnetic storm effects [*Rishbeth*, 1975; *Abdu*, 1997]. Recently, there has been a growing interest in studying the low-latitude ionosphere during major magnetic storm [*Kelley et al.*, 2004; *Lin et al.*, 2005].

1.3 The Middle-Latitude Ionosphere

The middle-latitude ionosphere is known to be the best understood ionospheric region, largely due to the relatively simple physics and the reasonably good coverage of measurements. In the middle-latitude ionosphere, transport of plasma is mostly caused by the combination of two facts, (1) the geomagnetic field line is inclined
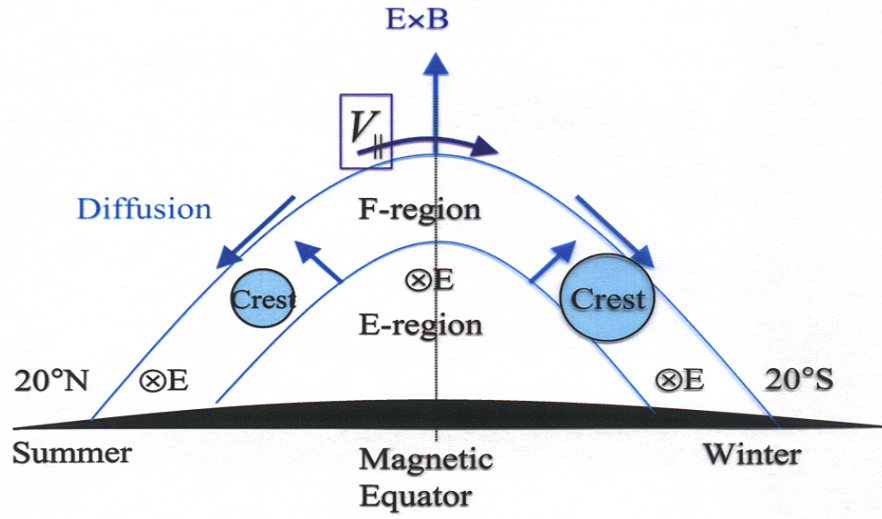
Figure 1.2. Fountain effects and asymmetry of the equatorial anomaly. An interhemispheric wind blowing from the summer to the winter hemisphere produces an asymmetry between two peak densities of the equatorial anomaly. **E** denotes an eastward electric field, and **B** is the northward geomagnetic field.

to the horizontal and (2) the ionospheric plasma is constrained to move along the geomagnetic field lines. Therefore, thermospheric neutral winds effectively transport the plasma along the field lines into higher or lower altitude regions in which recombination rates are different resulting in changes of the plasma density. As shown in Figure 1.3, during the day, the typically poleward neutral winds move plasma down to lower altitudes where the recombination rate is large. This results in a reduced peak height of F_2 and a decrease in the peak electron density. On the contrary, during the night, the typically equatorward winds move plasma up. Therefore the recombination of the plasma with neutrals decreases, the peak height increases, and the nighttime peak electron density is maintained.

1.4   Total Electron Content (TEC)

One of the widely used ionospheric parameter is Total Electron Content (TEC),
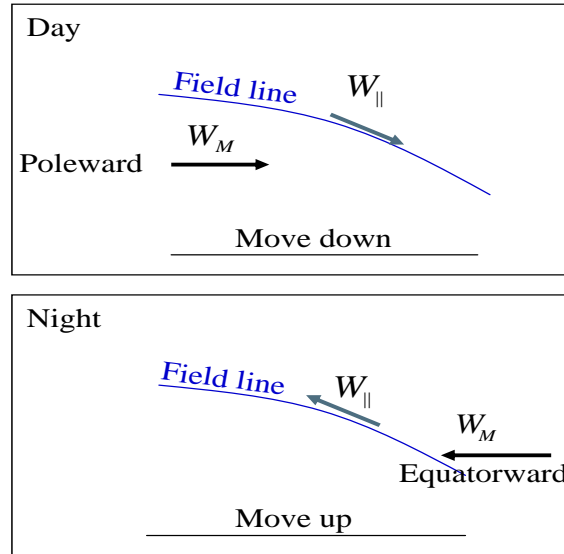
Figure 1.3. Vertical plasma drifts due to the meridional neutral wind W_M. $W_{||}$ is the meridional wind along the geomagnetic field line.

which is the number of electrons in a column of one-meter-squared cross section that extends all the way up from the ground through the ionosphere. TEC not only can provide an overall description of the ionization in the ionosphere, but also can be used for practical applications of radio wave propagation. Single frequency Global Positioning System (GPS) users can use TEC measurements to correct their signal, since TEC is proportional to the radio signal delay that a GPS signal experiences in the ionosphere. In this section, the effects of the ionosphere on radio wave propagation and the TEC measurement methods will be described.

1.4.1   Radio Wave Propagation in the Ionosphere

Radio wave propagation in the ionosphere is affected by the dispersive nature of the ionospheric plasma and the refraction of a radio wave depends on the wave frequency. However, the complex expression of the ionospheric refractive index n

represented by the Appleton-Hatree equation [*Hargreaves*, 1992] can be simplified to the following form in high-frequency limit:

$$n = \left(1 - \frac{f_p^2}{f^2}\right)^{\frac{1}{2}} \approx 1 - \frac{1}{2} \cdot \frac{f_p^2}{f^2} = 1 - \frac{40.30N}{f^2}, \qquad (1.1)$$

where $f_p \left(= \frac{Ne^2}{8\pi^2 \varepsilon_0 m_e}\right)$ is the electron plasma frequency in Hz, N is the electron number density in m^{-3}, and the unit of the numerical constant (40.30) is m^3/sec^2. In this high-frequency approximation $(f_p \ll f)$, electron collisions $(\nu \ll f)$ and the geomagnetic field $(\omega_B \ll \omega = 2\pi f)$ can be ignored.

Using Equation 1.1, the magnitude of the phase velocity can be derived as follows:

$$v_p = \frac{\omega}{k} = \frac{c}{n} = c\left(1 - \frac{40.30N}{f^2}\right)^{-1} \approx c\left(1 + \frac{40.30N}{f^2}\right), \qquad (1.2)$$

where c is the free space speed of light.

The carrier of a radio wave carries no information until it is modulated. The modulation information does not travel at the phase velocity but at the group velocity, which is always less than c. Using the relation $k = \frac{n\omega}{c}$ and Equation 1.1, the group velocity can be derived as follows:

$$v_g = \frac{\partial \omega}{\partial k} = \frac{c}{\frac{\partial (nf)}{\partial f}} = c\left(1 + \frac{40.30N}{f^2}\right)^{-1} \approx c\left(1 - \frac{40.30N}{f^2}\right). \qquad (1.3)$$

According to Equations 1.2 and 1.3, the propagation speed of radio waves varies all along their path through the ionosphere as the refractive index varies with the electron number density and radio wave frequency; therefore, time required for a signal to traverse the ionosphere is affected by the integrated effect of the ionosphere

as shown below:

$$\tau_{g/p} = \int_S \frac{ds}{v_{g/p}} = \frac{1}{c} \int \left(1 \pm \frac{40.30N}{f^2}\right) ds = \tau_0 \pm \frac{40.30}{cf^2} \int Nds, \qquad (1.4)$$

where S is the path of the radio wave, and τ_0 is the wave propagation time through vacuum. The ionosphere group signal propagation time (τ_g) increases (group time delay) by the presence of the ionosphere, whereas the phase propagation time (τ_p) is reduced (phase time advance) by the same amount $\int Nds$ that corresponds to the total number of electrons in a tube of unit cross section extending through the ionosphere along the path of the wave. This integral is often called the slant Total Electron Content (TEC) between a transmitter and a receiver. TEC is measured in TEC units (TECU), where 1 TECU equals 10^{16} electrons/m^2. Therefore, in the high-frequency approximation ($fp \ll f$) changes of the propagation time due to the plasma density in the ionosphere, by Equation 1.4, $\delta\tau_{g/p}(= \tau_{g/p} - \tau_0)$ are proportional to TEC and inversely proportional to the square of the wave frequency, f.

1.4.2   TEC Measurements

For TEC measurements, the Ionospheric effect on radio wave propagation mentioned in the previous subsection is often used. TEC has been measured for decades using the Faraday rotation effect on a linear polarized propagating plane wave. But today TEC measurements are made mostly using GPS data because of the good global coverage of the GPS observation network.

The Faraday rotation method uses the polarization property of E-M wave propagating through a magnetized plasma. As is well known, linear polarized plane waves can be expressed as a sum of right- and left-hand polarized waves. When this plane wave is propagating through plasma with an equilibrium magnetic field, the

difference in the phase velocities between the right- and left-hand polarized waves makes a rotation of the polarization. This angle of rotation (Ω) is proportional to TEC:

$$\Omega(rad) = \frac{e^3}{2\varepsilon_0 m_e^2 c} \frac{1}{\omega^2} \int_S NB_0 \cos\theta ds = 2.365 \times 10^4 \frac{1}{f^2} \int_S NB_0 \cos\theta ds, \qquad (1.5)$$

where B_0 is the magnetic field, and θ is the angle between the magnetic field B and the direction of the wave propagation [*Hargreaves*, 1992]. Even though this method has historically been heavily used for TEC observations, it has become less relevant in the past decade due to the rapid expansioned the ground GPS network.

GPS satellites transmit on two frequencies ($f_1 = 1575.42$ MHz and $f_2 = 1227.6$ MHz), which allows us to calculate two important values, (1) differential time delay

$$\delta\Delta\tau_g = \delta\tau_{g,1} - \delta\tau_{g,2} = \frac{40.30}{c}\left(\frac{1}{f_1^2} - \frac{1}{f_2^2}\right) \cdot TEC, \qquad (1.6)$$

and (2) differential phase , which are obtained from Equation 1.4

$$c\delta(\Delta\tau_{p,2} - \Delta\tau_{p,1}) = 40.30\left(\frac{1}{f_1^2} - \frac{1}{f_2^2}\right) \cdot TEC. \qquad (1.7)$$

Absolute TEC values can be obtained from Equation 1.6 by monitoring the differential time delay. Although it appears that TEC can also be obtained from Equation 1.7, a measurement of the differential phase has a typical 2π ambiguity. However, by monitoring the differential phase relative TEC can be measured with high fidelity. Unfortunately, the absolute TEC values obtained from time delay observations are less accurate. However, a more accurate TEC estimate with less than 0.1 TECU error can be obtained by a combination of the absolute and relative measurements, which is called leveling. Here, the 2π ambiguity of the accurate relative

TEC measurements is adjusted by a constant value to match the absolute, but noisy, absolute TEC observations [*Mannucci et al.*, 1993].

In practice, slant TEC values, which are measured along the ray path from a GPS satellite to a ground receiver, are converted to equivalent vertical TEC assuming the ionosphere to be compressed into a thin shell at a shell height of h as shown in Figure 1.4. The vertical TEC values (VTEC) are assigned to an ionospheric pierce point, which is the intercept of the line-of-sight ray and the thin shell at the altitude h. Often, vertical TEC (VTEC) is obtained from the slant TEC (STEC) by use of a mapping function [*Mannucci et al.*, 1993] as follows:

$$VTEC = M(e) \times STEC, \tag{1.8}$$

$$M(e) = \left[1 - \left(\frac{\cos(e)}{1 + h/R_E} \right)^2 \right]^{\frac{1}{2}}, \tag{1.9}$$

where e is an elevation angle of a satellite, h is ionospheric shell height, and R_E is the Earth's mean radius. This mapping functions takes the curvature of the Earth into account.

It should be mentioned that in addition to the GPS observations, a significant amount of TEC observations has also been obtained from the TOPEX/Poseidon and the JASON-1 satellites. These satellites use dual frequency transmitters/receivers to measure the sea surface height. As a byproduct, TEC can be extracted from these measurements over the oceans.

1.5 Ionospheric Modeling

In order, not only to specify the ionosphere, but also to understand the physics that control the dynamics of the ionosphere, several ionospheric models have been developed over the last several decades. The ionospheric models can be broadly di-
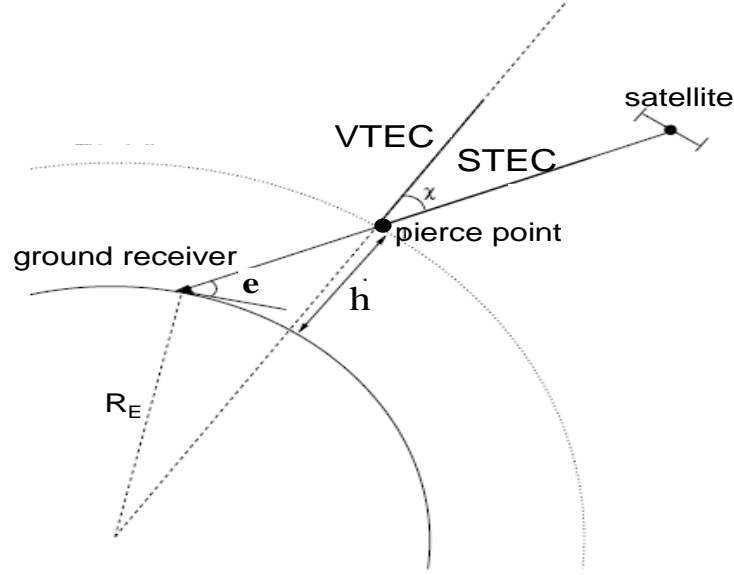
Figure 1.4. Geometry for the conversion of slant TEC to vertical TEC.

vided into three main categories, empirical, theoretical, and data assimilation models [*Schunk et al.*, 2004; *Scherliess et al.*, 2004].

Empirical models yield an average behavior of the ionosphere based on observational data. Therefore, empirical models are limited by the amount of data and the spatial and temporal coverage of the data that were used in their construction. For example, Figure 1.5 shows, in the right column, the longitudinally averaged TEC maps for equinox from the most comprehensive and widely used empirical model for the ionosphere, the International Reference Ionosphere (IRI) [*Bilitza*, 2004] in the left column. The large overestimates of the IRI TEC compared to the TEC maps (middle column) obtained from TOPEX TEC measurements at low latitudes around 7 MLT (magnetic local time) are shown [*Jee et al.*, 2005]. Despite these limitations, empirical model are widely used because of their ease of use.

Theoretical/numerical ionospheric models yield a representative ionosphere by numerically solving the equations which govern the production, loss and dynamics
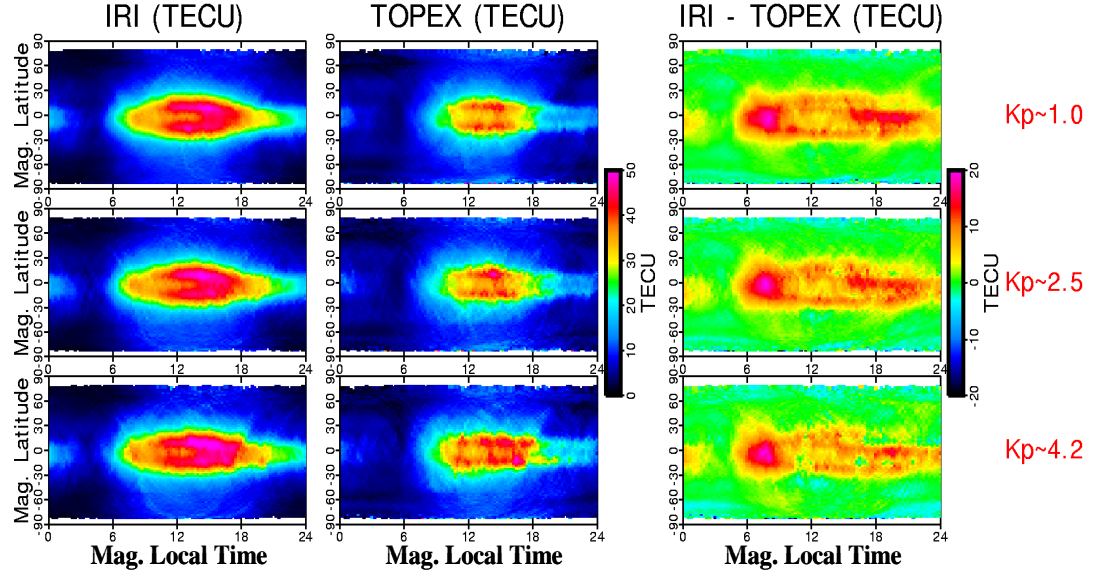
Figure 1.5. TEC maps from both IRI simulations and TOPEX measurements, and TEC difference between them as a functions of magnetic latitude and magnetic local time for the equinox, low solar flux and three different geomagnetic conditions [*Jee et al.* 2005].

of the plasma. However, theoretical/numerical ionospheric models require numerous input parameters associated with coupling processes to the magnetosphere, thermosphere, and plasmasphere. The accuracy of the ionospheric model output, therefore, depends strongly on the accuracy of these input parameters (e.g., the neutral densities, temperatures, and winds, dynamo electric fields, and the auroral electron precipitation). Unfortunately, these parameters are often only vaguely known.

Nevertheless, in order to model the overall ionospheric morphology, the model input parameters are typically provided by empirical models. For instance, a physics-based numerical model, IPM(Ionosphere/Plasmasphere Model) [*Schunk et al.*, 2004; *Scherliess et al.*, 2004] uses empirical representations for the thermospheric neutral

winds and for the low-latitude plasma drifts. In this case, the neutral composition is given by MSIS-90 model [*Hedin*, 1991], the neutral wind is given by the Horizontal Wind Model 93 (HWM93) [*Hedin et al.*, 1991], and the low-latitude plasma drifts are given by the Scherliess and Fejer plasma drift model [*Scherliess and Fejer*, 1999].

Another approach is to couple, in a self-consistent manner, a theoretical/numerical model of the ionosphere to theoretical/numerical models of the thermosphere, magnetosphere, plasmasphere, and lower atmosphere. One of the most widely known model that couples the ionosphere to the thermosphere and the lower atmosphere is the NCAR TIME-GCM (Thermosphere-Ionosphere-Mesosphere-Electrodynamics General Circulation Model) model [*Roble*, 1996]. However, even in this approach additional input parameters are needed and unreliable model outputs can be produced due to error propagation from model to model.

The ionospheric empirical and physics-based models are capable to reproduce many of climatological features of the ionosphere; however, they have limitation for reproducing ionospheric weather during quiet and storm times due to the aforementioned limitations. Recently, data assimilation models have also been developed that allow for specification of the state of the ionosphere from a combination of measurements and a physics-based model. These models promise a reliable specification of the ionosphere and a global ionospheric weather forecast by using powerful data assimilation techniques [*Schunk et al.*, 2002; *Scherliess et al.*, 2006].

1.6 Overview of This Work

As described in Section 1.1, in the upper atmosphere of the Earth positively charged ions and free electrons can be found. Variability in the distribution of the charged particles can degrade communication, navigation, and surveillance systems. Over the past decade, large efforts have been undertaken to continuously monitor

and specify these particles throughout the entire upper atmosphere. Unfortunately, the density of the charged particles cannot be measured everywhere all the time. However, changes in their number density are typically not localized, but rather extend over large or small areas. Therefore, an observed change in the density at one location might be used to predict the change in the number density at another location. In this work, the detailed relationship between observed changes in the total number of electrons above a given location with those at different locations was determined. The results of this study will not only help to better understand the physical processes that cause variations in the densities, but also can be used to improve predictive models for the Earth's upper atmosphere. In a second step, in order to better understand the causes of these changes, a computer model was used. In the following, an overview of these two studies is given in more detail.

Ground-based GPS/TEC observations from hundreds of GPS ground receivers allow us to study the global and regional TEC morphology during both geomagnetically quiet and disturbed times. Despite many studies of the climatological and storm-time variations of TEC, there only has been limited information about the spatial and temporal correlation of day-to-day variations in TEC on a global scale. These correlations, which indicate a statistical relationship between ionospheric parameters (TEC) at different locations or times, are not only important for a better understanding of the physical mechanisms that cause ionospheric weather variability, but are also a crucial component of modern-day data assimilation systems that provide improved ionospheric specifications and forecasts. In this work, detailed study of the spatial correlations of day-to-day ionospheric TEC variations on a global scale was performed for four 30-day-long periods in 2004 (January, March/April, June/July, September/October) using observations from more than 1000 ground-based GPS re-

ceivers. In Chapter 2, a detailed analysis of day-to-day TEC correlations is presented.

In an effort to better understand the effects of physical drivers on the ionospheric TEC variations, the relative importance of the neutral wind and the electric field for TEC variability was studied. The results of this study are presented in Chapter 3. For this study, a physics-based numerical Ionosphere/Plasmasphere Model (IPM) [*Schunk et al.*, 2004; *Scherliess et al.*, 2004] was used. The model solves the transport equations for the six ions, O^+, NO^+, O_2^+, N_2^+, H^+ and He^+, on convecting flux tubes that realistically follow the geomagnetic field. Two of the inputs required by the IPM are the thermospheric neutral wind and the low-latitude electric field, which can be given by existing empirical models or externally specified. To study the relative importance of the neutral wind and the electric field for the TEC variations, these two model inputs were externally modified and the resulting variations in TEC were compared. Neutral wind and electric field modifications were introduced at three different local times in order to investigate the effect of different start times of the imposed perturbations on TEC. This study focused on modeled low- and middle-latitude TEC variations in the afternoon and post-sunset period at three different longitude sectors for medium solar activity and low geomagnetic activity.

References

Abdu, M. A. (1997), Major phenomena of the equatorial ionospherethermosphere system under disturbed conditions, *J. Atmos. Sol. Terr. Phys., 59* (13), 1505- 1519.

Anderson, D. N., and R. G. Roble (1981), Neutral wind effects on the equatorial *F*-region ionosphere, *J. Atmos. Sol. Terr. Phys., 43*, 835.

Appleton, E.V. (1946), Two anomalies in the ionosphere, *Nature 157*, 691.

Banks, P. M., R. W. Schunk, and W. J. Raitt (1976), The topside ionosphere: A region of dynamic transition, *Annl. Rev. Earth Planet. Sci., 4*, 381.

Bilitza, D. (2004), 35 years of International Reference Ionosphere - Karl Rawer's legacy, *Adv. Radio Sci., 2*, 283-287.

Hargreaves, J. K. (1992), *The Solar-Terrestrial Environment*, Cambridge Atmospheric and Space Science Series, Cambridge Univ. Press, New York.

Hedin, A. E. (1991), Extension of the MSIS thermospheric model into the middle and lower atmosphere, *J. Geophys. Res., 96*, 1159.1172.

Hedin, A. E., et al. (1991), Revised global model of thermospheric winds using satellite and ground-based observations, *J. Geophys. Res., 96*, 7657-7688.

Jee, G., R. W. Schunk, and L. Scherliess (2005), Comparison of IRI-2001 with TOPEX TEC measurements, *J. Atmos. Sol. Terr. Phys.*, 67, 365-380.

Kelley, M. C., M. N. Vlasov, J. C. Foster, and A. J. Coster (2004), A quantitative explanation for the phenomenon known as storm-enhanced density, *Geophys. Res. Lett., 31*, L19809, doi:10.1029/2004GL020875.

Lin, C. H., A. D. Richmond, J. Y. Liu, H. C. Yeh, L. J. Paxton, G. Lu, H. F. Tsai, and S. Y. Su (2005), Large-scale variations of the low-latitude ionosphere during the October- November, 2003 superstorm: Observational results, *J. Geophys. Res., 110*, A09S28, doi:10.1029/2004JA010900.

Mannucci, A. J., B. D. Wilson, and C. D. Edwards (1993), A new method for monitoring the Earth's ionospheric total electron content using the GPS global network, in *Proceedings of ION GPS-93, the 6th International Technical Meeting of the Satellite Division of The Institute of Navigation, Salt Lake City, UT, 22-24 September*, pp. 1323-1332, The Institute of Navigation, Alexandria, Va.

Rishbeth, H. (1975), F-region storms and thermospheric circulation, *J. Atmos. Terr. Phys., 37*, 1055-1064.

Roble, R. G. (1996), The NCAR Thermosphere-Ionosphere-Mesosphere-Electrodynamics General Circulation Model (TIME-GCM), *STEP Handbook of Ionospheric Models*, edited by R. W. Schunk, Utah State Univ., Logan, pp. 281-288.

Scherliess, L., and B. G. Fejer (1999), Radar and satellite global equatorial F region vertical drift model, *J. Geophys. Res., 104*, 6829-6842.

Scherliess, L., R. W. Schunk, J. J. Sojka, and D. C. Thompson (2004), Development of a physics-based reduced state Kalman filter for the ionosphere, *Radio Sci., 39*, RS1S04, doi:10.1029/2002RS002797.

Scherliess, L., R. W. Schunk, J. J. Sojka, D. C. Thompson, and L. Zhu (2006), Utah State University global assimilation of ionospheric measurements Gauss-Markov Kalman filter model of the ionosphere: Model description and validation, *J. Geophys. Res., 111*, A11315, doi:10.1029/2006JA011712.

Schunk, R. W., and A. F. Nagy (2000), *Ionospheres*, Cambridge Univ. Press, New York.

Schunk, R. W., L. Scherliess, and J. J. Sojka (2002), Ionospheric specification and forecast modeling, *J. Spacecraft Rockets*, 39(2), 314-324.

Schunk, R. W., et al. (2004), Global Assimilation of Ionospheric Measurements (GAIM), *Radio Sci., 39*, RS1S02, doi:10.1029/2002RS002794.

CHAPTER 2

SPATIAL CORRELATIONS OF DAY-TO-DAY IONOSPHERIC TOTAL ELECTRON CONTENT VARIABILITY OBTAINED FROM GROUND-BASED GPS [1]

Abstract

The spatial correlations of day-to-day ionospheric TEC variations for four 30-day-long periods in 2004 (January, March/April, June/July, September/October) were determined using more than 1000 ground-based GPS receivers. The spatial correlations were obtained in a two-step process. Initially, the day-to-day variability was calculated by first mapping the observed slant TEC values for each five-minute GPS ground receiver-satellite pair to the vertical using a simple geometrical factor and then differencing it with its corresponding value from the previous day. This resulted in more than 150 million values of day-to-day change in TEC (ΔTEC). Next, statistics were performed on the ΔTEC values to obtain their spatial correlations. Our study indicates strong correlations between geomagnetic conjugate points and these correlations are larger at low latitudes ($r = 0.63 - 0.73$) than at middle latitudes ($r = 0.32 - 0.43$). Typical correlation lengths, defined as the angular separation at which the correlation coefficient drops to 0.7, were found to be larger at middle latitudes than at low latitudes. The meridional correlation lengths are about 7 degrees and 4 degrees at middle and low latitudes, respectively. The zonal correlation lengths are approximately 20 degrees at middle latitudes and 11 degrees at low latitudes. The correlation lengths are larger during daytime (1100 - 1300 MLT) than during nighttime (2300 - 0100 MLT). The results indicate that the spatial correlation is largely independent of season. These spatial correlations are important for under-

---

[1]Coauthored by J. S. Shim, L. Scherliess, R.W. Schunk, and D. C. Thompson.

standing the physical mechanisms that cause ionospheric weather variability and are also relevant to data assimilation.

2.1 Introduction

It is well known that the ionosphere varies markedly with altitude, latitude, longitude, universal time, season, solar cycle, and geomagnetic activity. This variability arises from the couplings, time delays, and feedback mechanisms that are inherent in the ionosphere-thermosphere system, as well as from effects of solar, interplanetary, magnetospheric, and mesospheric processes. Variations in the electric field, neutral winds, and neutral composition, all affect the global ionosphere over a multitude of temporal and spatial scales.

Total electron content (TEC) measurements have been used extensively to study the general morphology and variability of the ionosphere during both geomagnetically quiet and disturbed conditions. *Codrescu et al.* [1999, 2001] and *Jee et al.* [2004] have used TEC observations from the TOPEX satellite to study the TEC climatology over the oceans at low and middle latitudes and presented its seasonal and solar cycle variations. *Jee et al.* [2004] also presented the longitudinal variation of the TOPEX TEC data in the Atlantic, Indian, and Pacific sectors. A more detailed study of the longitudinal dependence of TEC at low-latitudes was presented by *Vladimer et al.* [1999] and recently by *Scherliess et al.* [2008] using the entire 13 years of TOPEX TEC data. The latter study pointed out the occurrence of a wavenumber-four pattern in the low-latitude TEC climatology.

Ground-based GPS/TEC observations from hundreds of GPS ground receivers have been used widely to study the global and regional TEC morphology during geomagnetic active periods [e.g., *Foster and Rideout*, 2005; *Foster et al.*, 2005]. These studies have, for example, pointed out the existence of large storm enhanced plasma

densities (SEDs), as observed during the strong October 2003 geomagnetic storm. *Foster and Rideout* [2007] also pointed out the conjugacy of the SED structures using a combination of ground-based GPS and Jason/TOPEX TEC data in the two hemispheres. They explained this conjugacy by the mapping of storm-time electric fields from one hemisphere to the other along geomagnetic field lines. A recent review of patterns and processes for TEC during geomagnetic storms is given by *Mendillo* [2006].

Ground-based GPS/TEC data have also been used to study the morphology and evolution of medium- and large-scale traveling ionospheric disturbances (TIDs) [e.g., *Saito et al.*, 1998; *Tsugawa et al.*, 2004, 2006; *Ho et al.*, 1998]. *Tsugawa et al.* [2006] studied the geomagnetic conjugacy of large-scale traveling ionospheric disturbances (LSTIDs) using TEC data obtained from GPS networks in Japan and Australia. Their observational results indicated that the LSTIDs observed almost simultaneously in both hemispheres were not connected electromagnetically through the geomagnetic field but were generated by atmospheric gravity waves that independently propagated equatorward in the two hemispheres. *Otsuka et al.* [2004] reported simultaneous observations of medium-scale traveling ionospheric disturbances (MSTIDs) at geomagnetic conjugate points in both hemispheres, using two all-sky airglow imagers at middle latitudes. Contrary to the *Tsugawa et al.* [2006] study, their result suggested that polarization electric field ($\mathbf{E}_p$) may play an important role in the generation of MSTIDs. They explained their results by the mapping of the polarization electric fields along geomagnetic field lines from one hemisphere to the other, causing the F region plasma to move upward or downward by $\mathbf{E} \times \mathbf{B}$ drifts. As a result, plasma density structures were mirrored in the northern and southern hemispheres.

Although the above studies have revealed many of the climatological and storm-time variations of TEC, information about the spatial and temporal correlation of day-to-day variations in TEC on a global scale is limited. These correlations, which describe a statistical relationship between ionospheric parameters (TEC) at different locations or times, are not only important for a better understanding of the physical mechanisms that cause ionospheric weather variability, but are also crucial component of modern-day data assimilation systems that provide improved ionospheric specifications and forecasts [e.g., *Daley*, 1991; *Scherliess et al.*, 2006].

Several studies of spatial TEC correlation using data obtained from the Faraday rotation technique at middle latitude have been conducted [e.g., *Kane*, 1975; *Klobuchar and Johanson*, 1977; *Soicher*, 1978; *Huang*, 1983]. *Kane* [1975] used TEC data obtained from geostationary satellites recorded at six locations for different seasons in 1967, and found that variations in TEC at locations separated by more than about 3000 km in latitude or longitude showed poor correlations. *Klobuchar and Johanson* [1977] used data from nine TEC stations for the solar maximum period (1968, 1969) and for the solar minimum period (1972, 1974), and computed correlation coefficients for the 1000-1600 local time sector. They pointed out that a 50 percent improvement in TEC predictions over monthly median values can be obtained, when TEC monitoring stations are spaced by approximately 2400 km in longitude and 1600 km in latitude. Correlations between TEC at Fort Monmouth, NJ (40.18° N, 74.06° W) and Richmond, FL (25.60° N, 80.40° W) were determined by *Soicher* [1978]. His analysis included TEC data from the two stations for the first five months of 1975 and September 1974. He obtained correlation coefficient larger than 0.9, and found no seasonal variation in the correlation coefficient. *Huang* [1983] studied correlation coefficients between Aberystwyth and Hawick, which are separated by 304 km, for the

period from November 1975 to July 1976. He confirmed that the daytime correlation coefficient of TEC between the two locations was of the order of 0.9. *Huang* [1984] studied the spatial correlation of TEC at the equatorial anomaly crest using Faraday rotation data at Lunping and Kaohsiung from December 1981 to November 1982. He found that the diurnal variations of the TEC correlation coefficient at the two locations, which are separated by 280 km, were different for each month. In addition, he pointed out that the correlation length during the day (1000-1600LT) was shorter in the crest zone of the equatorial anomaly compared to the region outside of the crest zone.

Gail et al. [1993] studied the spatial and temporal correlations of local middle-latitude TEC data from GPS ground receivers to extrapolate single-point measurements of TEC to other locations and times. They used a four-channel receiver that tracked coded signals from the NAVSTAR GPS satellites for morning and midday over a 4-week period near the autumnal equinox in 1989. Their study indicated that the correlation coefficient during midday decreased linearly with latitude, longitude, and time separation, with values of about 0.91 for a 1000 km separation and 0.98 for a 1-hour separation.

TOPEX observations of the ionospheric TEC were also used to obtain spatial correlation lengths in order to improve single frequency altimeter measurements by adaptive modeling techniques [*Angell et al.*, 2006]. They calculated the correlation coefficient using a data set consisting of 100 consecutive ascending tracks over a range of geographic latitude from 45° S to 45° N and over all local times, and found that the spatial coherence distance for TEC, which is defined as the separation at which the spatial correlation coefficient falls to 0.7, varied between 200 km to 3600 km depending on latitude and local time. However, their study was limited since the TOPEX

satellite does not allow simultaneous TEC measurements in both hemispheres (the satellite takes 112 minutes to complete a single orbit).

In this study, TEC measurements from more than 1000 ground-based GPS receivers were used to determine the global morphology of day-to-day TEC changes. In Section 2.2, we present our initial preparation of the ground-based GPS TEC data for our statistical analysis. The statistical analysis technique of the global day-to-day variability, as well as and our results for different geophysical conditions, are presented in Section 2.3. Our conclusions are discussed in Section 2.4.

2.2   TEC Data

In order to statistically determine the global day-to-day TEC variability, as well as its spatial correlations, we have analyzed instantaneous ground-based GPS/TEC observations from more than 1000 ground GPS receivers with a 5-minute cadence during four 30-day-long periods. These 30-day-long periods covered different seasonal conditions and included January 2004, March/April 2004, June/July 2004 and September/October 2004, and their average geophysical conditions are given in Table 2.1. At any instant in time, each GPS ground receiver observes between about four to nine GPS satellites with elevation angles above 15°, with the actual number of satellites in view depending on the current satellite positions and to a lesser extent on the geographic latitude of the receiver. On the average, each GPS receiver observes about five GPS satellites at each instant and as a result our data set consists of more than 150 million ΔTEC values (4×30 days$\times24$ hours/day$\times12$ times/hour$\times1000$ receivers$\times5$ GPS satellites).

For our analysis, we have used differential phase and pseudorange observations. These data were used to obtain accurate slant TEC values by a leveling process in which the integer ambiguity of the highly accurate carrier phase measurement

Table 2.1. Average geophysical conditions for the four 30-day-long study periods

	Day of Year	$\overline{K_p}$	$\overline{F10.7}$	% of time $K_p \geq 5.0$
January 2004	001-029/2004	3.36	111.8	6.8
Mar./Apr. 2004	080-110/2004	2.23	108.5	3.2
Jun/July 2004	172-202/2004	1.60	112.5	0.8
Sep./Oct. 2004	266-296/2004	1.60	92.5	1.2

difference (error < 0.1 TECU) is adjusted by a constant value to match the absolute, but noisy, pseudorange observations [*Mannucci et al.*, 1993]. This procedure resulted in slant TEC observations that potentially include ground receiver and satellite-specific differential time delay biases. These biases, however, will cancel out in our analysis, as outlined below.

In order to combine the slant TEC data from different viewing geometries, the observed slant TEC (STEC) values were mapped to the vertical direction for each GPS ground receiver-satellite pair using a thin shell approximation with an ionospheric shell height of 350 km [*Mannucci et al.*, 1993] and assigned to the locations of the ionospheric pierce points. In order to reduce the errors associated with our mapping procedure, as well as to reduce a possible multipath contamination of the TEC data, we have excluded data with elevation angles below 15°. With this elevation angle cutoff, the locations of the pierce points form a circle around the location of the receiver with a radius of about 850 km.

Next, the day-to-day changes in TEC were obtained by subtracting previous day's TEC value from current day's corresponding TEC value

$$\Delta TEC(x, d, t) = TEC(x, d, t) - TEC(x, d-1, t+5\ min), \qquad (2.1)$$

where x denotes geographic latitude and longitude of the ionospheric pierce point, and d and t denote day and universal time, respectively. Here, we took advantage of the fact that the GPS satellites nearly follow the same ground tracks from one day to the next (4 min earlier each day), e.g., each ground receiver collects TEC data along almost the same ionospheric path on consecutive days. The shift of 5 minutes in Equation 2.1 approximately takes account of the 4-min shift of the GPS satellite orbits (we use 5 min instead of 4 min because of the 5-min cadence of our data). The errors from the 1-min difference between the shift of the GPS satellite orbit and the cadence of our data were found to be negligible, due to the insignificant difference in the latitude and longitude of the ionospheric pierce points (less than $0.04°$). Therefore, for example, ΔTEC at 1930 UT on day 2004/85 is the difference between TEC at 1930 UT on day 2004/85 and TEC at 1935 UT on day 2004/84 for each ground receiver-satellite pair.

Figure 2.1 shows a typical example of day-to-day TEC variability (ΔTEC), as obtained from Equation 2.1, for a magnetically quiet time (Kp < 2). Positive and negative values in ΔTEC indicate increases and decreases of TEC from one day to the next, respectively. Note that a significant amount of TEC variability is noticeable even during this quiet period.

There are several sources for errors in the analysis of the TEC data that could potentially affect our analysis. As mentioned above, systematic errors in the slant TEC data, associated with differential time delay biases in the satellite transmitter and the ground receivers, are the largest sources of error [*Mannucci et al.*, 1993]. However, as evident from Equation 2.1, these biases cancel out in our analysis under the assumption that they remain constant for the two consecutive days [*Wilson and Mannucci*, 1993]. A second, potentially important, source of error is associated with
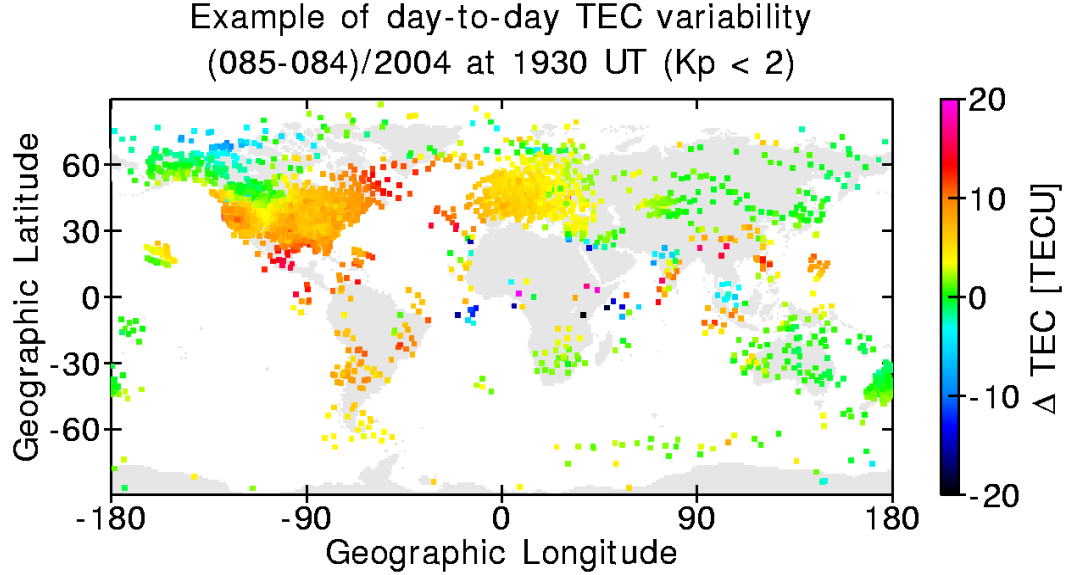
Figure 2.1. Examples of day-to-day TEC variability (085-084/2004) at 1930 UT shown in a geographic coordinate system.

the corruption of slant TEC with multipath errors. This uncertainty is, however, drastically reduced in our study due to the elimination of slant TEC data associated with low elevation angles ($< 15°$), and we do not anticipate this error to be significant.

An additional error that could potentially influence our results is associated with the mapping of the slant TEC data to the vertical direction and consecutive binning of the data into spatial bins. Generally, this error is associated with gradients in the ionosphere and consists of at least three contributing terms. The first term is associated with the slant range mapping error that is introduced when the GPS radio signal traverses the ionosphere across a gradient region. The second term is associated with the fact that any ionospheric gradient will result in different TEC values for different ionospheric piercing points regardless of any slant range mapping error. Finally, the third term is associated with the variability of the gradient region and possibly with changes in the height of the ionosphere from one day to the next. Although our analysis of these errors will not separate the three terms, we will provide

an estimate for the overall error that is introduced by the combination of the three terms. Since each GPS ground receiver at any given time observes about five satellites randomly distributed in the sky and more than one GPS receiver could be located in a given spatial bin, we have estimated the overall error by calculating the spread in the mapped TEC data about its mean value. If the ionosphere would be spatially uniform, all mapped slant TEC data would result in the same vertical TEC value. However, due to horizontal gradients in the ionosphere and changes in these gradients and in the height of the ionosphere from one day to the next, the mapping introduces errors in the individual estimated vertical TECs that lead to a spread of the obtained values. In order to obtain an estimate of this error, we have used our entire 30-day data base of five minute ΔTEC values corresponding to the March/April 2004 period. All ΔTEC data for a given UT were sorted into a $2° \times 4°$ geographic latitude$\times$ longitude bin, and the average ($\overline{\Delta TEC}$) and the standard deviation in each bin were calculated for every five minute UT step. For the calculation of the standard deviation, only ΔTEC values were considered that deviated less than three sigma from the average values in each bin. We found that in more than 92% of all bins, the standard deviation was less than 1.5 TECU. Next, a global average of all standard deviations was separately calculated for the daytime (1100-1300 LT) and for the nighttime (2300-0100 LT) by averaging overall spatial bins and all 30 days. The global average values of the standard deviations were found to be nearly independent of the time of the day with values of 0.65 TECU and 0.67 TECU during the day and night, respectively. Note that these values correspond to about 15 % of the mean of the averaged ΔTEC absolute values (i.e., mean of $|\overline{\Delta TEC}|$) during the day and to about 33% during the night. A further refinement of our analysis, separating the data into low and mid latitudes, revealed that the errors at low latitudes ($-20°$ to $+20°$) are slightly

larger with values of 0.75 TECU and 0.99 TECU for the day and nighttime periods, respectively. Surprisingly, these estimated errors of less than 1 TECU associated with the mapping and binning of the slant ΔTEC data are significantly smaller than the corresponding errors of several TECU caused by a mapping of absolute slant TEC value to the vertical direction in regions of large horizontal electron density gradients [*Mannucci et al.*, 1993]. We speculate that the error in mapping our ΔTEC values is smaller than the error of mapping the original slant TEC, because of the correlated nature of these errors on two consecutive days. As a result, we speculate that much of the mapping errors associated with the first two terms mentioned above have canceled out in our differencing scheme (Equation 2.1) and the major contributing error in our analysis is associated with day-to-day changes in the gradients and/or the height of the ionosphere. However, due to the currently sparse data coverage over the low-latitude region, our error estimations in this region need further investigation in the future.

2.3   Analysis and Results

For our global analysis of day-to-day TEC changes, we have used two statistical parameters, e.g., the local standard deviation of these variations and their spatial correlation coefficient. The first one is a measure of the local deviation of TEC changes about a mean value (which is zero in our analysis) and the second one, namely the spatial correlation coefficient, is a measure of the statistical correlation between TEC changes at different locations on the globe.

2.3.1   Standard Deviations

In order to statistically describe the local day-to-day changes in TEC, we have used the standard deviation of these changes about their respective mean TEC

changes. For all of our four study periods, the TEC changes were found to closely exhibit Gaussian distributions around zero mean value, indicating that on the average, TEC experienced as many increases and decreases from one day to the next over the 30-day-long time periods. Consequently, the standard deviation is an adequate measure of the day-to-day variations in TEC.

Following the analysis of *Codrescu et al.* [1999, 2001] and *Jee et al.* [2004], who have shown that the general TEC morphology is best described in a geomagnetic frame, we have also adopted this frame for our analysis of TEC variability. In particular, we have calculated for each ΔTEC value the corresponding magnetic latitude and magnetic local time (MLT) pair using quasi-dipole coordinates [*Richmond*, 1995].

Next, for each of the 30-day-long periods, the ΔTEC values were sorted according to their magnetic latitude and MLT and binned into $2°\times20$ min magnetic latitude/ MLT bins. Finally, in each bin the standard deviation was determined. As a result, global maps of the standard deviation as a function of magnetic local time and latitude were created. Figure 2.2 shows the resulting standard deviation maps for our four study periods. Note that the magnetic latitude-MLT coordinate system is fixed in space. Therefore, as the Earth rotates, all geographic longitudes contribute to each magnetic latitude-MLT bin. Hence, Figure 2.2 shows zonally averaged ΔTEC.

Clearly evident in Figure 2.2 is the enhanced variability around the locations of the equatorial anomaly with values ranging from about 8 to 17 TECU. These enhancements in the standard deviation are approximately located at $\pm15°$ magnetic latitude on both sides of the magnetic equator and last from about 1000 MLT until about 0200 MLT, with their largest values around 1500-1700 MLT. During equinoxes (right panels in Figure 2.2) the standard deviation appears to be nearly symmetric
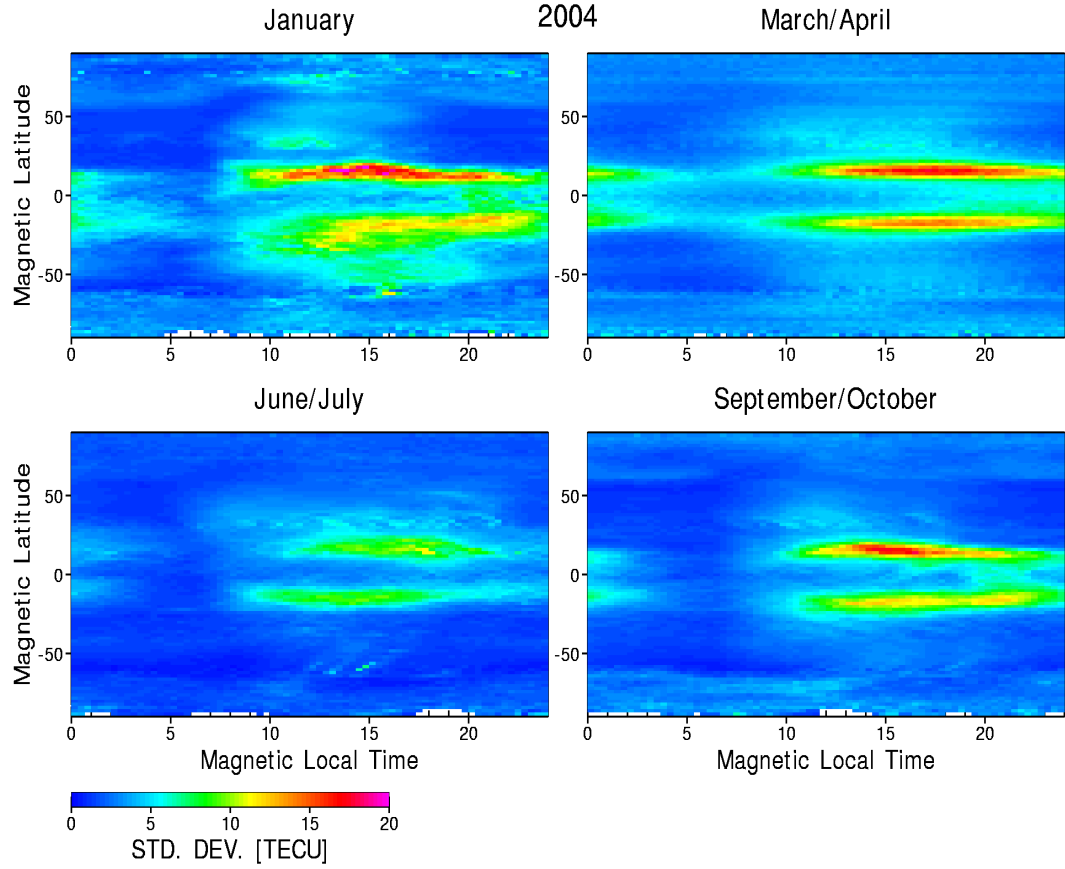
Figure 2.2. Maps of standard deviation of zonally averaged ΔTEC as functions of geomagnetic latitude and magnetic local time for four 30-day-long periods (January (001-029), March/April (080-110), June/July (172-202), and September/October (266-296)) in 2004.

about the magnetic equator with slightly smaller values in the southern hemisphere. During the December solstice period (upper left panel in Figure 2.2), a pronounced difference of about 30% in the standard deviation between the northern and southern anomalies can be seen. During June solstice (lower left panel), the standard deviation around the anomaly peaks does not display a clear asymmetry.

Near the magnetic equator the standard deviation is significantly reduced when compared to the off-equatorial enhancements at all local times. Here, the standard deviation is nearly always below 5 TECU and comparable to the middle-

latitude values.

At middle latitudes, the standard deviations are nearly symmetric in the northern and southern hemispheres during the equinoxes with values near 5 TECU during the day and 2-3 TECU at night. During June solstice (lower left panel), the standard deviations are also close to symmetric, although slight enhancement in the variability can be seen during daytime in the northern (summer) hemisphere when compared to the southern (winter) hemisphere. However, the standard deviations during the December solstice period (upper left panel) are significantly elevated during the daytime when compared to the other seasons and exhibit clear asymmetries. Here, deviations of about 10 TECU are observed in the southern hemisphere and deviations of about 7-8 TECU are seen in the northern hemisphere, indicating that the larger TEC variations occur in the summer hemisphere (southern hemisphere) for this time period. Based on our limited analysis of the seasonal dependence of the standard deviation, using only January 2004 to characterize December solstice conditions, it is not clear whether this apparent seasonal difference is due to a true seasonal variation or associated with the enhanced geomagnetic activity seen during this month (see Table 2.1)

The seasonal asymmetry in the day-to-day TEC variability, with larger variability in the summer hemisphere than in the winter hemisphere during daytime, is in contrast to the well-known seasonal anomaly in the peak F region densities (N_mF_2) [*Jee et al.*, 2004; *Rishbeth et al.*, 2000]. The seasonal anomaly refers to the observation that during daytime N_mF_2 at middle latitudes is larger during winter than during summer conditions. *Codrescu et al.* [1999, 2001] and *Jee et al.* [2004] reported that the seasonal anomaly was not evident in their global TEC analysis. Our results indicate that this anomaly is also absent or opposite in the day-to-day TEC changes.

The annual anomaly, however, can clearly be seen in Figure 2.2 (left panels). This anomaly describes the fact that N_mF_2 during December solstice conditions is on the average larger than during June solstice conditions. This anomaly, which was clearly seen in the absolute TEC values by *Codrescu et al.* [1999] and *Jee et al.* [2004], is also clearly evident in our day-to-day TEC changes. Figure 2.2 indicates that the TEC variability is reduced by about 50% from December to June solstice conditions.

Due to the uneven distribution of our data with a significantly denser data distribution in the northern hemisphere when compared to both the southern hemisphere and the equatorial region (see Figure 2.1), it is important to test the robustness of the results for different data distributions. For these tests, we estimated the uncertainty in the true standard deviation, which is inversely proportional to the square root of the sample size. The uncertainty in estimating the standard deviation was found to be less than three percent of the ΔTEC value, even in the data starved southern hemisphere. This indicates that the observed north-south variability is a real feature rather than an artifact due to the poor sampling in the southern hemisphere. However, additional robustness tests were performed using a random sub sampling of our data base. The analysis was than redone with a 50% reduction in the number of data points and the results were compared with those of our full analysis using all available data. Although small, statistically insignificant differences in the standard deviation maps were observed, none of them affected our results presented above. However, note that there are well-known longitudinal variations in the low- and middle-latitude ionosphere [*Immel et al.*, 2006; *Scherliess et al.*, 2008], and some of our hemispheric asymmetries might be the result of the non-uniform data coverage in the two hemispheres.

2.3.2   Spatial Correlations

In order to establish the statistical correlation of the day-to-day TEC changes (ΔTEC) between different locations on the globe, we have used the linear spatial correlation coefficient. This coefficient, which ranges from a value of 1 (perfect correlation) to a value of -1 (anti correlation), statistically describes the strength of a linear relationship between ΔTEC at one location to ΔTEC at another location on the globe. A correlation coefficient of zero indicates the variables are independent.

The linear spatial correlation coefficient is of significant value and can, for example, be used to determine the optimum station spacing in a network of ground receivers for improved TEC predictions [*Klobuchar and Johanson*, 1977; *Gail et al.*, 1993; *Rush*, 1976], or to improve single frequency altimeter measurements by adaptive modeling techniques [*Angell et al.*, 2006]. Furthermore, spatial correlation coefficients are an important part of modern data assimilation systems and help to statistically distribute information away from observing systems into unobserved domains.

We have determined the spatial correlation coefficients (r_{ij}) for ΔTEC between different geographic locations on the globe by first binning and averaging the individual ΔTEC observations for a given universal time (UT) in $5° \times 15°$ geographic latitude and longitude bins and then calculating the correlation coefficient between the different pairs of bins (i,j) using a standard method [*Maybeck*, 1994]:

$$r_{ij} = \frac{\sum_{d,t}\left[\left(\overline{\Delta TEC_i(d,t)} - M_i\right)\left(\overline{\Delta TEC_j(d,t)} - M_j\right)\right]}{\left[\sum_{d,t}\left(\overline{\Delta TEC_i(d,t)} - M_i\right)^2\right]^{\frac{1}{2}}\left[\sum_{d,t}\left(\overline{\Delta TEC_j(d,t)} - M_j\right)^2\right]^{\frac{1}{2}}}. \qquad (2.2)$$

Here, the subscripts i and j correspond to the different geographic bin, $\overline{\Delta TEC_i(d,t)}$ is the average value of $\Delta TEC_i(d,t)$ in the ith bin at a given time t and a day d, and $\overline{\Delta TEC_i(d,t)}$ is the mean value of over a given time period. As mentioned above,

these mean values are close to zero in our analysis and can be ignored.

In our study, relatively large spatial bins ($5° \times 15°$) were used in order to acquire a sufficient amount of data in each bin in both hemispheres. This was necessary due to the relatively sparse data coverage in the southern hemisphere (see Figure 2.1). As a result of these large bin sizes, observations from several different ground-receiver sites typically contribute to a given bin at any time. The observations were averaged in our analysis and the average value was used to represent the bin. It is interesting to note that the spread of the individual ΔTECs from the different stations in each bin about the average value was found to be less than 2 TECU for most of our cases (more than 90%).

Figure 2.3 shows the spatial correlation coefficients of ΔTEC between different locations on the globe for the March/April 2004 period. Each of the nine panels in Figure 2.3 shows the correlation coefficient of ΔTEC between a fixed reference point (black dot) and the rest of the globe. Nine different reference points were chosen covering three geographic longitude sectors ($-67.5°$E, $22.5°$E, and $127.5°$E) and three geographic latitude sectors (northern hemisphere, southern hemisphere and near the equator). The correlation coefficients shown in Figure 2.3 are color-coded, with green indicating only small correlations between ΔTEC at the reference point and the corresponding geographic location, and red and blue indicating strong correlations and anticorrelations, respectively.

Figure 2.3 indicates that the correlation coefficients are significantly smaller at low and equatorial latitudes when compared to the middle-latitude values. An interesting observation in Figure 2.3 is the correlation between magnetic conjugate points. This conjugacy can clearly be seen in all three longitude sectors but is best observed in the American and East Asian sectors (left and right panels) due to the

good data coverage in these sectors. However, it is difficult to obtain reliable estimates of the correlation lengths from Figure 2.3 due to the data distribution.

In order to further investigate the spatial correlation coefficients and to take advantage of the apparent alignment of the observed correlations in Figure 2.3 with magnetic coordinates, we have calculated zonally averaged correlation coefficients using again quasi-dipole coordinates. First, we have calculated the geomagnetic latitude and longitude for each ΔTEC value and binned the data in $5° \times 15°$ geomagnetic latitude and longitude bins. At this step, zonal information is retained. Next, the longitudinal separation ($\Delta Longitude$) between the bins was determined and the correlation coefficient was calculated as a function of the magnetic latitudes of the bins and their longitude separation. This second step resulted in zonally averaged correlation coefficients that, however, preserved the zonal correlations coefficients.

Figure 2.4 shows as an example of the variation of the ΔTEC values for selected pairs of reference and comparison points. The reference points were selected for four magnetic latitudes ($47.5°$, $2.5°$, $-12.5°$, and $-42.5°$), comprising the four rows in Figure 2.4, and for three relative comparison locations (magnetic conjugate, $\Delta Longitude = 30°$, and $\Delta Longitude = 120°$), comprising the three columns in Figure 2.4. For example, consider $47.5°$ magnetic latitude and the conjugate point comparison (top row, left column). At $47.5°$ magnetic latitude, the ΔTEC from all of the days in the four 30-day periods and all longitudes are considered, and ΔTEC bins are created. The ΔTEC bins vary from -10 to $+10$ TECU in increments of 1 TECU (x-axis). For each ΔTEC value at 47.5 (x-axis), there are corresponding ΔTEC values at the conjugate point (y-axis). The open squares show the average ΔTEC values at the conjugate points, and the bars show the spread about the average values (standard deviation). The middle and right columns show a similar comparison, but
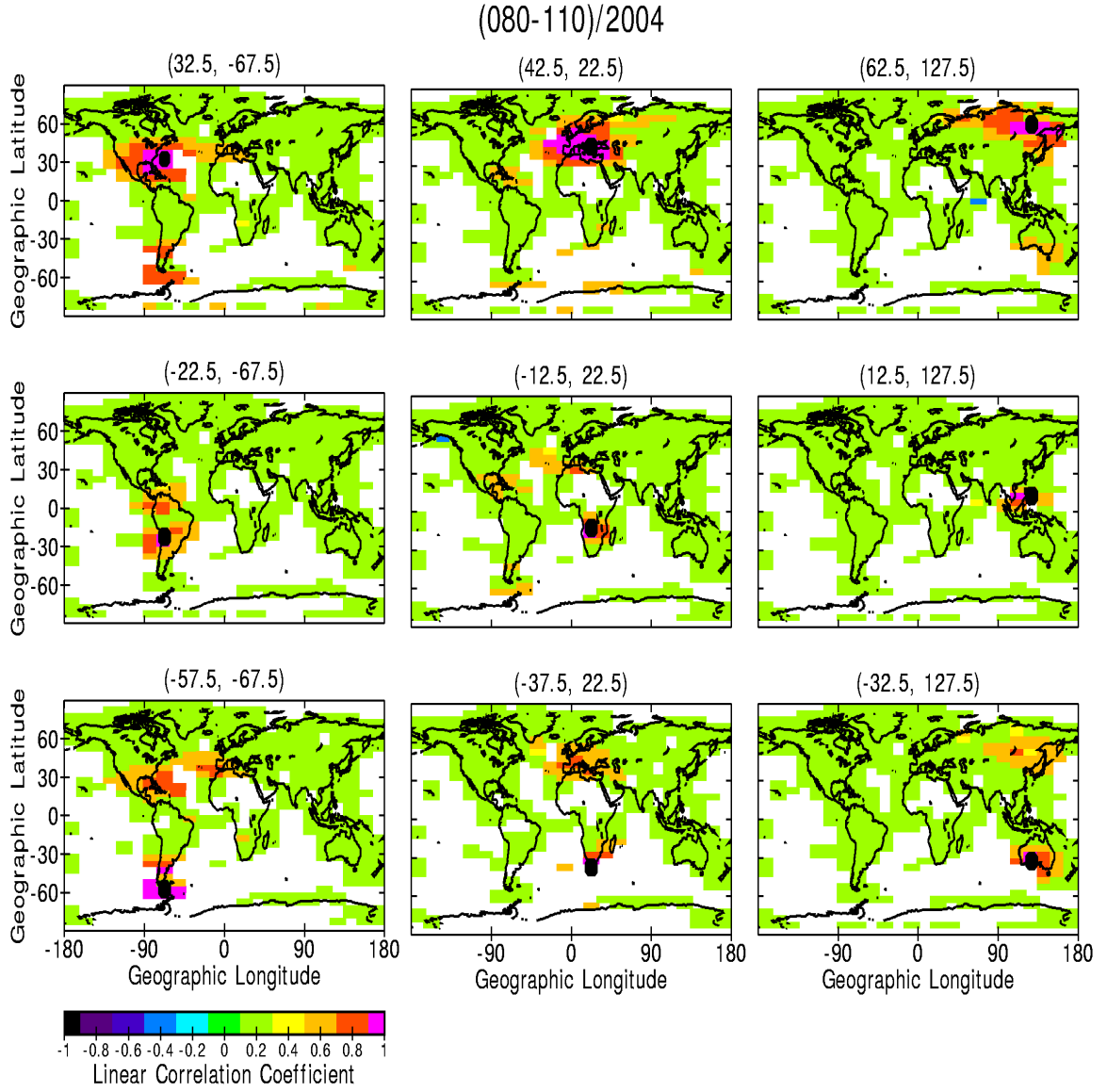
Figure 2.3. Spatial correlation coefficients of day-to-day change in TEC between a reference point (black dot) and the rest of the globe for March/April (080-110) in 2004 in a geographic coordinate system.

in $\Delta Longitude$ instead of conjugate points. For these comparisons, the x-axis again displayed ΔTEC values in 1 ΔTEC bins from -10 to $+10$ TECU. For each ΔTEC, there are corresponding ΔTEC values 30° to the East ($\Delta Longitude =30°$) and 120° to the East ($\Delta Longitude =120°$) (y-axis). The open squares show the average values

and the bars show the standard deviations.

Figure 2.4 also shows the correlation coefficients for all twelve presented and between zonally separated ($\Delta Longitude$=30°) points at middle latitudes. For larger zonal angular separations ($\Delta Longitude$=120°), the correlation coefficients are close to zero, indicating uncorrelated variations.

Figure 2.4 shows that the average relationship between the ΔTEC changes is nearly linear between the various locations, indicating that a day-to-day change in TEC at one location can be statistically related using a linear relationship to expected TEC variations at other locations, where measurements might not be available. Furthermore, the linear relationship between the ΔTEC at the different locations, in retrospect, justifies our use of the linear correlation coefficient in our analysis.

Figure 2.5 shows the zonally averaged correlation coefficients in much more detail. Shown are zonally averaged maps of the correlation coefficients as a function of magnetic latitude and longitudinal difference ($\Delta Longitude$) between reference points displayed as black dots and the locations on the globe (comparison points). Here, $\Delta Longitude$ is positive (negative) when a comparison point is east (west) of the reference point. The results are shown in the top four rows for our four 30-day-long time periods (January 2004, March/April 2004, June/July 2004, and September/October 2004) and at four different reference magnetic latitudes (−42.5°, −12.5°, 2.5°, and 47.5°). The bottom row of Figure 2.5 shows the seasonally averaged correlation coefficients obtained by combining the data from our four data periods. Note that these four data periods cover all four seasons.

Figure 2.5 shows that the correlation length (as indicated by the size of the red regions) is larger at middle latitudes (1st and 4th column) and smaller at low and equatorial latitudes (2nd and 3rd column) and generally larger in the zonal than in
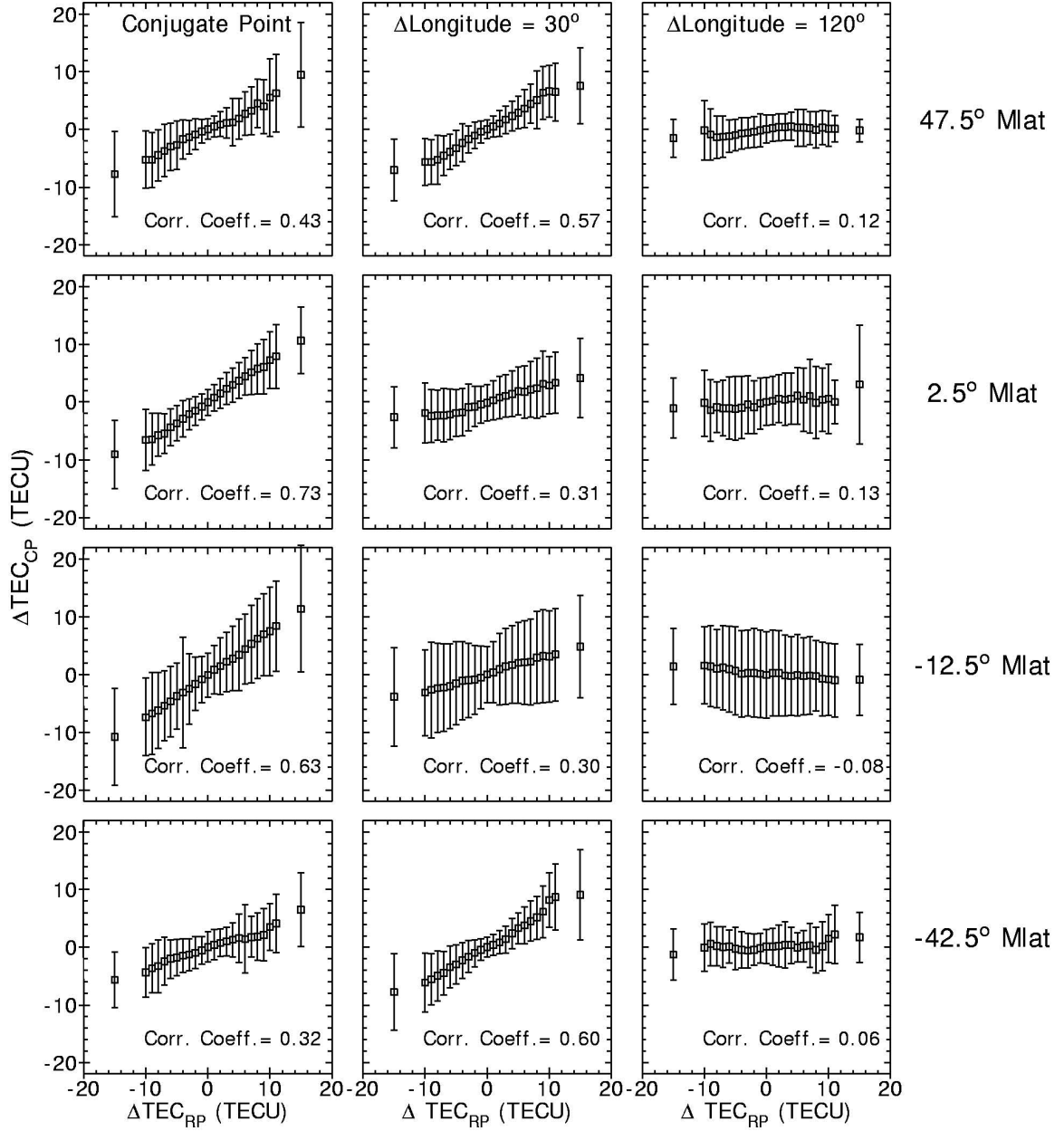
Figure 2.4. ΔTEC_{RP} versus ΔTEC_{CP} selected pairs of reference/comparison points. The x axes represent ΔTEC_{RP} at reference points located on each of the four magnetic latitudes: $47.5°$, $2.5°$, $-12.5°$, and $-42.5°$; from the top to the bottom), and y axes represent average ΔTEC_{CP} at conjugate points of the reference points (leftmost column), at points $30°$ apart (middle column), and $120°$ apart (rightmost column) from the reference points in longitude.

the meridional direction (a detailed analysis of the correlation length is given below). Furthermore, the correlation lengths, as well as the correlation values, only differ slightly between the different seasons at all latitudes.

Figure 2.5 clearly shows the correlation of the TEC variations between magnetic conjugate points. These correlations are found to be largest at low latitudes with correlation coefficients up to 0.8 and smaller values of 0.4-0.6 at middle latitudes and can be seen during all seasons, as well as in our multi-seasonal average (bottom row).

The conjugacy in the correlation coefficient can be seen even more clearly in Figure 2.6, which shows in the left panel the correlation coefficient for our multi-seasonal case as a function of the geomagnetic latitude of the reference points. Here, the x-axis represents the geomagnetic latitude of the reference point and the y-axis represents the geomagnetic latitude of the comparison points. As in Figure 2.5, the correlation coefficients correspond to zonally averaged values. The black diagonal line denotes the locations where the reference and comparison points are identical and naturally their correlation coefficient is 1.

The meridional variation of the correlation coefficient for a given magnetic latitude can be obtained from Figure 2.6a by fixing the magnetic latitude under consideration along the x-axis and reading off the corresponding values along the y-axis. Figure 2.6a shows that the correlation length exhibits a significant latitude dependence with the largest values seen in both hemispheres at middle latitudes, between about $\pm 30°$ - $\pm 60°$ magnetic latitude.

The correlation between magnetically conjugate points (black dashed line) also exhibits a strong latitudinal dependence. Here, the larger correlation lengths are also seen at middle latitudes, but the larger correlation values are observed at low latitudes
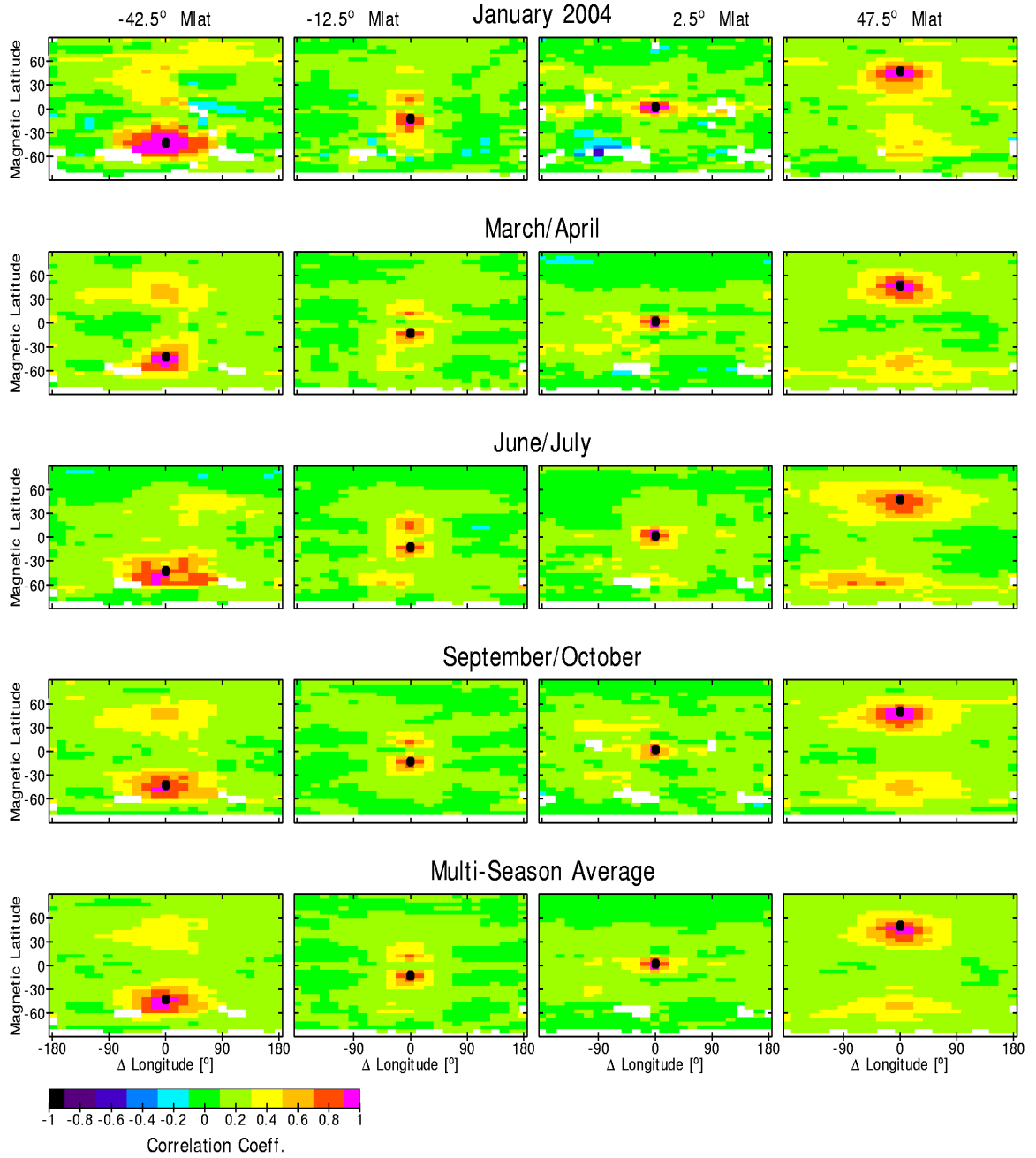
Figure 2.5. Longitudinally averaged correlation coefficients shown as functions of magnetic latitude and $\Delta Longitude$ (magnetic longitude difference between reference points (black dots) and all other points in the globe) at different magnetic latitudes $(-42.5°, -12.5°, 2.5°,$ and $47.5°)$ for four 30-day-long periods (January, March/April, June/July, and September/October in 2004), as well as multi-season average.

(below about 30° magnetic latitude). Near the magnetic equator, the correlations are confined to the local near-equatorial region. At higher latitudes (above about 65° magnetic latitude) correlations with the conjugate points are drastically reduced probably owing to the highly dynamic plasma transport processes and/or to the strongly reduced number of TEC observations at these latitudes.

Figure 2.6b (right panel) shows the variations of the spatial correlation coefficients of day-to-day change in TEC in the zonal direction as the geomagnetic latitude of the reference point varies. Here, the x-axis represents the separation in longitude ($\Delta Longitude$) between the reference points and the comparison points and the y-axis corresponds to the geomagnetic latitude of the reference points. Again, zonally averaged correlation coefficients are shown. The vertical black line (at $\Delta Longitude =0$) indicates the locations where the reference and comparison points are identical, and consequently have a correlation of 1. Figure 2.6b shows that the zonal correlation lengths are also larger at middle latitudes, between about ±30°- ±60° magnetic latitude and fall off toward the low and high latitudes. Note that the zonal correlation length drastically increases again in the northern polar cap region, but these increased correlations are most likely an artifact due to a lack of sufficient data coverage at these latitudes.

In order to more precisely determine the correlation length, we have averaged our data into two latitudinal bins corresponding to geomagnetic low ($-30°$ to $+30°$) and middle latitudes (±30° to ±60°). Figure 2.7 shows, for these two cases, the dependence of the correlation coefficient on the angular separation from a reference point in the meridional (upper panels) and in the zonal (lower panels) direction. Here, the angular separation is given as the difference in the latitude and longitude of the reference and the comparison points, respectively. In order to avoid a contamination
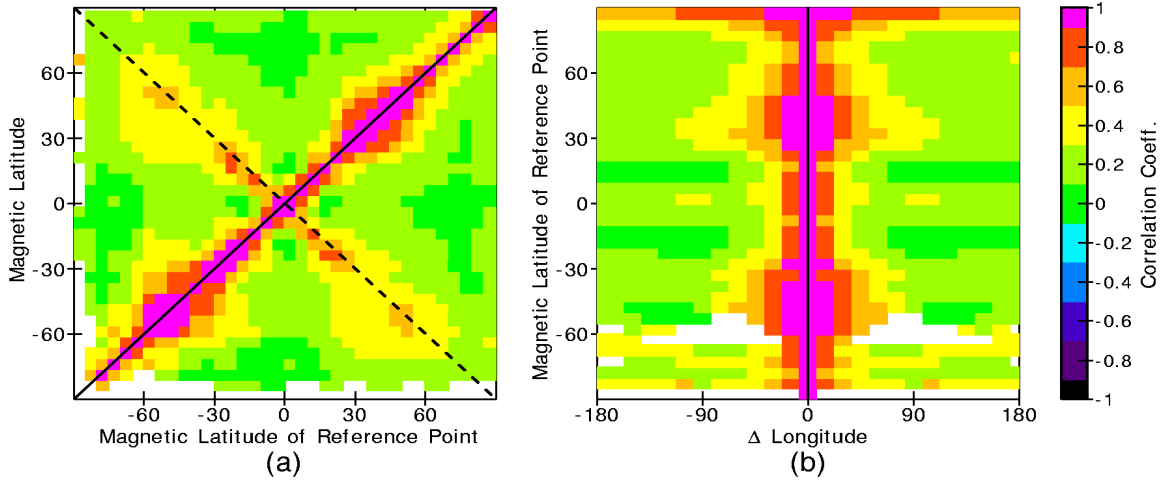
Figure 2.6. Change in the (a) meridional and (b) zonal correlation coefficients as the latitude of the reference point changes. In (a), the x-axis represents the geomagnetic latitude of the reference point and the y-axis represents geomagnetic latitude of the location that the reference is compared to. The correlation coefficient of 1 (diagonal black line) corresponds to the correlation of ΔTEC at a reference point with itself. In (b), the x-axis represents the difference in longitude ($\Delta Longitude$) between the reference point and comparison points, and y-axis is the geomagnetic latitude of the reference point. The correlation coefficient of 1 (vertical black line) corresponds to the correlation of ΔTEC at a reference point with itself.

of the correlation coefficient at low latitudes (left panels) with the strong correlations between conjugate points, only poleward $\Delta latitude$ separations were considered. For the middle-latitude case (right panels) no distinction between poleward and equatorward separations were made.

Figure 2.7 shows that the typical correlation lengths, defined as the angular separation at which the correlation coefficient drops to 0.7, is larger at middle latitudes than at low latitudes. For the multi-season case (solid lines) the meridional correlation length (top panels) is about 7° and 4° at middle and low latitudes, respectively. The zonal correlation lengths (bottom panels) are approximately 20° at middle latitudes and 11° at low latitudes. The reason for the different correlation lengths at low and middle latitude is possibly due to the different driving forces

(e.g., neutral winds at middle latitudes and zonal electric fields at low latitudes) that mainly control the plasma distribution in these two regions.

In order to investigate a possible seasonal dependence of the correlation length, Figure 2.7 also shows the correlation coefficients separated into winter, spring, summer and fall conditions. Here, for example, the winter data were obtained by combining the southern hemisphere data obtained during June solstice conditions with the northern hemisphere data obtained during December solstice conditions, and similar combinations were done for the other seasons. Figure 2.7 shows that the correlation coefficients are largely independent of the seasonal conditions and are well represented by our multi-seasonal case, with the exception of the meridional correlation coefficients at low-latitudes during summer conditions, which are slightly larger compared to the other seasons.

So far, all of our results pertained to local time averaged conditions and no distinctions between daytime and nighttime conditions were made. Figure 2.8 shows the spatial correlation coefficient maps separately for daytime (1100-1300 MLT) and nighttime (2300-0100 MLT) conditions. The maps are shown for our multi-season case and for the same four magnetic latitudes shown in Figure 2.4. The sizes of the red regions about the reference points, indicating the regions of high correlations, are significantly larger during daytime than during nighttime. Furthermore, the correlations between geomagnetic conjugate points at middle latitude essentially disappear during the night, but are evident at low latitudes. During daytime, the conjugate correlations are well established at both middle and low latitudes, with values of about 0.7 at low latitudes and 0.5 at middle latitudes. Note that the daytime correlation coefficients are larger than nighttime correlation coefficients in all cases.

In order to more precisely determine the correlation lengths for the two cases,
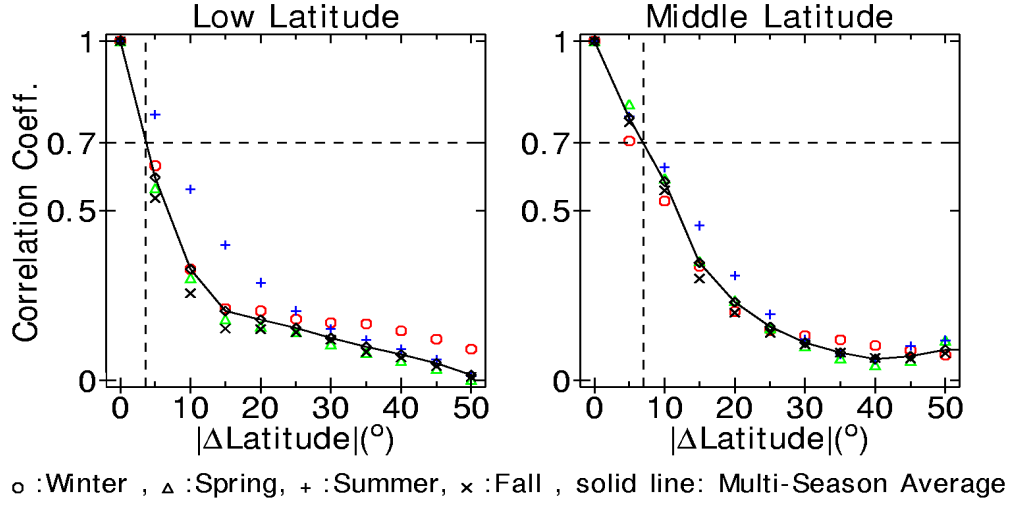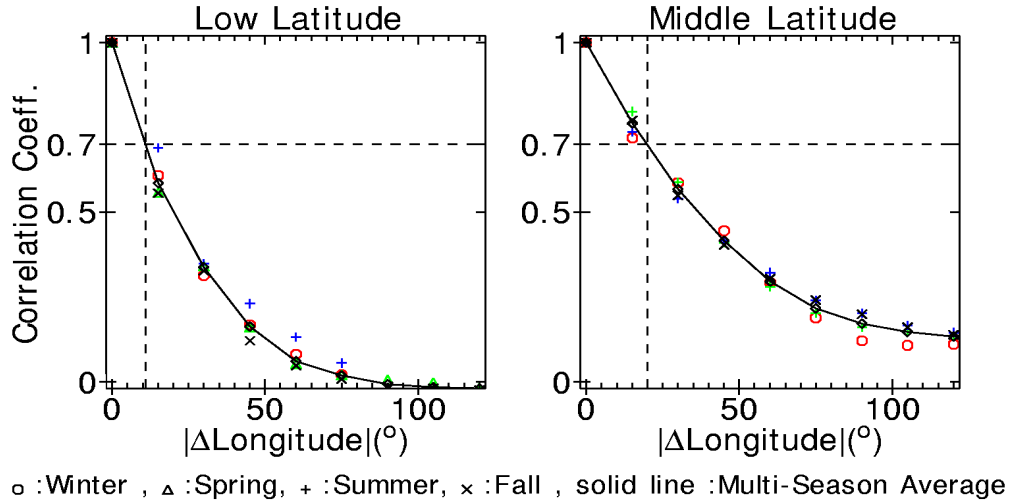
Figure 2.7. Spatial correlation coefficient versus (a) latitude separation and (b) longitude separation in degrees at low and middle latitudes for four seasons and multi-season average. Open circles, triangles, crosses, and Xs denote winter, spring, summer, and fall, respectively. The solid line corresponds to the multi-season average.

we have similar to Figure 2.7, averaged our data into two latitudinal bins corresponding to geomagnetic low and middle latitudes and then plotted the resulting correlation coefficients (Figure 2.9) as a function of the angular separation from a reference point in the meridional (upper panels) and zonal (bottom panels) direc-
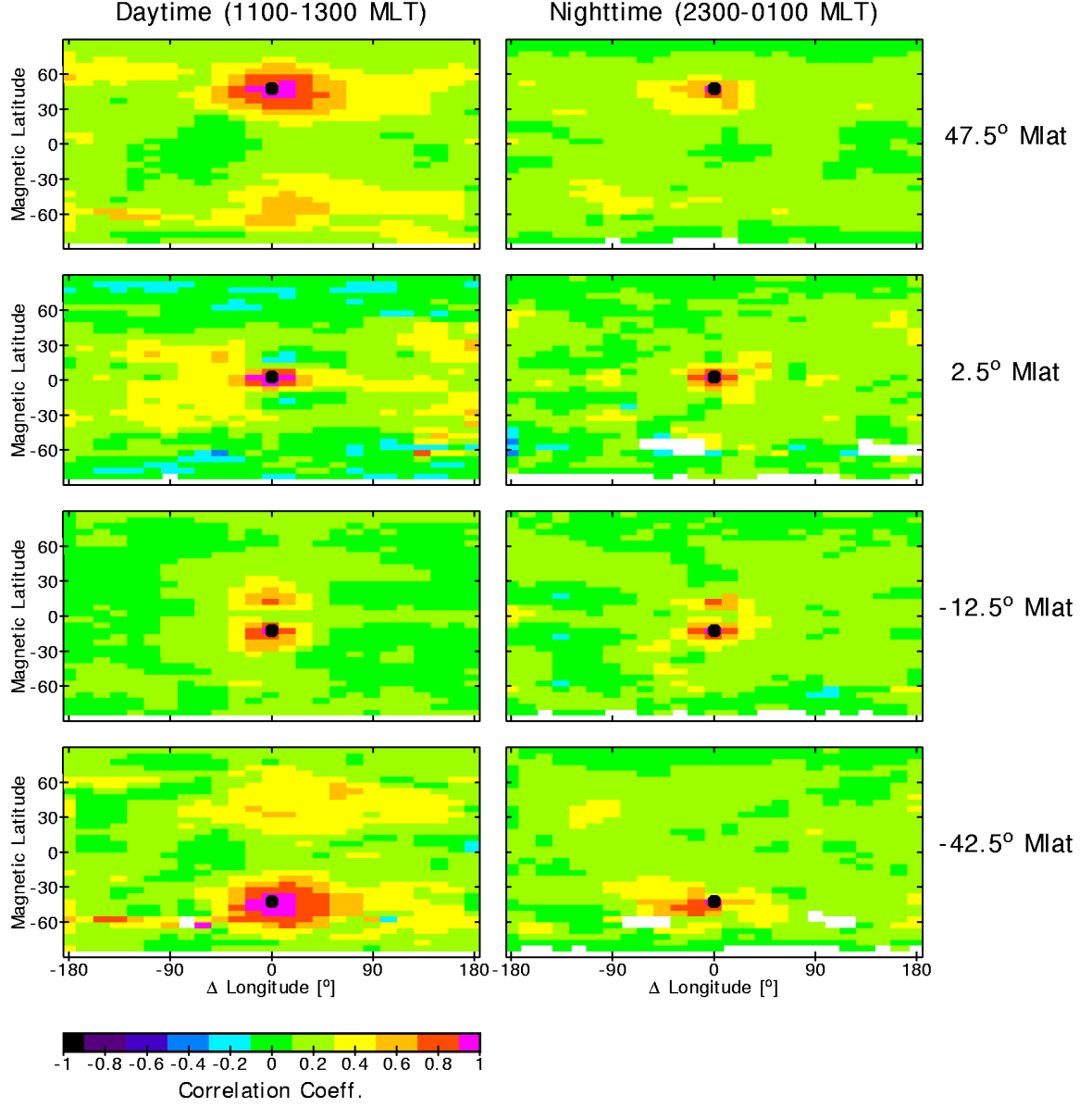
Figure 2.8. Daytime (1100-1300 MLT) and nighttime (2300-0100 MLT) longitudinally averaged correlation coefficients shown as a function of magnetic latitude (mlat) and magnetic longitudinal difference ($\Delta Longitude$) at four different magnetic latitudes ($-42.5°$, $-12.5°$, $2.5°$, and $47.5°$). Four periods are combined (January, March/April, June/July, and September/October in 2004).

tion. Each panel shows two lines corresponding to daytime (1100-1300 MLT) and nighttime (2300-0100 MLT) conditions, respectively.

During daytime, the meridional correlation lengths are about 9° and 5° at middle and low latitudes, respectively, whereas during nighttime these values are significantly reduced and of the order of $2° - 3°$ at both latitudes. The larger daytime correlation lengths compared to the nighttime agrees well with the results of *Rush* [1976], who used 18 months of f_oF_2 measurements from 32 ionosonde stations. Although their use of f_oF_2 and our use of ΔTEC are not directly comparable, these results indicate that the general trends are similar. *Huang* [1983] studied correlation coefficients using nine months of TEC observations from one pair of TEC stations. In contrast to our results, this study indicated that the nighttime correlation coefficients in TEC were larger than the corresponding daytime values. We speculate that the relatively small sampling size used in the *Huang* study might explain the discrepancy in the results.

The bottom panel of Figure 2.9 shows that the zonal correlation lengths during the day are approximately 23° at middle latitudes and 15° at low latitudes. During the night, these values are also reduced to about 11° at middle latitudes and 10° degrees at low latitudes. *Klobuchar and Johanson* [1977] found that, at middle latitudes, the daytime correlation length is about 18° (or about 2900 km) in the East-West direction and about 16° (or 1800 km) in the North-South directions. A comparison of their results with our values reveals that our values are slightly larger in the zonal direction (23° > 18°) and smaller in the meridional direction (9° < 16°). However, it needs to be noted that our correlation coefficients correspond to day-to-day changes in TEC, whereas the *Klobuchar and Johanson* values correspond to instantaneous TEC variations.
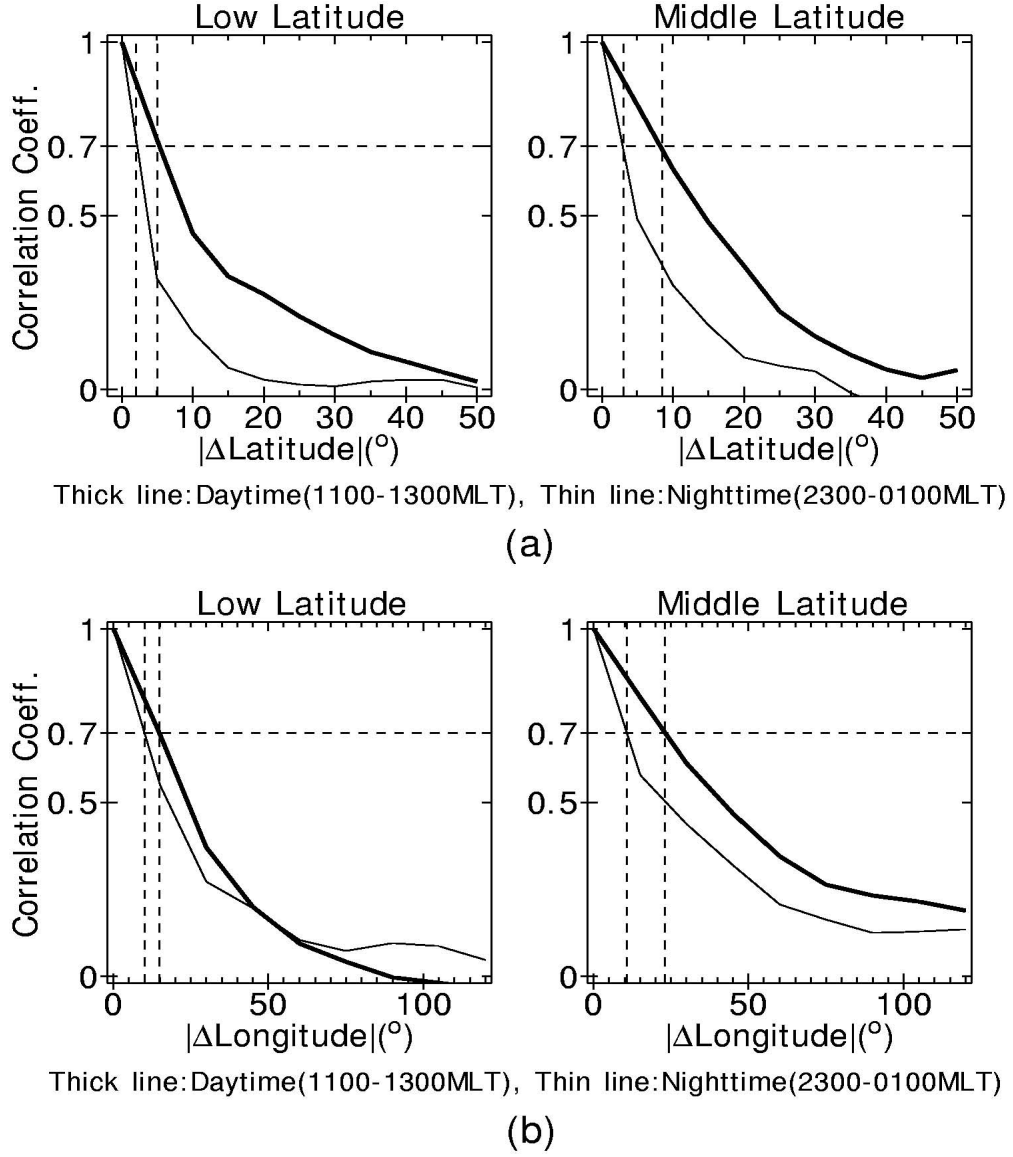
Figure 2.9. Daytime and nighttime spatial correlation coefficients as functions of (a) latitude separation and (b) longitude separation in degrees at low and middle latitudes. Four periods are combined (January, March/April, June/July, and September/October in 2004). Thick and thin lines denote daytime and nighttime, respectively.

Manoj et al. [2006] used CHAMP satellite and ground-based observations of the equatorial electrojet (EEJ) during the solar maximum conditions from 2000 to 2002 and found that the spatial correlation coefficient between the satellite and

the ground-based observations is significantly reduced for longitudinal separations of more than 15°. A 15° zonal correlation length in the EEJ was also found by *Alken and Maus* [2007] using magnetic observations from the CHAMP, Ørsted, and SAC-C satellites. Our zonal correlation length of 15° at low latitudes during daytime is in excellent agreement with the results of these studies and suggests that during daytime the TEC variability at low latitudes is also mainly driven by variations in the equatorial electric fields.

2.4   Summary and Discussion

We have used more than 150 million TEC observations from more than 1000 globally distributed GPS ground receivers to study the local and spatial morphology of day-to-day ionospheric variability. Our study included four 30-day-long periods in 2004 covering the different seasonal conditions.

In order to investigate day-to-day TEC variability, we have calculated the changes in TEC from one day to the next by differencing the individual GPS/TEC observations obtained at the same location on consecutive days using all available GPS ground stations. The resulting TEC changes (ΔTEC) were statistically analyzed and the global day-to-day TEC variability, as well as its spatial correlation, were determined. Two statistical parameters, e.g., the local standard deviation and the spatial correlation coefficient, were used to describe the global day-to-day TEC variability. The standard deviation was used to describe the local variability in TEC and the spatial correlation coefficients were used to measure statistical correlations between TEC changes at different locations on the globe.

Our results indicate that the local TEC variability, as indicated by the standard deviation, is largest around the locations of the equatorial anomaly with maximum values occurring in the afternoon sector between about 1500-1700 MLT. During

equinox, the variability is found to be nearly symmetric about the magnetic equator, but the variability exhibits asymmetries during the solstices at both low and middle latitudes. During the solstices, the daytime TEC variations at middle latitudes are found to be larger in the summer hemisphere than in the winter hemisphere in contrast to the well-known seasonal anomaly in the ionospheric F region peak densities (c.f., *Schunk and Nagy*, 2000). The well-known annual anomaly, on the other hand, with reduced peak densities during June solstice conditions, is also observed in the TEC variability with a reduction of about 50% in the standard deviation from December to June solstice.

Our study of the spatial correlation indicates that typical correlation lengths, defined as the angular separation at which the correlation coefficient drops to 0.7, are largest at middle latitudes and smaller at low and high latitudes. The correlation lengths are found to be largely independent of season. The seasonally and local time-averaged meridional correlation lengths are about 7° and 4° at middle and low latitudes, respectively. The zonal correlation lengths are about 20° at middle latitudes and 11° at low latitudes.

The daytime zonal and meridional correlation lengths are both found to be larger than their corresponding nighttime values. The daytime meridional correlation lengths are approximately 9° and 5° at middle and low latitudes, and the nighttime values are about 3° and 2° at middle and low latitudes, respectively. The zonal correlation lengths are 23° at middle latitudes and 15° at low latitudes during the day, and are 11° at middle latitudes and 10° at low latitudes during the night.

One of the interesting results of our study is the observation of correlations between geomagnetic conjugate points. These correlations are strongest at low latitudes with correlation coefficients of about 0.8 ($r \approx 0.8$) during both daytime and

nighttime. At middle latitudes, the conjugate correlation coefficients are smaller with values of about $0.4 - 0.6$ (r = $0.4 - 0.6$) during daytime and are not observed during the night.

There are several factors that could potentially lead to correlated responses at conjugate points (c.f., *Schunk and Nagy*, 2000). During daytime, day-to-day changes in the solar illumination leads to a correlated response, but these correlations would be observed over the entire illuminated disk and would not be constrained to the conjugate points. Neutral meridional winds, on the other hand, could potentially cause correlated (or anti-correlated) responses at conjugate points. For example, interhemispheric transport, driven by neutral winds would lead to a flow of ionization along magnetic field line from one hemisphere to its conjugate point in the other hemisphere. Furthermore, equatorward traveling waves (e.g., TIDs), that are simultaneously generated in the two hemispheres, could lead to a correlated response at conjugate points and some of our observed correlations might be due to these structures.

The most promising candidate to explain the observed conjugate correlations, however, are electric fields. Electric fields can be locally generated through neutral wind dynamo action in one hemisphere and then map along magnetic field lines to the conjugate point located in the opposite hemisphere. The resulting transport of the ionization due to the presence of these electric fields in the two hemispheres would lead to a correlated response in TEC at the two conjugate points. The mapping of electric fields along geomagnetic field lines has, for example, recently been reported by *Otsuka et al.* [2004] using simultaneous observations of medium-scale traveling ionospheric disturbances (MSTIDs) at geomagnetic conjugate points, and by *Foster and Rideout* [2007], who investigated conjugate SED structures using a combination of ground-

based GPS and Jason/TOPEX TEC data in the two hemispheres. Assuming that the correlations between conjugate points are associated with the forcing by electric fields that map along the magnetic field lines, the observed correlation coefficient between conjugate points of r = 0.5 during the day at middle latitudes indicates that about 25% of the observed TEC variability can be explained by variations in the electric field forcing. The significantly larger correlation coefficient of 0.8 between conjugate points at low latitudes indicates that more than 50% of the observed variability is related to changes in the electric field forcing. It is interesting to note that at middle latitudes the conjugate correlations are only observed during daytime, indicating that during the night the electric field variations are either small or washed out by other local processes.

It is also interesting to note that the TEC changes over most parts of the illuminated disk are largely uncorrelated, indicating that day-to-day changes in the solar illumination only add a statistically insignificant contribution to the day-to-day changes in TEC. This statistical analysis, of course, does not imply that on any given day (for example during solar flares) changes in the solar illumination could not have important effects on TEC.

Although our study has revealed many of the scale sizes of day-to-day TEC variability, questions about the physical mechanisms that are responsible for the observed variations remain. For example, it remains unclear how much of the observed variability is due to inherent variations in the ionosphere-thermosphere system, and how much can be attributed to effects due to magnetospheric and mesospheric processes. Clearly, further studies are needed. Furthermore, information about the spatial and temporal correlation of day-to-day variations of other ionospheric parameters (e.g., N_mF_2, h_mF_2, and topside scale height) on a global scale is limited. In

addition, our study was based on TEC observations obtained during medium solar flux conditions. The dependence of the spatial correlation coefficients on the phase of the solar cycle needs to be addressed in future studies.

An improved understanding and specification of these correlations is not only important for a better understanding of the physical mechanisms that cause ionospheric weather variability, but is also a crucial component of modern-day data assimilation systems that provide improved ionospheric specifications and forecasts.

References

Alken, P., and S. Maus (2007), Spatio-temporal characterization of the equatorial electrojet from CHAMP, Ørsted, and SAC-C satellite magnetic measurements, *J. Geophys. Res., 112*, A09305, doi:10.1029/2007JA012524.

Angell, J., T. R. Robinson and S. P. Lawrence (2006), TOPEX observations of the ionospheric electron content coherence distance: Applications to altimetric correction modeling. (Available at http://ion.le.ac.uk/remote_sensing/TEC_correl.html, accessed May 2006)

Codrescu, M. V., S. E. Palo, X. Zhang, T. J. Fuller-Rowell, and C. Poppe (1999), TEC climatology derived from TOPEX/POSEIDON measurements, *J. Atmos. Sol. Terr. Phys., 61*, 281-298.

Codrescu, M. V., K. L. Beierle, T. J. Fuller-Rowell, S. E. Palo, and X. Zhang (2001), More total electron content climatology from TOPEX/Poseidon measurements, *Radio Sci., 36*, 325-333.

Daley, R. (1991), *Atmospheric Data Analysis*, Cambridge Atmospheric and Space Science Series, Cambridge Univ. Press, New York.

Foster, J. C., and W. Rideout (2005), Midlatitude TEC enhancements during the October 2003 superstorm, *Geophys. Res. Lett., 32*, L12S04, doi:10.1029/2004GL021719.

Foster, J. C., and W. Rideout (2007), Storm enhanced density: Magnetic conjugacy effects, *Ann. Geophys., 25*(8), 1791-1799.

Foster, J. C., et al. (2005), Multiradar observations of the polar tongue of ionization, *J. Geophys. Res., 110*, A09S31, doi:10.1029/2004JA010928.

Gail, W. B., A. B. Prag, D. S. Coco, and C. Coker (1993), A statistical characterization of local mid-latitude total electron content, *J. Geophys. Res., 98*, 15717-15727.

Ho, C. M., A. J. Mannucci, L. Sparks, X. Pi, U. J. Lindqwister, B. D. Wilson, B. A. Iijima, and M. J. Reyes (1998), Ionospheric total electron content perturbations monitored by the GPS global network during two northern hemisphere winter storms, *J. Geophys. Res., 103* (A11), 26,409-26,420.

Huang, T. X. (1983), Average horizontal gradients and spatial correlations of mid-latitude total electron content at solar minimum, in Proceedings of the International Symposium on Beacon Satellite Studies of the Earth's Environment, pp. 403-408, Radio Science Division, National Physical Laboratory, New Delhi.

Huang, Y. N. (1984), Spatial Correlation of the Ionospheric Total Electron Content at the Equatorial Anomaly Crest, *J. Geophys. Res., 89* (A11), 9823-9827.

Immel, T. J., E. Sagawa, S. L. England, S. B. Henderson, M. E. Hagan, S. B. Mende, H. U. Frey, C. M. Swenson, and L. J. Paxton (2006), Control of equatorial ionospheric morphology by atmospheric tides, *Geophys. Res. Lett., 33*, L15108, doi:10.1029/2006GL026161.

Jee, G., R. W. Schunk, and L. Scherliess (2004) Analysis of TEC data from the TOPEX/Poseidon mission, *J. Geophys. Res.*, 109, A01301, doi:10.1029/2003JA010058.

Kane, R. P. (1975), Day-to-Day Variability of Ionospheric Electron Content at Mid-Latitudes, *J. Geophys. Res., 80*(22), 3091-3099.

Klobuchar, J. A., and J. M. Johanson (1977), Correlation Distance of Mean Daytime Electron Content, *Rep., AFGL-TR-77-0185*, Air Force Geophys. Lab. Bedford, Mass.

Mannucci, A. J., B. D. Wilson, and C. D. Edwards (1993), A New Method for Monitoring the Earth's Ionospheric Total Electron Content Using the GPS Global Network, in *Proceedings of ION GPS-93, the 6th International Technical Meeting of the Satellite Division of The Institute of Navigation, Salt Lake City, UT, 22-24 September*, pp. 1323-1332, The Institute of Navigation, Alexandria, Va.

Manoj, C., H. Lühr, S. Maus, and N. Nagarajan (2006), Evidence for short spatial correlation lengths of the noontime equatorial electrojet inferred from a comparison of satellite and ground magnetic data, *J. Geophys. Res.*, 111, A11312, doi:10.1029/2006JA011855.

Maybeck, P. S. (1994), *Stochastic models, estimation, and control*, vol.1, Navtech Press, Arlington, Va.

Mendillo, M. (2006), Storm in the ionosphere: Patterns and processes for total electron content, *Rev. Geophys., 44*, RG4001, doi:10.1029/2005RG000193.

Otsuka, Y., K. Shiokawa, and T. Ogawa (2004), Geomagnetic conjugate observations of medium-scale traveling ionospheric disturbances at midlatitude using all-sky airglow imagers, *Geophys. Res. Lett., 31*, L15803, doi:10.1029/2004GL020262.

Richmond, A. D. (1995), Ionospheric electrodynamics using magnetic apex coordinates, *J. Geomagn. Geoelectr., 47*, 191-212.

Rishbeth, H., I. C. F. Muller-Wodarg, L. Zou, T. J. Fuller-Rowell, G. H. Millward, R. J. Moffett, D. W. Idenden, and A. D. Aylward (2000), Annual and semiannual variations in the ionospheric F_2-layer: 2. Physical discussion, *Ann. Geophys., 18*, 945-956.

Rush, C. M. (1976), An ionospheric observation network for use in short-term propagation predictions, *Telecommun. J., 43*(8), 544-549.

Saito, A., S. Fukao, and S. Miyazaki (1998), High resolution mapping of TEC perturbations with the GSI GPS network over Japan, Geophys. *Res. Lett., 25(16)*, 3079-3082.

Scherliess, L., R. W. Schunk, J. J. Sojka, D. C. Thompson, and L. Zhu (2006), Utah State University global assimilation of ionospheric measurements Gauss-Markov Kalman filter model of the ionosphere: Model description and validation, *J. Geophys. Res., 111*, A11315, doi:10.1029/2006JA011712.

Scherliess, L. D. C. Thompson, and R. W. Schunk (2008), Longitudinal variability of low-latitude total electron content: Tidal influences, *J. Geophys. Res., 113*, doi:10.1029/2007JA012480.

Schunk, R. W., and A. F. Nagy (2000), *Ionospheres*, Cambridge University Press, New York.

Soicher, H. (1978), Spatial correlation of transionospheric signal time delays, *IEEE Trans. Antennas Propag., AP-26*, 311-314.

Tsugawa, T., A. Saito, Y. Otsuka (2004), A statistical study of large-scale traveling ionospheric disturbances using the GPS network in Japan, *J. Geophys. Res., 109*, A06302, doi:10.1029/2003JA010302.

Tsugawa, T., K. Shiokawa, Y. Otsuka, T. Ogawa, A. Saito, and M. Nishioka (2006), Geomagnetic conjugate observations of large-scale traveling ionospheric disturbances using GPS networks in Japan and Australia, *J. Geophys. Res., 111*, A02302, doi:10.1029/2005JA011300.

Vladimer, J. A., P. Jastrzebski, M. C. Lee, P. H. Doherty, D. T. Decker, and D. N. Anderson (1999), Longitude structure of ionosphere total electron content at low latitudes measured by the TOPEX/Poseidon satellite, *Radio Sci.*, 34, 1239-1260.

Wilson, B. D., and A. J. Mannucci (1993), Instrumental biases in ionospheric measurements derived from GPS data, presented at the ION-GPS Symposium, Salt Lake City, Utah, September.

CHAPTER 3

NEUTRAL WIND AND PLASMA DRIFT EFFECTS ON LOW- AND MIDDLE-LATITUDE TEC [1]

Abstract

A physics-based numerical Ionosphere/Plasmasphere Model (IPM) was used to study the effects of daytime neutral wind and electric field perturbations on the subsequent evolution of the afternoon and post-sunset TEC during vernal equinox conditions. The model solves the transport equations for the six ions, O^+, NO^+, O_2^+, N_2^+, H^+ and He^+, on convecting flux tubes that realistically follow the geomagnetic field. The IPM covers geomagnetic latitudes from about 60°N to 60°S and equatorial crossing altitudes from 90 to 30,000 km. Two of the input parameters required by the IPM are the thermospheric neutral wind and the low-latitude electric field, which can be provided by existing empirical models or externally specified. To study the relative importance of the neutral wind and the electric field for the TEC variations, these two model inputs were externally modified and the resulting TEC variations were compared. Neutral wind and electric field modifications were introduced at three different local times in order to investigate the effect of different start times of the imposed perturbations on TEC. Three longitude sectors (78°, 273° and 318° E) were considered and the results correspond to medium solar activity (F10.7 = 150) and low geomagnetic activity (Kp = 2) conditions. The largest TEC changes were found predominantly in the equatorial anomaly, and a significant longitudinal dependence was observed. The simulation results indicate that TEC variations at 2100 LT vary non-linearly with the elapsed time after the imposed neutral wind and electric field perturbations. An important outcome of this study is that daytime neutral wind

---

and/or electric field modifications can lead to essentially identical TEC changes in the 2100 local time sector.

3.1 Introduction

In the ionosphere, the plasma density distribution depends not only on production and loss processes but also on transport processes associated with electric fields and neutral winds [*Schunk and Nagy, 2000*]. The electric field plays an important role on the morphology of the low-latitude ionosphere and is responsible for the equatorial ionization anomaly. Meridional neutral winds also play an important role in controlling the peak height and density of the F layer and are largely responsible for maintaining the nighttime ionosphere at middle latitudes [*Rishbeth*, 1972, 1974]. During the day, the generally poleward winds at middle latitudes drive plasma down along magnetic field lines into regions of greater neutral density, where it will more rapidly be lost via recombination. At night the opposite holds true.

Integrated measurements, such as Total Electron Content (TEC) and airglow emissions, obtained both from ground and space have become widely available over the past decade and have been used extensively to study the general morphology and variability of the ionosphere [*Codrescu et al.*, 1999, 2001; *Jee et al.*, 2004; *Immel et al.*, 2006; *Scherliess et al.*, 2008]. These measurements have also helped to understand the effect of electric fields and neutral winds on the low- and middle-latitude ionosphere [*Kil et al.*, 2006; *Scherliess et al.*, 2008]. *Su et al.* [1994], for example, used ground-based TEC observations in the low-latitude region to study the seasonal and solar activity variations of nighttime TEC enhancements and their latitude and longitude dependence in the northern equatorial anomaly region. Their study suggested that post midnight TEC enhancements observed on the poleward shoulder of the equatorial anomaly result from not only the evening $\mathbf{E} \times \mathbf{B}$ drifts, but also

from the effects of neutral winds on the plasma distribution. The morphology of the plasma distribution at low and mid latitudes in the Australian region was studied by *Horvath and Essex* [2000] using GPS and TOPEX TEC data during a period of low solar activity. Their results suggested that downward $\mathbf{E} \times \mathbf{B}$ drifts after sunset together with the downward plasma flow along the magnetic field lines from greater heights can produce the TEC enhancements observed around midnight in the middle-latitude regions. These studies, however, have been limited by uncertainties in the knowledge of the neutral wind and plasma drift velocities.

Model calculations, on the other hand, have been used to obtain a better understanding of the relative importance of the $\mathbf{E} \times \mathbf{B}$ drift and neutral winds on the plasma distribution. *Balan et al.* [1997] used SUPIM (Sheffield University Plasmasphere-Ionosphere model) under magnetically quiet equinoctial conditions at high solar activity to study the temporal evolution of the equatorial plasma fountain and equatorial anomaly. They found that the neutral wind, which causes large hemispheric asymmetries in the plasma fountain during both daytime and nighttime, becomes less effective during the time of the evening prereversal enhancement of the upward drift. *Jee et al.* [2005] used a one-dimensional middle-latitude ionosphere model to study the sensitivity of quiet-time TEC to the atmospheric and ionospheric parameters including the neutral wind. Their study showed that during both, day and night, the magnetic meridional component of the neutral wind significantly affects TEC, and that the geographic zonal wind can cause noticeable longitudinal variations in TEC due to the longitudinal variation of the declination angle. *England et al.* [2008] used SAMI2 (Sami2 is Another Model of the Ionosphere) [*Huba et al.*, 2000] to demonstrate that the recently observed zonal variations in the E-region dynamo electric fields are sufficient to explain the observed variation in brightness and

latitude of the airglow bands. They calculated the contribution made to the overall change in the simulated 135.6 nm airglow brightness by changes in the E-region dynamo electric fields during different periods of the day. Their results indicated that changes at all local time periods make a significant contribution to the total change in the airglow at 2100 LT, with the most significant being close to local noon and during the late afternoon. *Su et al.* [1995] used TEC observations and model results from SUPIM to study the longitudinal differences in TEC in the northern equatorial anomaly region during summer. They suggested that the daytime longitudinal differences in TEC are caused mainly by the differences in neutral wind velocities while the nighttime differences are due to a combination of the differences in both the neutral wind and $\mathbf{E} \times \mathbf{B}$ drift velocities. However, more recently, *McDonald et al.* [2008] found that winds, as well as solar conditions, play an important role in determining the effect that the daytime and prereversal enhancement drifts have on the evening densities and anomaly crest separations. They investigated the relative contributions of the daytime and evening vertical $\mathbf{E} \times \mathbf{B}$ drifts to the nighttime plasma distributions in the low-latitude F-region ionosphere under both solar minimum and maximum conditions on an equinox day with low geomagnetic activity at $122°$ E longitude using SAMI2. Their results suggested that the prereversal enhancement and neutral winds, in addition to the daytime upward plasma drifts, might play an important role in sustaining the recently found wave number four pattern [*Immel et al.*, 2006; *Scherliess et al.*, 2008] in the nighttime ionosphere.

However, the relative contribution of the daytime neutral wind and vertical drift to the nighttime TEC variability is still not fully understood. In this study, we have systematically studied the relative effects of the meridional wind and vertical drift on the afternoon and post-sunset TEC for spring equinox (DOY 080) using a

physics-based numerical Ionosphere/Plasmasphere Model (IPM). In order to investigate the wind and vertical drift effects on TEC, three kinds of wind perturbations (poleward, equatorward and northward) and two kinds of vertical drift perturbations (upward and downward) were externally supplied to the IPM at three different local times (five different perturbations × three different perturbation starting times). In the following, we will first describe briefly the physics-based IPM model followed by a more detailed description of the applied wind and drift perturbations.

3.2   Ionosphere/Plasmasphere Model and Model Inputs

We have used a physics-based numerical Ionosphere/Plasmasphere Model (IPM) to study the effects of neutral winds and electric fields on the afternoon and post-sunset TEC variability. In the following, we briefly describe the IPM and the modifications that we have applied to the neutral wind and the low-latitude drifts.

3.2.1   Ionosphere/Plasmasphere Model

The IPM [*Schunk et al.* 2004; *Scherliess et al.*, 2004] solves the transport equations for the six ions, O^+, NO^+, O_2^+, N_2^+, H^+ and He^+, on convecting flux tubes that realistically follow the geomagnetic field. The IPM covers geomagnetic latitudes from about 60°N to 60°S corresponding to equatorial crossing altitudes from about 90 to 30,000 km. The equations are solved along magnetic field lines for individual convecting plasma flux tubes of plasma, and the 3-D nature of the model is obtained by following a large number of plasma flux tubes. The IPM uses the International Geomagnetic Reference Field (IGRF), which properly accounts for displacement between the geomagnetic and geographic equators and the bending of the B- field lines with latitude. These features are important at low and middle latitudes where the declination angle can play an important role on the plasma distribution and TEC

[*Jee et al.*, 2004] The inclusion of He^+ as a major ion is also important because, at Arecibo, it is frequently observed to be a dominant ion in a distinct altitude range [*Gonzales and Sulzer*, 1996].

For the present study, the three-dimensional plasma distribution at low and middle latitudes was calculated by diurnally running the IPM over a three-day time period for a given geophysical condition. The first two days of each model run were used to remove effects associated with the initial condition and the plasma densities from the third day were used for our study. The model TEC was then obtained by integrating the model plasma densities from the bottom boundary (~ 100 km) up to an altitude of 1350 km. Even though the IPM also provides values for the plasmaspheric TEC, an upper boundary of 1350 km was chosen in our TEC calculations in order to be able to compare our results with direct TEC observations from the TOPEX and Jason-1 satellites. These satellite data have been used extensively in previous studies [e.g., *Codrescu et al.*, 1999, 2001; *Jee et al.*, 2004; *Scherliess et al.*, 2008] to investigate the general morphology and variability of low- and middle-latitude TEC.

3.2.2   Ionosphere/Plasmasphere Model Inputs

The IPM as a stand-alone Ionosphere-Plasmasphere model requires several inputs that pertain to thermospheric and electrodynamic parameters. Two of the main inputs to the model are the thermospheric neutral winds and the low-latitude plasma drifts. In its default mode, the model uses empirical representations for these parameters given by the Horizontal Wind Model 93 (HWM93) [*Hedin et al.*, 1991] and the Scherliess and Fejer equatorial vertical plasma drift model [*Scherliess and Fejer*, 1999]. However, these two parameters can also be externally specified, which allows for a systematic study of their effects on the resulting electron density distribution and TEC. In the current study, we have systematically varied the thermospheric

neutral winds and the low-latitude electric field by changing one parameter at a time while keeping the others at their default values. In the following sections, default values for the wind and plasma drifts, and the applied variations from these values are described.

3.2.2.1 Neutral Winds

In the upper F region, transport processes due to wind-induced drifts along **B** field lines become important, especially in the middle-latitude ionosphere. In order to investigate meridional wind effects on TEC variations, poleward, equatorward and northward wind perturbations were systematically added to the default values of the geographic meridional wind obtained from the horizontal wind model (HWM93). Theses perturbations were only applied on the third day of the three-day IPM runs. The construction of the perturbation winds was guided by the latitude variation observed in the HWM winds. Figure 3.1 shows the HWM meridional wind (positive for northward) at three different longitude sectors from 1200LT through 2100LT as a function of geographic latitude. To first order the HWM winds vary linearly with latitude below about ±45°latitude. Consequently, we also adopted for the poleward and equatorward wind perturbations that they vary linearly with geographic latitude as shown in Figure 3.2a. For example, for the poleward perturbation we applied a 100 m/s (northward) wind at 45° geographic latitude and a −100 m/s (southward) wind at −45° geographic latitude. These wind perturbations in both hemispheres were linearly decreased to zero at the geographic equator. Similarly, for the equatorward perturbation, a −100 m/s wind at 45° geographic latitude and a 100 m/s wind at −45° geographic latitude were applied. The linear decrease of the equatorward perturbations with latitude was taken to be the same as for the poleward perturbation. The northward wind perturbations were held at a constant value of 100 m/s
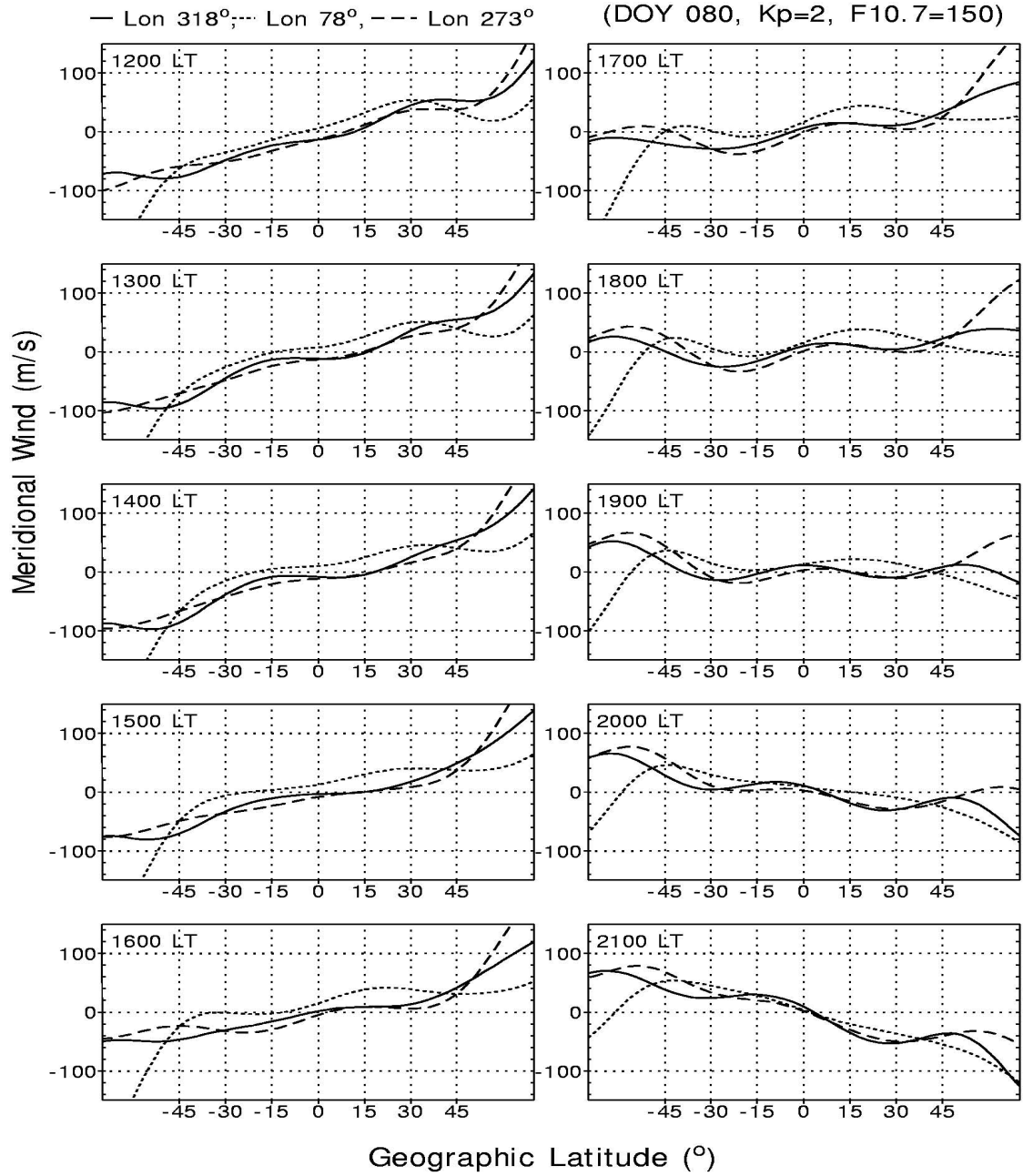
Figure 3.1. HWM meridional winds as a function of geographic latitude at three longitude sectors (78°, 273°, and 318°E) from 1200LT through 2100LT for medium solar activity (F10.7 = 150) and quiet geomagnetic (Kp =2) conditions at an altitude of 350 km on an equinox day (DOY 80).
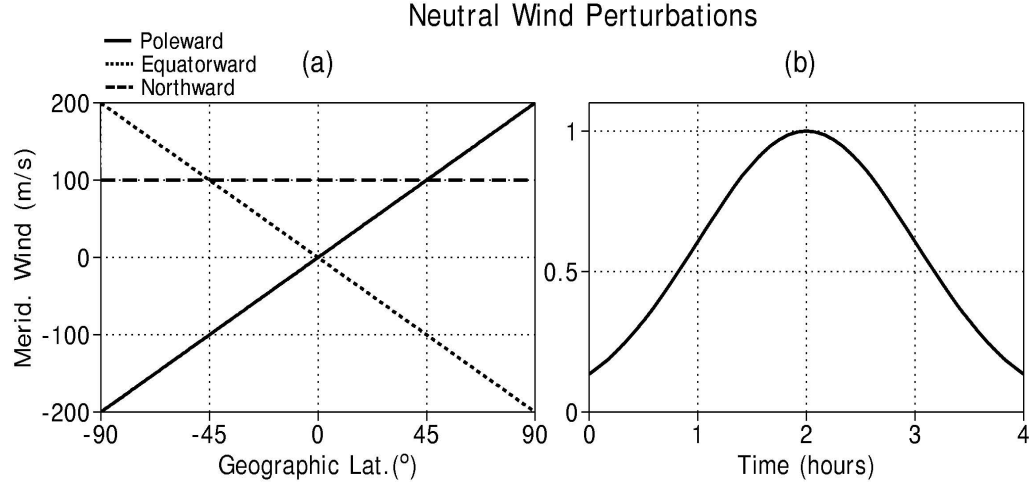
Figure 3.2. (a) Neutral wind perturbations superimposed to the default geographic meridional wind obtained from the horizontal wind model (HWM93). Solid, dotted, and dashed lines represent poleward, equatorward, and northward wind perturbations, respectively. (b) Neutral wind perturbations with a Gaussian shape as a function of time. The perturbations last for 4 hours and the local time, at which the perturbation reaches the maximum value, will be called a time when the perturbation starts or is added.

at all latitudes. The perturbation winds were then separately superposed on the background HWM wind values for individual test cases.

The wind perturbations mentioned above were introduced in a Gaussian shape as a function of local time. As shown in Figure 3.2b, the perturbations last for 4 hours and reach their maximum value after 2 hours at 1500 LT. However, in order to investigate the effect of different start times of the imposed perturbations on TEC, three local times (1200, 1500, and 1800 LT) were considered. The local time at which the wind perturbation reaches the maximum value will be used to identify the perturbation, even though the perturbation starts 2 hours earlier. For example, Case P12, E15, and N18 represent the addition of the poleward wind at 1200 LT, equatorward wind at 1500 LT and northward wind 1800 LT, respectively. For each case, three longitude sectors, 78°, 273°, and 318° were selected in order to investigate

the longitudinal dependence of TEC changes.

3.2.2.2 Vertical Drift

At low latitudes, within $\pm 20°$ dip latitude, the $\mathbf{E} \times \mathbf{B}$ vertical drift is the primary cause of the redistribution of the ionospheric plasma density. In order to investigate the $\mathbf{E} \times \mathbf{B}$ vertical drift effects on TEC, variations in the vertical drift were introduced by adding downward and upward drifts to the default drift values obtained from the Scherliess and Fejer equatorial vertical drift model. As before, these perturbations were only applied on the third day of the three-day IPM runs. The same time-dependent Gaussian-shaped vertical drift variations were applied as used for the neutral wind perturbations. The variations start at three different local times (1000, 1300, and 1600 LT), reach their peak value of 22 m/s 2 hours later, and then decrease back to zero during the next 2 hours. Figure 3.3 shows two examples of the vertical drifts at $273°$ of longitude as a function of local time. The downward vertical drift perturbations (dotted lines) started at 1300 LT and 1600 LT and reached their maximums (22 m/s) at 1500 LT and 1800 LT, respectively. In Figure 3.3, the solid lines represent the default vertical drift velocities given by the Scherliess and Fejer model, while the dotted lines denote the vertical drift perturbations and the dashed lines denote the applied vertical drift obtained from the superposition of the background and perturbation drifts. In a manner similar to the wind modification cases, Case U15 and D18 denote an additional vertical drift in the upward direction at 1500 LT and in the downward direction at 1800 LT, respectively.
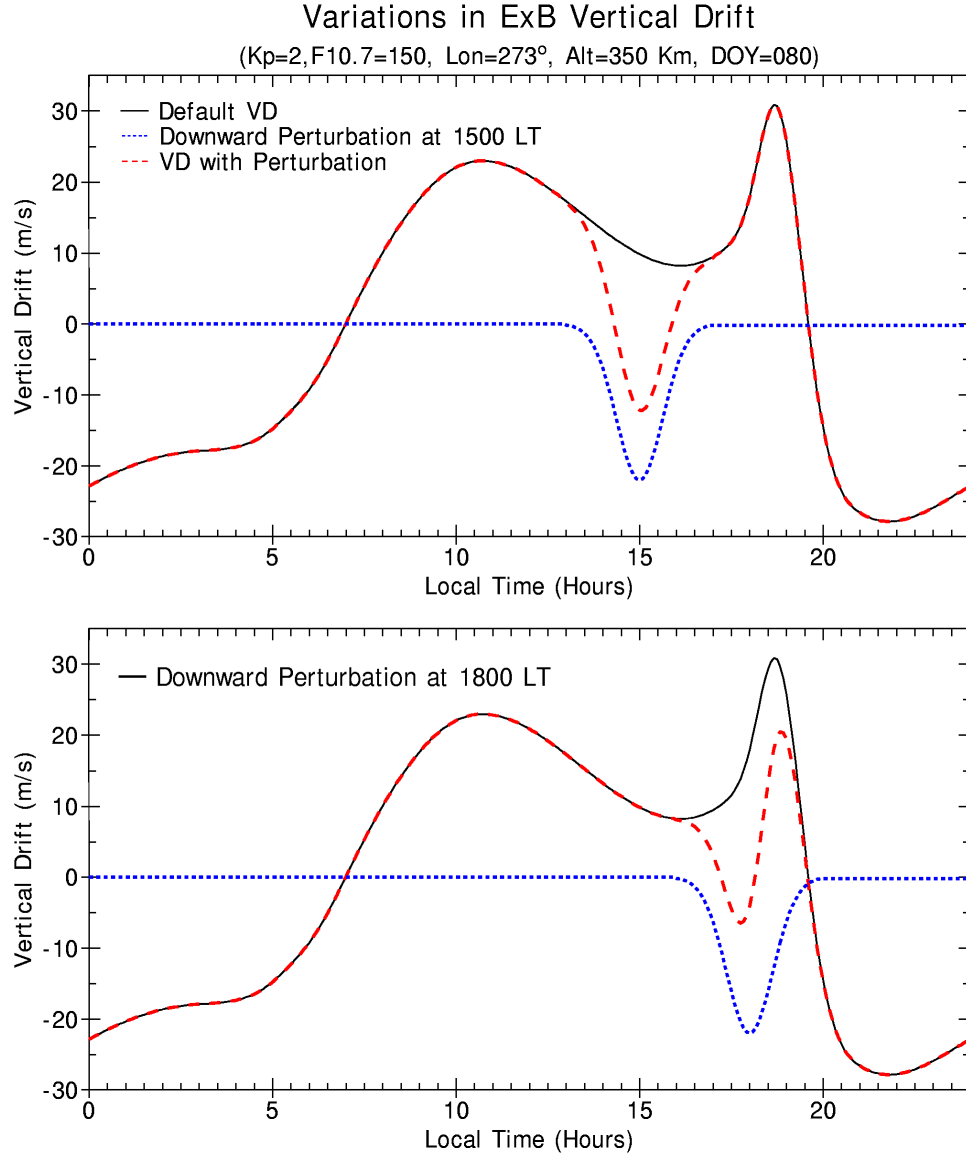
Figure 3.3. $\mathbf{E} \times \mathbf{B}$ vertical drifts at 273° longitude as a function of local time for medium solar activity (F10.7 = 150) and quiet geomagnetic (Kp =2) conditions at an altitude of 350 km on an equinox day (DOY 80). The solid lines represent the default vertical drift velocity of the Scherliess and Fejer model, the dotted lines represent the perturbation, and the dashed lines denote the vertical drift with the perturbation.

3.3 Ionospheric Simulations and Discussion

3.3.1 Meridional Wind Perturbations

For the wind perturbations, nine global simulations of the IPM were performed. Three case studies for each of three imposed wind directions (poleward, equatorward and northward) were performed by adding the perturbations at three different local times (1200, 1500, and 1800 LT). In order to investigate the longitudinal dependence of TEC on the meridional wind variations, three longitude sectors (78°, 273°, and 318°) were selected for medium solar activity (F10.7 = 150) and low geomagnetic activity (Kp = 2) conditions for each case.

Figure 3.4 shows examples of TEC at 2100 LT. For these examples, wind
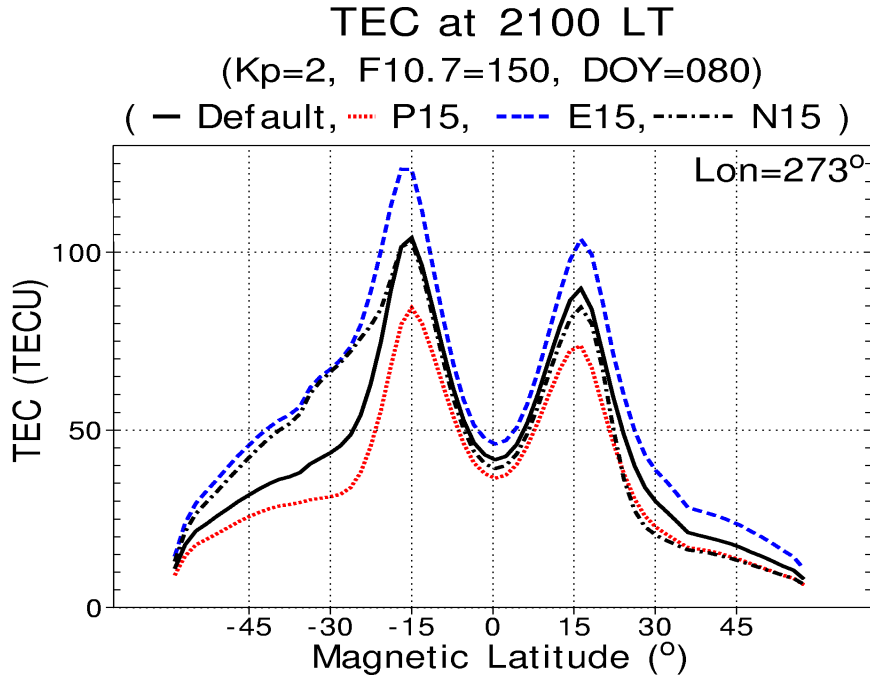
Figure 3.4. Examples of TEC at 273° longitude with the wind perturbations added at 1500 LT. Dotted, dashed and dashed-dotted lines represent TEC values at 2100 LT, 6 hours after poleward (P15), equatorward (E15), and northward (N15) perturbations were imposed, respectively. The solid line represents TEC with the default wind and vertical drift (1TECU = 10^{16} electrons/m^2).

perturbations were added at 1500 LT and the results are shown at 273° longitude. Also shown in Figure 3.4 are the default TEC values (solid line) that were obtained from the IPM run with unperturbed wind and vertical drift values (default). The TEC values for Case P15 (poleward at 1500 LT), E15 (equatorward at 1500 LT) and N15 (northward at 1500 LT) are denoted by the dotted, dashed and dashed-dotted lines, respectively. Case P15 shows a decrease in TEC of up to 20 TECU (20%) in the regions of the equatorial anomaly, and a decrease of about 5 TECU (10%) at the magnetic equator. For Case E15, a TEC increase of roughly the same magnitude as the decrease in Case P15 is seen. The northward wind perturbation (Case N15) does not affect TEC significantly in the low latitudes. In the middle latitudes, increases in TEC for Cases E15 and N15 are approximately 22 TECU (50% in the southern hemisphere). Furthermore, TEC for Case N15 is similar to Case E15 in the southern hemisphere and Case P15 in the northern hemisphere.

In the following subsections, the effects of the wind perturbations on TEC are systematically described for each of the Cases P15, E15, and N15.

3.3.1.1 Poleward Wind Perturbation at 1500 LT (Case P15)

The solid lines in Figure 3.5 show the changes in TEC (ΔTEC) as a function of geomagnetic latitude obtained by subtracting the default TEC values obtained from our unperturbed model run from those obtained from our model run with the poleward perturbation added at 1500 LT (Case P15). This ΔTEC denotes the change in TEC that can be attributed to the poleward wind perturbations. The results correspond to vernal equinox (DOY 80), medium solar activity, and geomagnetic quiet conditions. Also shown in Figure 3.5 are the default meridional wind velocities (depicted as crosses) at a height of 350 km and the meridional wind velocities with the perturbations added (depicted as squares). The rows in Figure 3.5 show ΔTEC
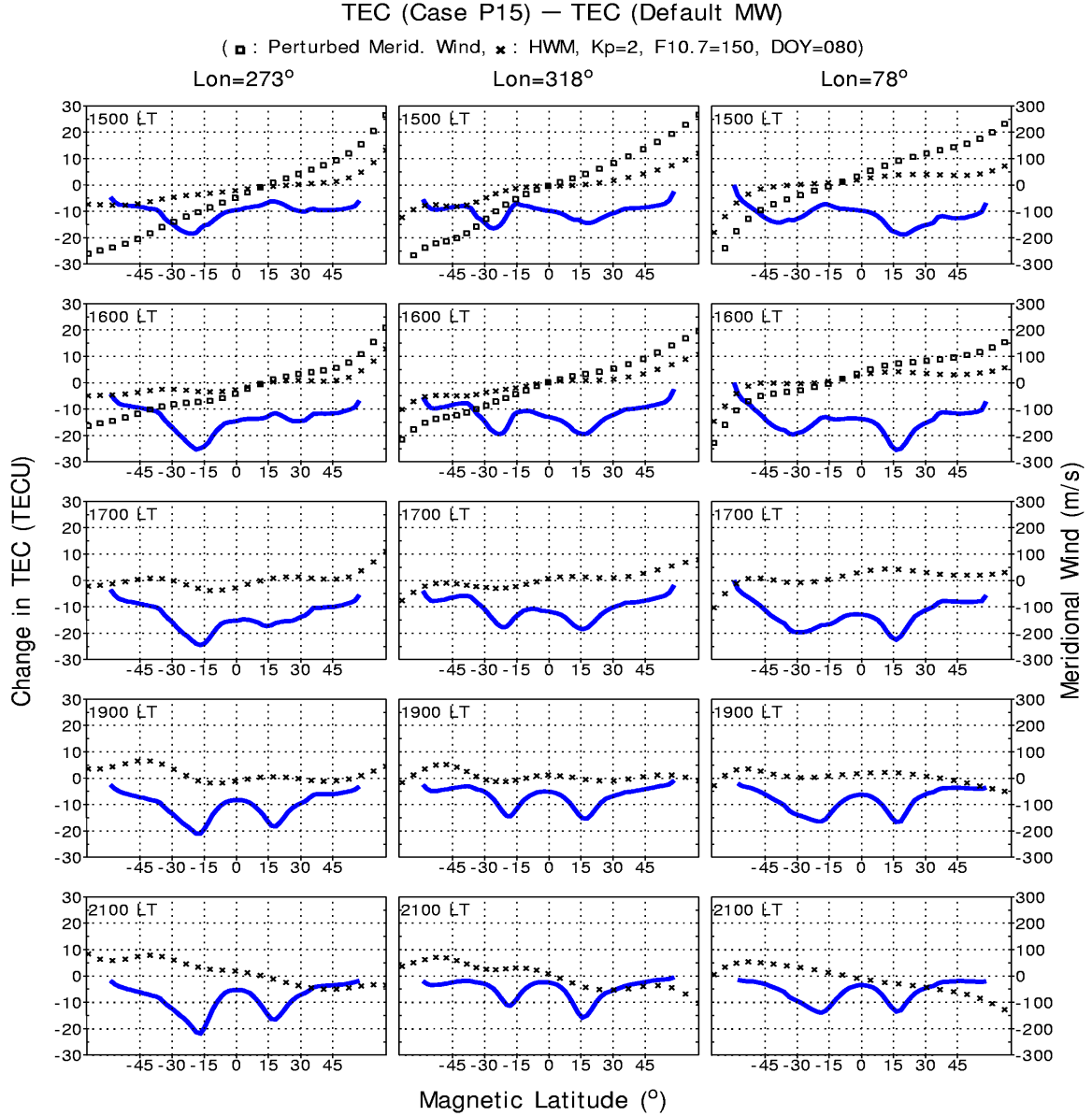
Figure 3.5. TEC difference (ΔTEC) (left scale) between TEC with a poleward wind perturbation added at 1500 LT (Case P15) and the TEC with the default wind. ΔTEC values (solid lines) are shown as a function of the geomagnetic latitude at three longitude sectors; 273° (left), 318° (middle), and 78° (right). Crosses represent the default meridional wind (m/s) (right scale) along the given longitude meridian at a height of 350 km and squares represent the meridional wind with the perturbation. The results shown are for medium solar activity and geomagnetic quiet conditions on DOY 80.

values over a range of local times. The columns in Figure 3.5 represent the results in the three longitude sectors; 273° (left), 318° (middle), and 78° (right). Note that the perturbed winds are not shown after 1700 LT (2 hours after the peak of the perturbation) since the perturbation is zero. In all three longitude sectors, the changes in TEC (ΔTEC) for Case P15 are negative as expected from the fact that the poleward wind moves plasma down to lower altitudes where the plasma density decreases due to a larger recombination rate. However, the changes in TEC are quite different in the three longitude sectors, even though the same variations of the neutral meridional wind were added and the default wind velocities in the three longitude sectors are similar. The differences in ΔTEC between the three longitude sectors are largest around the time when the wind perturbations were imposed (1500 LT), but the general shape of the ΔTEC corves at the three longitudes become similar as time progresses.

The maximum change in TEC occurs around the location of southern equatorial anomaly in the 273° longitude sector, which is where the magnetic equator is roughly 11° south of the geographic equator. At 78° longitude, where the magnetic equator is roughly 8° north of the geographic equator, the ΔTEC values are larger in the northern equatorial anomaly region than the southern region until 1900 LT. However, at 318° longitude, where the magnetic equator nearly coincides with the geographic equator, a nearly symmetric response is seen in ΔTEC during the afternoon. At 2100 LT, an asymmetry in ΔTEC has also developed in this sector. The longitude differences in the responses can be understood by considering that the superposed wind perturbations have the same magnitudes at the same geographic latitudes in both hemispheres but are different in the geomagnetic reference frame. Therefore, the perturbations in the geomagnetic frame have different magnitudes at

the geomagnetic conjugate latitudes owing to the offset between the geomagnetic and geographic equators. For example, at 273° longitude, the southern hemisphere has larger perturbations than the northern hemisphere.

As mentioned above, this longitude dependency is more noticeable during the time when the perturbations are applied. The ΔTEC peak value in the southern hemisphere is larger than that in the northern hemisphere at 273° longitude, and the opposite is observed at 78° longitude, while at 318° longitude, the ΔTEC peak values in the two hemispheres are similar to each other as mentioned above. However, 6 hours after the wind perturbations, the changes in TEC in the three different longitude sectors show similar features, except for the differences in peak values.

3.3.1.2   Equatorward Wind Perturbation at 1500 LT (Case E15)

For Case E15, a maximum equatorward wind perturbation was imposed at 1500 LT and the corresponding ΔTEC values are shown in Figure 3.6. For this case, increases in TEC are observed because the upward movement of the plasma by the equatorward wind reduces plasma loss through recombination. The ΔTEC responses in the three longitude sectors are similar but opposite to those for Case P15 shown in Figure 3.5. However, there are some subtle differences between Case E15 and Case P15. Generally, Case E15 shows larger changes in TEC at middle latitudes than Case P15 and the peaks of ΔTEC for Case E15 are shifted by up to about 10° poleward compared to Case P15. For example, at 78° longitude, from 1500 through 1700 LT, the peaks of changes in TEC occur at about 30° N for Case E15, while Case P15 has the maximum change in TEC near 15° N in the northern hemisphere. The ΔTEC in the latitude range from 30° N to 50° N is larger for Case E15 than for Case P15. A similar differences are also found in the southern hemisphere at 273° longitude and in both hemispheres at 318° longitude.
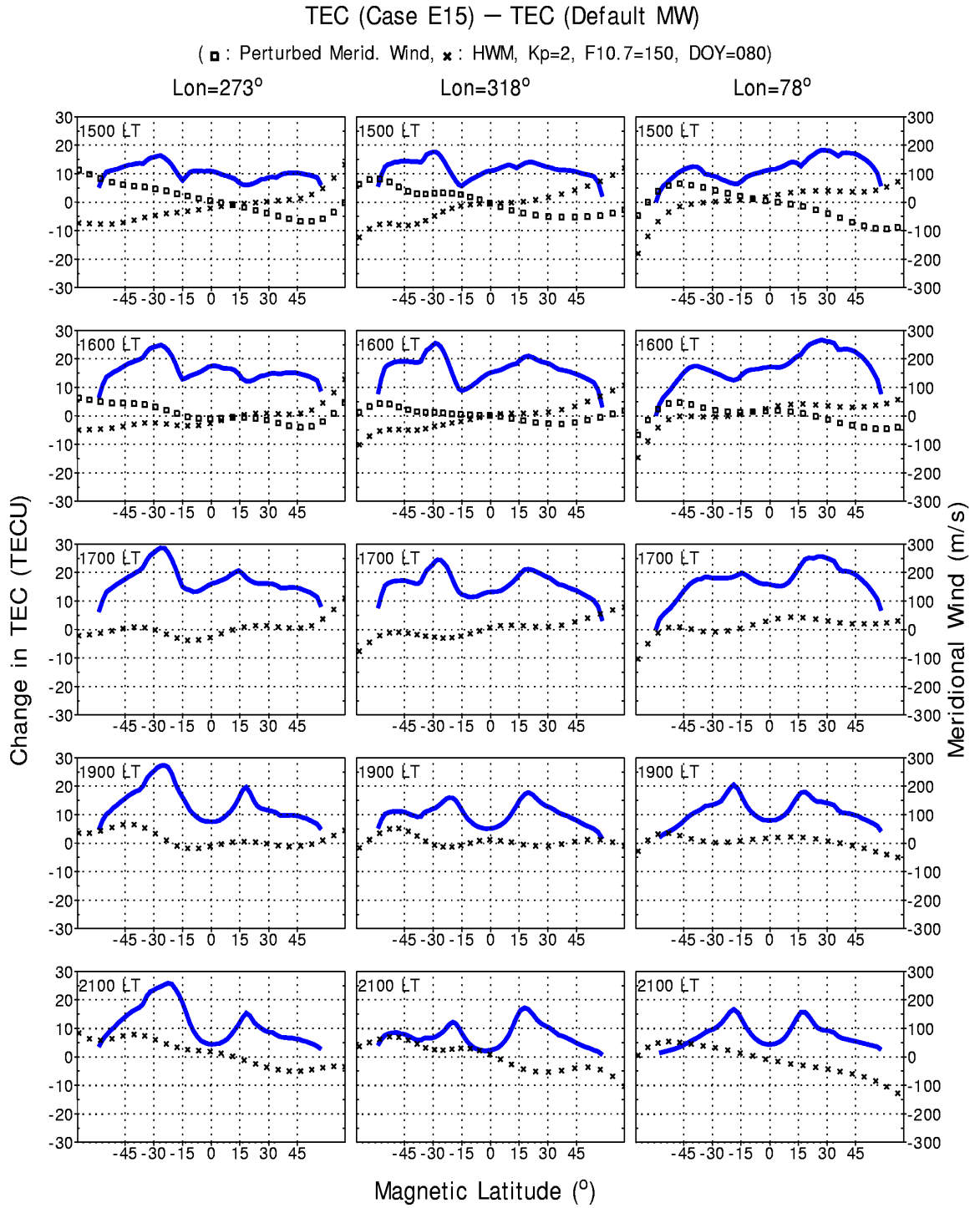
Figure 3.6. Same as Figure 3.5, but for the equatorward wind perturbation (Case E15).

During the evening hours, the locations of the peaks of ΔTEC move closer toward the location of the equatorial anomaly ($\sim 15°$ latitude), and the difference in the locations of the ΔTEC peaks for Case E15 and Case P15 becomes smaller. At 2100 LT, 6 hours after the perturbations, the maximum value of ΔTEC at 273° longitude in the southern hemisphere is larger than the maximum value in the northern hemisphere, and the peak of ΔTEC in the southern hemisphere is still shifted slightly poleward compared to Case P15 in Figure 3.5. This differs from 318° where the maximum value of ΔTEC is smaller in the southern hemisphere than in the northern hemisphere. However, the ΔTEC peak values in both hemispheres are almost the same at 78° longitude, similar to Case P15.

At middle latitudes, in the 273° and 318° longitude sectors, variations in TEC are larger in the northern than in the southern hemisphere. The opposite is found at 78° longitude. These results again indicate the complex response of the ionospheric plasma density for even the same imposed wind perturbation.

3.3.1.3   Northward Wind Perturbation at 1500LT (Case N15)

Figure 3.7 shows the TEC changes associated with a northward wind perturbation imposed at 1500 LT (Case N15). Similar changes in TEC (solid lines) are observed in the three longitude sectors at the time of the perturbation (1500 LT). However, as time evolves, the ΔTEC features in the northern hemisphere start to differ significantly from each other with the greatest difference in ΔTEC occurring in the latitude range between about 15° N and 30° N at 1700 LT. For example, at 1700 LT, around 20° N, the ΔTEC values at 273°, 78°, and 318° are negative, near zero, and positive, respectively. These differences develop despite the fact that there are no significant differences in the wind pattern (crosses in Figure 3.7).

At all three longitudes, a decrease in TEC is found in the southern low lati-
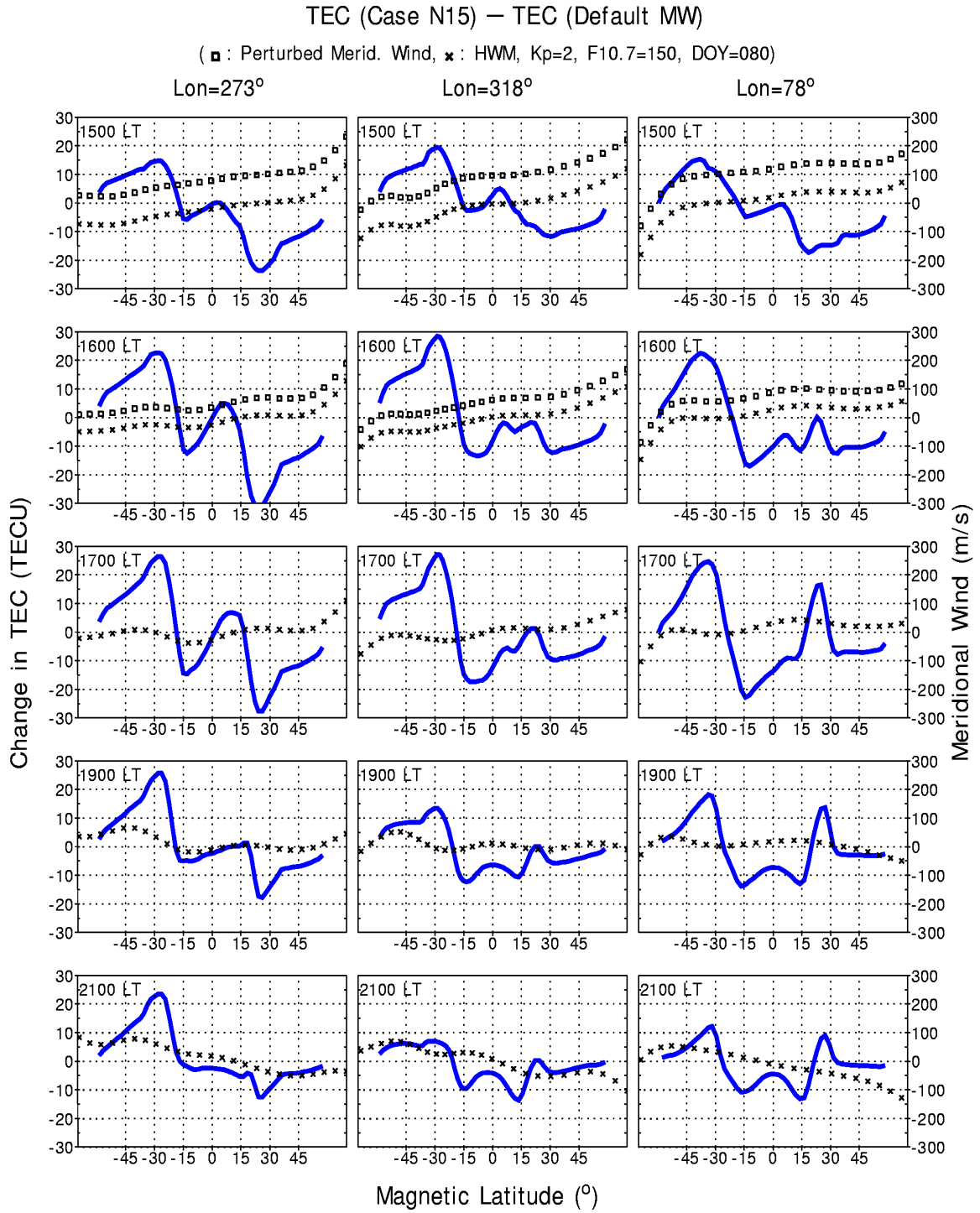
Figure 3.7. Same as Figure 3.5, but for the northward wind perturbation (Case N15).

tudes (about $-20° \sim 0°$) throughout the afternoon and evening hours. In the northern low latitudes ($0° \sim 20°$) a more complex evolution is observed, as mentioned above. For example, at 273° longitude a positive change in TEC observed at 1600 and 1700 LT between 0° and 10° latitude develops into a negative response after sunset. Similarly, an initial negative response in the 78° longitude sector between 15° and 30° latitude at 1500 LT develops into a strong positive response 2 hours later. One might expect that the imposed northward interhemispheric wind reduces TEC near the southern equatorial anomaly region and increases TEC in the northern equatorial anomaly region. However, as indicated above, the morphology of the TEC responses in the northern hemisphere follows a more complex pattern. This can be understood by considering the competing processes of enhanced recombination (decrease in plasma density) due to the northward (poleward in the northern hemisphere) wind perturbation and the enhanced plasma transport of equatorial plasma toward the equatorial anomaly region by the poleward wind (increase in plasma density).

At middle latitudes ($> |35|°$), the TEC variations show similar increases in the northern hemisphere for Case N15 and Case P15, and similar decreases in the southern hemisphere for Case N15 and Case E15. However, at low-latitudes, the ΔTEC responses for Case N15 differ significantly from Case P15 and Case E15 in both hemispheres due to the imposed interhemispheric wind.

So far, only wind perturbations added at 1500 LT were considered. In order to investigate the effects that different starting times for wind perturbations have on the changes in TEC, we also considered wind perturbations imposed at two other local times (1200 LT and 1800 LT), as well as the 1500 LT cases. In the next subsection, we present the TEC variations at 2100 LT caused by these three different wind perturbations.

3.3.1.4   TEC Variations at 2100LT

Figure 3.8 shows TEC changes at 2100 LT due to the wind perturbations added at three local times; 1200 LT (solid lines), 1500 LT (dotted lines), and 1800 LT (dashed lines). In the left column, thin lines represent ΔTEC due to equatorward wind perturbations (Cases E), while the thick lines represent ΔTEC due to poleward wind perturbations (Cases P). ΔTEC values for northward perturbations (Cases N) are shown in the right panel. Results are shown for the three longitude sectors, 273° (top), 318° (middle), and 78° (bottom).

Figure 3.8 shows that the changes in TEC at 2100 LT generally have, as expected, their largest magnitudes for those cases when the perturbation time was closest to 2100 LT, e.g., for the cases when the wind perturbations were centered around 1800 LT. However, there are several important exceptions to this rule. For example, the TEC changes observed in the southern hemisphere at 273° longitude are significantly larger for Cases E15 (and N15) than for Cases E18 (and N18), respectively. This unexpected behavior might be understood when considering that the imposed equatorward wind at 1800 LT in addition to the also generally equatorward nighttime winds impede the downward plasma flow associated with the prereversal enhancement in the equatorial vertical drifts [*Su et al.*, 1995]. This mechanism, however, does not explain why this characteristic is not observed in the other two longitude sectors and additional investigations are needed. However, as a good rule Figure 3.8 shows that the ΔTEC response at 2100 LT nearly linearly decreases with the elapsed time at middle latitude (poleward of about $\pm 35°$ latitude) and a more complex nonlinear characteristic is prevalent at lower latitudes (equatorward of $\pm 35°$ latitude).

At low latitudes, between about $\pm 15°$ latitude, the ΔTEC responses for Cases
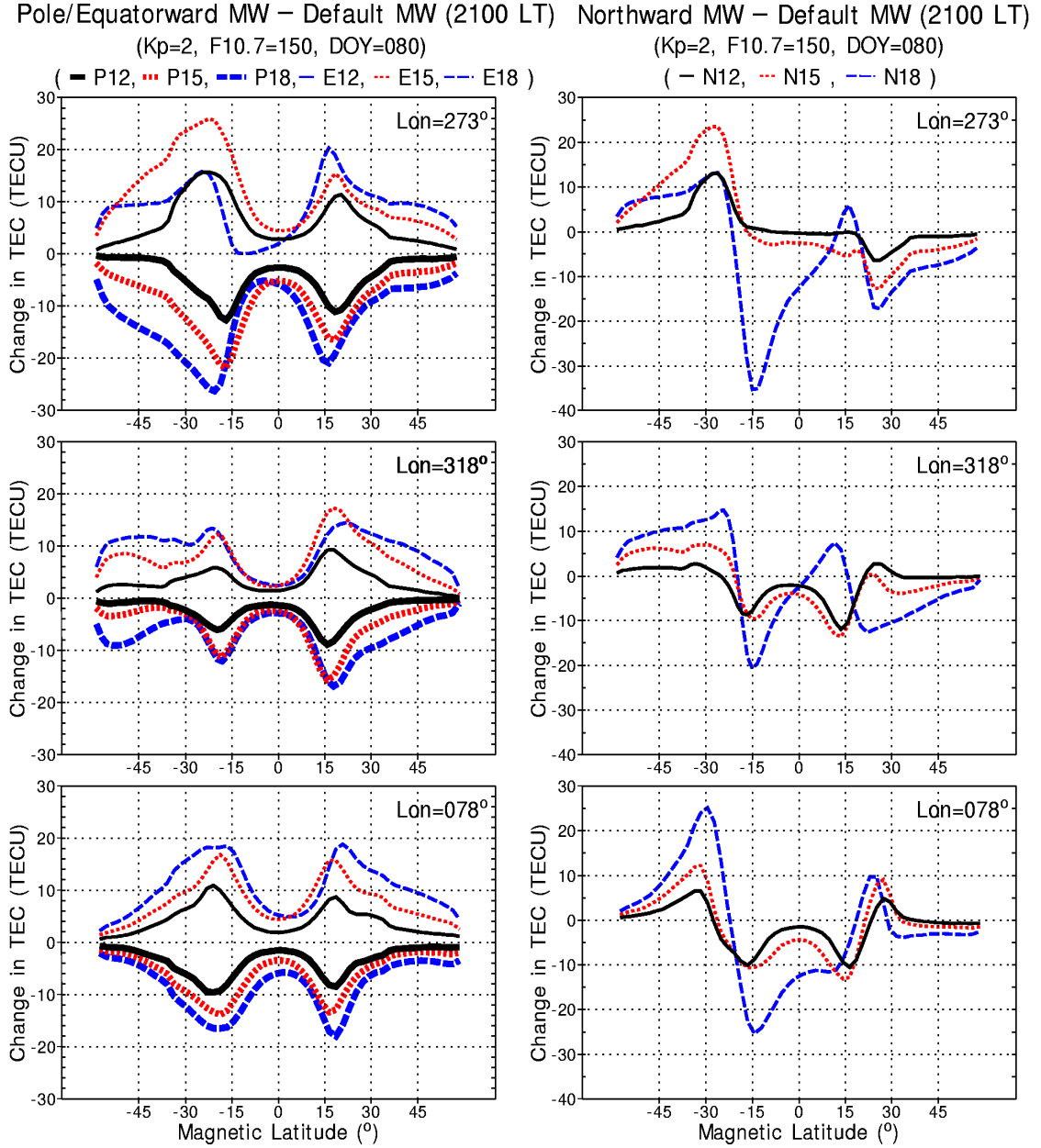
Figure 3.8. TEC changes (ΔTEC) from the default TEC at 2100 LT caused by poleward, equatorward (left panel) and northward (right panel) wind perturbations at three longitude sectors, 273° (top), 318° (middle), and 78° (bottom). Solid, dotted, and dashed lines represent ΔTEC due to perturbations added at 1200 LT, 1500 LT, and 1800 LT, respectively. The thin (thick) lines in the left panel represent ΔTEC due to the equatorward (poleward) wind perturbation.

N12 and N15 are very similar with slightly smaller magnitudes for Case N12. In particular, for these two cases, ΔTEC has nearly relaxed back to a value of zero in the 273° longitude sector. At the other two longitude sectors, two nearly symmetric negative peaks are seen near $\pm 15°$ latitude. The ΔTEC response for Case N18, however, differs significantly from Cases N12 and N15. For this case, a generally anti-symmetric response is seen in the lower latitude region with a negative peak near $-15°$ latitude and a positive peak near $+15°$ latitude. The development of the positive peak in the northern hemisphere is, however, suppressed in the 78° longitude sector. The development of this anti-symmetric response is attributed to the effects of interhemispheric plasma transport and modifications in the plasma fountain due to the northward wind perturbation. It is important to note that the observed anti-symmetric response for Case N18 is also seen for cases N12 and N15 (see Figure 3.7) right after the wind perturbations were imposed. With ongoing time, however, the anti-symmetric response develops into a symmetric response seen at 2100 LT. The longitudinal differences seen at low latitude are most likely due to the interplay of plasma transport processes associated with the default background wind pattern and the imposed wind perturbations.

At middle latitudes, poleward of about $\pm 20°$ latitude, the ΔTEC response follows a more systematic pattern. In particular in the southern hemisphere, a positive ΔTEC response is seen that diminishes in magnitude as the elapsed time between the imposed wind perturbation and 2100 LT increases. These positive ΔTEC responses are due to the uplift of the ionospheric plasma associated with the northward wind perturbation. In the northern hemisphere a more complex structure is observed at middle latitudes. For example, in the northern middle latitudes, a negative change in TEC can be seen at 273° longitude whereas a positive response is seen at 78° lon-

gitude. For the 318° longitude sector, a positive response is observed for Case N12 and negative responses are associated with Cases N15 and N18.

These complex responses in the change of TEC indicate the nonlinear interaction of the plasma transport, loss, and production mechanisms. Depending on the default background wind pattern and the background plasma densities, large difference in the TEC responses can occur for even the same applied wind perturbation. Furthermore, the dependence of the ΔTEC response over elapsed time is often nonlinear and strongly depends on the background conditions.

3.3.2 Vertical Drift Perturbations

In addition to the study of the effects of wind perturbations on TEC presented above, we have also studied the effect of changes in the equatorial vertical drift velocity on the afternoon and post-sunset TEC. Here, two drift perturbations were considered, upward (Case U) and downward (Case D). Again, like in the wind perturbation cases, three case studies for each of the two drift perturbations (see Figure 3.3) were performed by adding the perturbation drifts at three different local times (1200, 1500, and 1800 LT). Next, the dependence of TEC on the vertical drift variations was investigated in the three different longitude sectors (318°, 78°, and 273°) for medium solar activity (F10.7 = 150) and low geomagnetic activity (Kp = 2) on day 80.

3.3.2.1 Vertical Drift Perturbations at 1500 LT (Case D15, Case U15)

Figure 3.9 TEC changes obtained by subtracting the TEC values associated with the default (unperturbed) model run from those with the upward (U) and downward (D) drifts imposed at 1500 LT. Solid lines denote TEC changes due to a downward vertical drift perturbation (Case D15), and dotted lines represent TEC changes
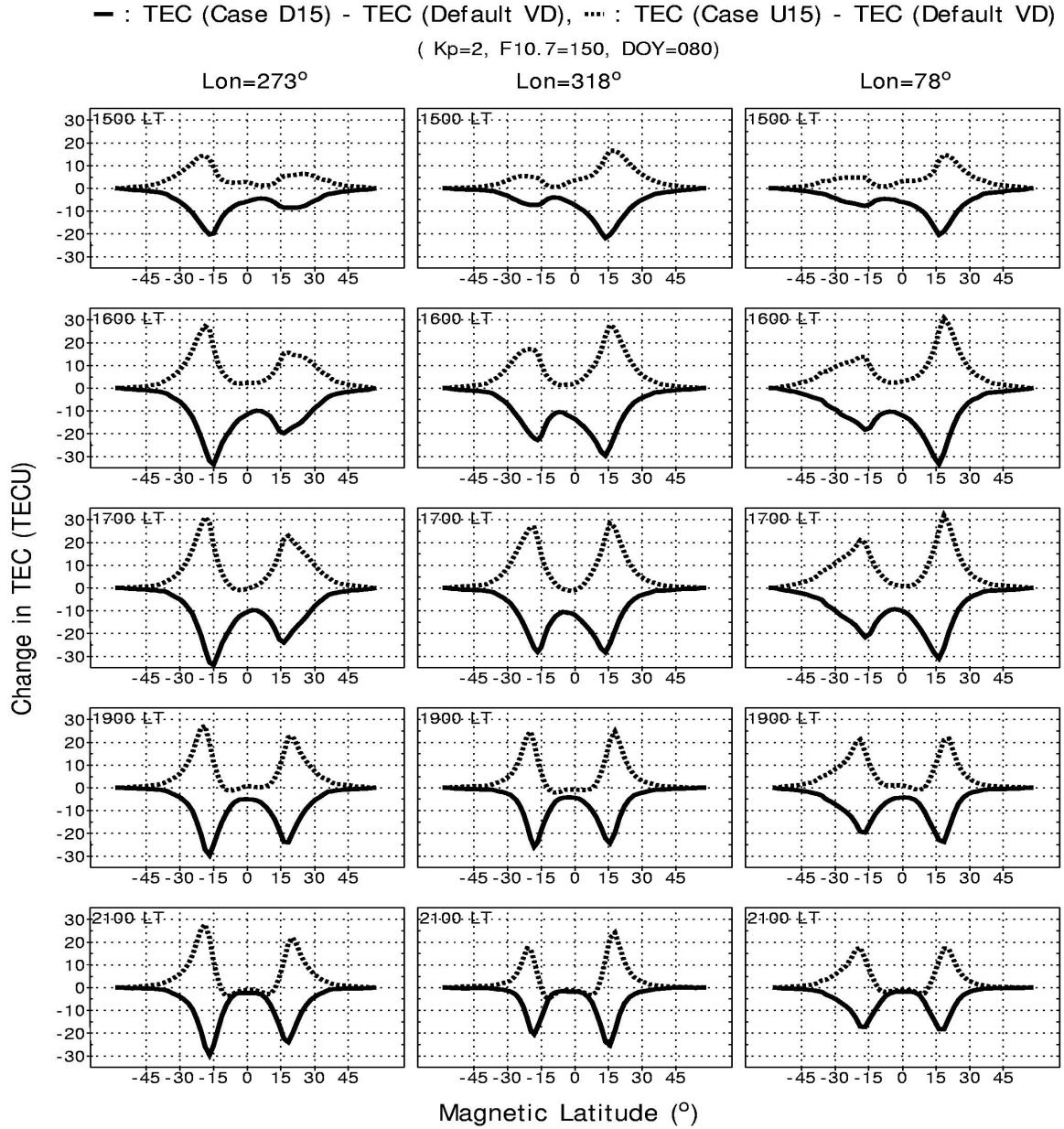
Figure 3.9. TEC difference (ΔTEC) between TEC with a vertical drift perturbation added at 1500 LT and TEC with the default $\mathbf{E} \times \mathbf{B}$ vertical drift. Solid (dotted) lines denote TEC changes due to a downward (upward) vertical drift perturbation. ΔTEC values are shown as a function of the geomagnetic latitude at three longitude sectors, 273° (left), 318° (middle), and 78° (right) for medium solar activity and geomagnetic quiet conditions on DOY 80.

due to an upward vertical drift perturbation (Case U15). As in Figures $3.5-3.7$, the ΔTEC values are shown as a function of geomagnetic latitude from 1500 LT to 1700 LT in 1-hour time steps, and at 1900 and 2100 LT, at three longitude sectors, 273° (left), 318° (middle), and 78° (right).

To first order the ΔTEC responses for Cases D15 and U15 are the same but opposite with Case U15 being positive and Case D15 being negative. Two peaks in ΔTEC can be seen for all cases and longitudes located symmetrically about the magnetic equator at about ±15° to ±20° magnetic latitude. These peaks are slightly shifted toward the poles for Case U15 compared to those for Case D15. Near the magnetic equator, ΔTEC for Case U15 is near zero, while TEC for Case D15 is decreased by up to -10 TECU shortly after the drift perturbations were imposed (1600, 1700 LT).

The evolution of ΔTEC variations with time for Case D15 (U15) is similar to those for Case P15 (E15) at low latitudes (see Figures 5 and 6). In both cases, the same asymmetry between ΔTEC peaks in the two hemispheres is found in the two longitude sectors, 273° and 78°, and the same symmetry feature at 318° longitude is also seen at 1700 LT. This suggests that TEC variations at 2100 LT due to variations of the neutral meridional wind and those due to variations in the vertical drift are nearly indistinguishable from one another, especially at low latitudes. We will come back to this important point below. At middle latitudes, on the other hand, ΔTEC for Case D15 and U15 are almost zero, while ΔTEC for Case P15 and E15 are not negligible. The main reason for this is that the imposed wind perturbations increase with latitude, while the imposed vertical drift perturbations decrease with latitude. For example, a 20 m/s vertical drift perturbation at the equator corresponds to an upward motion of only about 2 m/s at 45° latitude [*Millward et al.*, 1996].

3.3.2.2 Vertical Drift Perturbations at 1800LT (Case D18, Case U18)

Figure 3.10 shows the TEC changes due to the vertical drift perturbation added at 1800 LT. The greatest differences between these cases and the previously discussed Cases U/D15 occur near the magnetic equator $(-10° \sim 10°)$. The ΔTEC values at 2100 LT for both Case D/U15 and Case D/U18 are similar, except for the
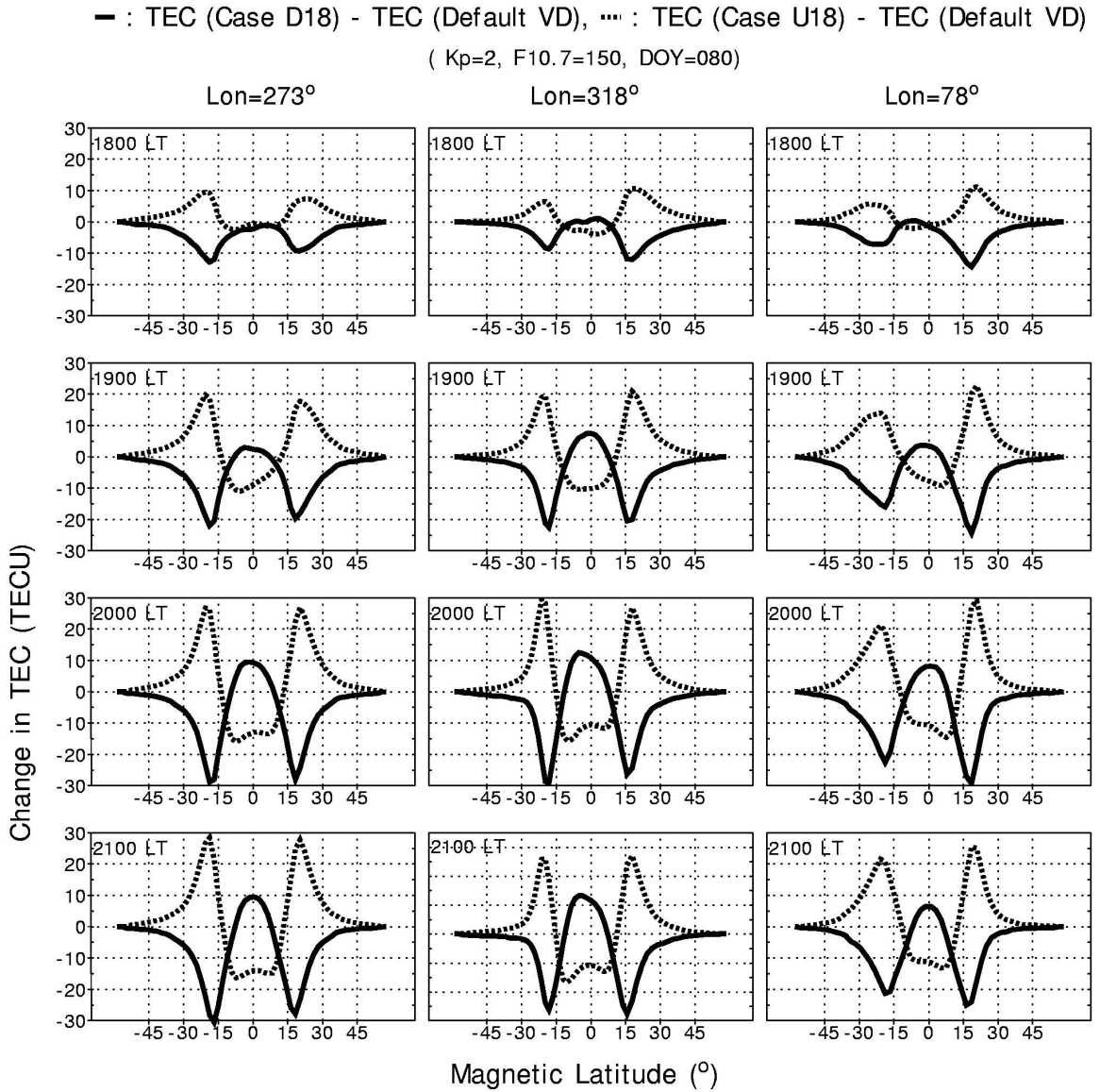

Figure 3.10. Same as Figure 3.9, but for a vertical drift perturbation added at 1800 LT. ΔTEC values are shown from 1800 LT to 2100 LT with a 1-hour step.

region near the equator. Here, the downward vertical drift perturbation (Case D18) results in a positive change in TEC, which is opposite to Case D15, while the upward vertical drift perturbation (Case U18) results in a negative change. The negative change in TEC due to the upward vertical drift perturbation is due to the absence of photoionization after sunset in combination with the plasma transport away from the magnetic equator toward the equatorial anomaly regions. As a result, TEC decreases in the equator region, while TEC in the equatorial anomaly increases. However, for Case U15, photoionization is still active when the upward perturbation is imposed and compensates for the loss of plasma due to the transport processes.

3.3.2.3   TEC Variations at 2100LT

Figure 3.11 shows the change in TEC at 2100 LT due to the downward (left panel) and upward (right panel) vertical drift perturbations imposed at 1200 LT (solid lines), 1500 LT (dotted lines), and 1800 LT (dashed lines), respectively. Again, ΔTEC responses are shown for the three longitude sectors, 273° (top), 318° (middle), and 78° (bottom).

Near the magnetic equator the ΔTEC responses at 2100 LT show significant differences depending on the elapsed time after the drift perturbation were imposed. For example, significant changes in TEC can be seen associated with cases D18 and U18 at all longitudes whereas in the case of the noontime and afternoon drift perturbation the change in TEC has nearly relaxed back to a zero value. The positive change in TEC near the magnetic equator associated with the downward drift perturbation imposed at 1800 LT is most likely a manifestation of the reduced evening plasma fountain, which will leave more plasma in the equatorial region leading to a positive ΔTEC response. As mentioned before, the negative change in TEC for Case U18 is possibly due to a combination of the lack of photoionization post sunset
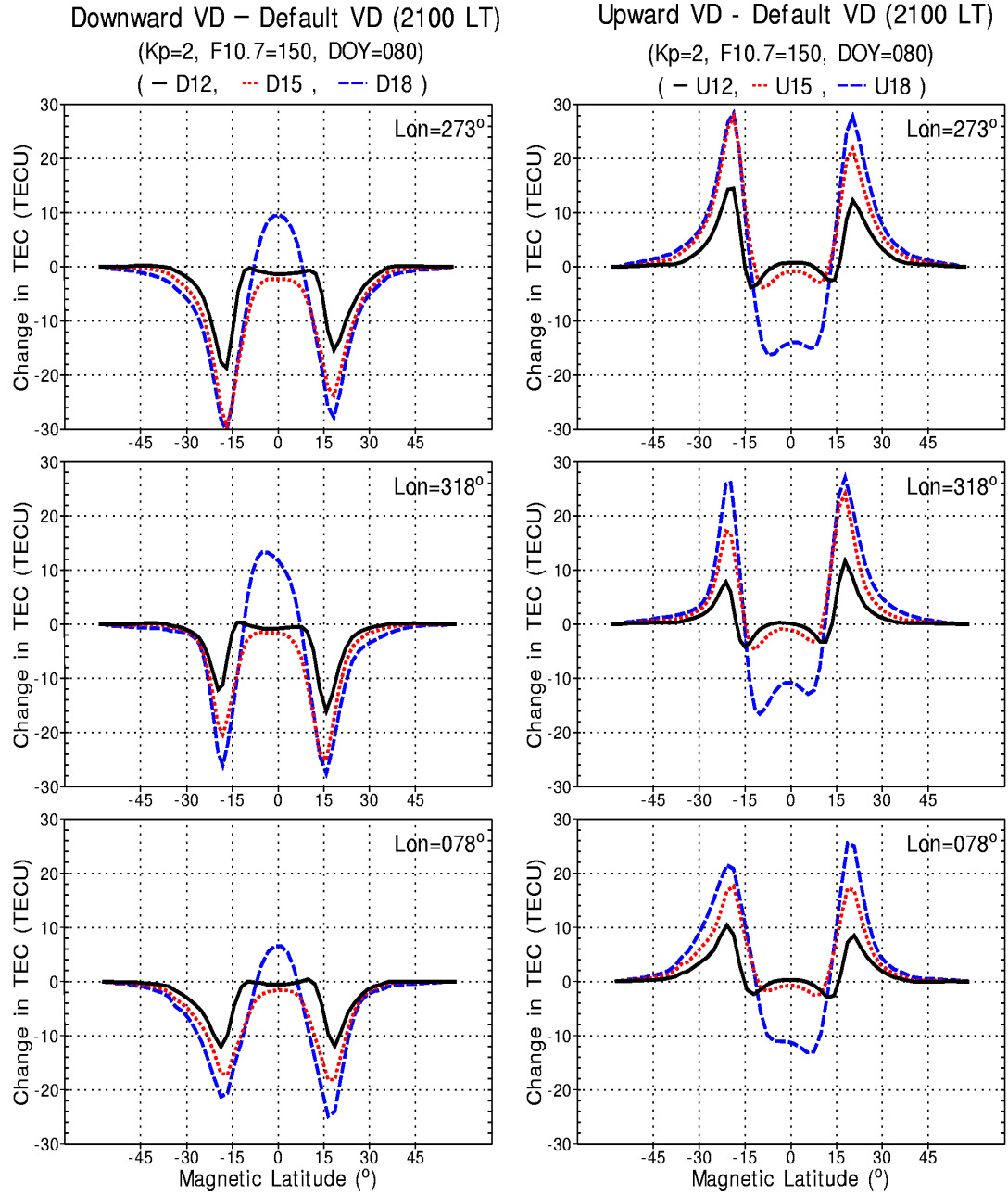
Figure 3.11. TEC changes (ΔTEC) from the default TEC at 2100 LT due to downward (left panel) and upward (right panel) vertical drift perturbations added at each of three local times; 1200 LT (solid lines), 1500 LT (dotted lines), and 1800 LT (dashed lines). ΔTEC values are shown at three longitude sectors; 273° (top), 318° (middle), and 78° (bottom).

and the increased transport of plasma away from the equator toward the equatorial anomaly regions.

Poleward of about $\pm20°$ latitude, the TEC responses associated with Cases U/D15 and U/D18 are nearly identical at all longitudes. However, significant differences in the magnitude of the TEC responses for Case U/D12 and U/D15 are seen.

There are several longitudinal differences in the response of ΔTEC that should be pointed out. Note that similar to the wind perturbation cases, 6 and 9 hours after the perturbations are applied (Case U/D12 and U/D15), an asymmetry is found between ΔTEC peaks in the two hemispheres at both 273° and 318° longitudes. Here, ΔTEC peak value in the southern hemisphere is larger than the peak value in the northern hemisphere at 273° longitude, while the opposite is found at 318° longitude. However, the asymmetry in the two longitude sectors is not clearly visible 3 hours after the perturbation (Case U/D18). At 78° longitude, on the other hand, the ΔTEC peak values in the two hemispheres are symmetric when the perturbations were added at 1200 LT or 1500 LT, while the ΔTEC peak values in the northern hemisphere are slightly larger than those in the southern hemisphere for Cases D18 and U18.

These results indicate that even for the same imposed drift perturbations significant difference in the TEC response can be seen. Similar to our neutral wind results presented above, this indicates the importance of the background conditions when evaluating the effects of variations in the equatorial plasma drift on the overall plasma distribution.

Furthermore, a comparison of Figure 3.5, 3.6, and 3.9 shows that often changes in the meridional wind and plasma drift can lead to basically the same TEC changes.

Consequently, the physical causes of observed changes in TEC can often not be uniquely determined from TEC alone. However, initial results indicate that even though the same TEC changes are observed difference in other ionospheric parameters, such as, $h_m F_2$ could be used to distinguish the effects of different driving mechanism.

3.4 Summary and Conclusion

We have studied the meridional wind and vertical drift effects on the afternoon and post-sunset TEC for spring equinox (DOY 080), medium solar activity (F10.7 = 150) and low geomagnetic activity (Kp = 2) conditions, using the physics-based numerical Ionosphere/Plasmasphere Model (IPM). In order to evaluate the effects of changes in the neutral wind on TEC, nine case studies were considered (three different wind perturbations × three different perturbation starting times). In detail, poleward, equatorward, and northward wind perturbations were superimposed on the background neutral winds obtained from HWM93. These perturbations were separately superimposed for each model run at three different local times (1200, 1500, and 1800 LT).

In addition to the nine wind cases, six model runs associated with imposed variations in the equatorial vertical plasma drifts were performed. Downward and upward vertical drift perturbations were superimposed on the default drifts obtained from the Scherliess and Fejer equatorial vertical drift model at the same three local times (1200, 1500, and 1800 LT). Moreover, in order to determine possible longitudinal variations in the TEC responses associated with these wind and drift perturbations, three longitude sectors ($78°, 273°$, and $318°$E) were considered. These sectors are distinguished from each other by their offset between the geomagnetic and geographic equators.

It was found that when a poleward/equatorward wind perturbation was imposed at 1500 LT (Cases P15 and E15), the resulting changes in TEC (ΔTEC) were found to be, as expected, similar but opposite throughout the afternoon and evening hours. However, the magnitude of ΔTEC at middle latitudes was found to be larger for Case E15 than for Case P15. Furthermore, the maximum ΔTEC responses for Case E15 were seen to be shifted poleward by up to 10° when compared to those of Case P15. At middle latitudes, Case N15 (northward wind perturbation at 1500 LT) and Case P15 show similar TEC decreases in the northern hemisphere, while Case N15 and Case E15 show similar TEC increases in the southern hemisphere. However, at low latitudes, the TEC responses differ significantly from each other due to an interhemispheric plasma flow associated with the northward wind perturbation.

Our simulations with imposed upward and downward drift perturbations indicate that, to first order, ΔTEC responses for these two cases have the same magnitude but opposite direction. Here an upward/downward perturbation drift results in an increase/decrease of TEC. Two peaks in ΔTEC were found located symmetrically about the magnetic equator at about ±15° to ±20° magnetic latitude. Near the magnetic equator, significant differences are seen associated with the local time of the imposed drift perturbation. While a downward/upward drift perturbation imposed at 1500 LT results in a decrease/increase in the equatorial TEC, the same perturbation imposed 3 hours later at 1800 LT results in the opposite response.

The TEC responses after an imposed drift or wind perturbation often exhibit a complex nonlinear temporal evolution throughout the afternoon and evening hours. For example, for Case N15 initially a hemispheric asymmetric response in TEC develops over the course of the next few hours changing into a symmetric response. Furthermore, large longitudinal differences are found for most of the TEC responses

for the same imposed wind or drift perturbations.

At 2100 LT, several hours after the imposed wind and drift perturbation, the changes in TEC generally have, as expected, their largest magnitudes for those cases when the perturbation time was closest to 2100 LT, e.g., for those cases when the wind perturbations were centered around 1800 LT. However, several important exceptions to this rule were found. For example, the TEC changes observed in the southern hemisphere at 273° longitude are significantly larger when perturbation winds were imposed in the afternoon hours (1500 LT) than for those cases when they were imposed at 1800 LT. These results indicate the complex interplay between production, loss, and transport processes.

Finally, when comparing the wind and drift induced changes in TEC, we found that at low latitudes the ΔTEC responses associated with downward/upward drift perturbations (Cases D15/U15) are nearly indistinguishable from those associated with the poleward/equatorward wind perturbations (Cases P15/E15). These results indicate the importance of additional information when interpreting the sources of observed variations in the afternoon and post-sunset TEC.

References

Balan, N, G. J. Bailey, M. A. Abdu, K. I. Oyama, P. G. Richards, J. MacDougall, and I. S. Batista (1997), Equatorial plasma fountain and its effects over three locations: Evidence for an dditional layer, the F3 layer, *J. Geophys. Res., 57* (4), 2047-2056.

Codrescu, M. V., S. E. Palo, X. Zhang, T. J. Fuller-Rowell, and C. Poppe (1999), TEC climatology derived from TOPEX/POSEIDON measurements, *J. Atmos. Sol. Terr. Phys., 61*, 281-298.

Codrescu, M. V., K. L. Beierle, T. J. Fuller-Rowell, S. E. Palo, and X. Zhang (2001), More total electron content climatology from TOPEX/Poseidon measurements, *Radio Sci., 36*, 325-333.

England, S. L., T. J. Immel, and J. D. Huba (2008), Modeling the longitudinal variation in the post-sunset far-ultraviolet OI airglow using the SAMI2 model, *J.*

Geophys. Res., 113, A01309, doi:10.1029/2007JA012536.

Gonzalez, S. A., and M. P. Sulzer (1996), Detection of He$^+$ Layering in the topside ionosphere over Arecibo during equinox solar minimum conditions, *Geophys. Res. Lett., 23* (18), 2509-2512.

Hedin, A. E., et al. (1991), Revised global model of thermospheric winds using satellite and ground-based observations, *J. Geophys. Res., 96*, 7657-7688.

Horvath, I., and E. A. Essex (2000), Using observations from the GPS and TOPEX satellites to investigate night-time TEC enhancements at mid-latitudes in the southern hemisphere during a low sunspot number period, *J. Atmos. Sol. Terr. Phys., 62* (5), 371-391.

Huba, J. D., G. Joyce, and J. A. Fedder (2000), Sami2 is Another Model of the Ionosphere (SAMI2): A new low-latitude ionosphere model, *J. Geophys. Res., 105*, 23,035-23,054.

Immel, T. J., E. Sagawa, S. L. England, S. B. Henderson, M. E. Hagan, S. B. Mende, H. U. Frey, C. M. Swenson, and L. J. Paxton (2006), Control of equatorial ionospheric morphology by atmospheric tides, *Geophys. Res. Lett., 33*, L15108, doi:10.1029/2006GL026161.

Jee, G., R. W. Schunk, and L. Scherliess (2004) Analysis of TEC data from the TOPEX/Poseidon mission, *J. Geophys. Res., 109*, A01301, doi:10.1029/2003JA010058.

Jee, G., R. W. Schunk, and L. Scherliess (2005), On the sensitivity of total electron content (TEC) to upper atmospheric/ionospheric parameters, *J. Atmos. Sol. Terr. Phys., 67*, 1040-1052.

Kil, H., R. DeMajistre, L. J. Paxton, and Y. Zhang (2006), Nighttime F-region morphology in the low and middle latitudes seen from DMSP F15 and TIMED/GUVI, *J. Atmos. Sol. Terr. Phys., 68*, 1672-1681.

McDonald, S. E., C. Coker, K. F. Dymond, D. N. Anderson, and E. A. Araujo-Pradere (2008), The relative importance of day and evening vertical $\mathbf{E} \times \mathbf{B}$ drift to nighttime equatorial anomaly evolution, *IES 2008*.

Millward, G. H., R. J. Moffett, S. Quegan, and T. J. Fuller-Rowell (1996), A coupled Thermosphere-Ionosphere-Plasmasphere Model (CTIP), *STEP Handbook of Ionospheric Models*, pp. 239-279.

Rishbeth, H. (1972), Thermospheric winds and the F region: A review, at midlatitudes, *J. Atmos. Terr. Phys., 34*, 1-47.

Rishbeth, H. (1974), Ionospheric dynamics 1945-1970, *J. Atmos. Terr. Phys., 36*, 2309-2319.

Scherliess, L., and B. G. Fejer (1999), Radar and satellite global equatorial F region vertical drift model, *J. Geophys. Res., 104*, 6829-6842.

Scherliess, L., R. W. Schunk, J. J. Sojka, and D. C. Thompson (2004), Development of a physics-based reduced state Kalman filter for the ionosphere, *Radio Sci., 39*, RS1S04,doi:10.1029/2002RS002797.

Scherliess, L. D. C. Thompson, and R. W. Schunk (2008), Longitudinal variability of low- latitude total electron content: Tidal influences, *J. Geophys. Res., 113*, doi:10.1029/2007JA012480.

Schunk, R. W., and A. F. Nagy (2000), *Ionospheres*, Cambridge Univ. Press, New York.

Schunk, R. W., et al. (2004), Global Assimilation of Ionospheric Measurements (GAIM), *Radio Sci., 39*, RS1S02, doi:10.1029/2002RS002794.

Su, Y. Z., G. J. Bailey, and N. Balan (1994), Night-time enhancements in TEC at equatorial anomaly altitudes, *J. Atmos. Sol. Terr. Phys., 56* (12), 1619-1628.

Su, Y. Z., G. J. Bailey, and N. Balan (1995), Modelling studies of the longitudinal variations in TEC at equatorial-anomaly latitudes, *J. Atmos. Sol. Terr. Phys., 57* (4), 433-442.

CHAPTER 4

CONCLUSION

In this chapter, we will summarize the results of our study on the ionospheric total electron content (TEC) variability: the spatial correlations of day-to-day ionospheric TEC variability obtained from ground-based GPS and the neutral wind and plasma drift effects on the nighttime TEC variability. Then, we will present the limitations of our study and suggestions for further studies.

4.1 Summary and Conclusion

It is well known that the ionosphere varies markedly with altitude, latitude, longitude, universal time, season, solar cycle, geomagnetic activity, and shows significant day-to-day variability. Total Electron Content (TEC) measurements and ionospheric model simulations have been used extensively to study the general morphology and variability of the ionosphere during both geomagnetically quiet and disturbed conditions. In an effort to better understand the TEC variability and its cause, the global day-to-day ionospheric TEC variability, particularly spatial correlations of day-to-day ionospheric TEC changes have been studied using GPS TEC measurements, and the relative importance of the neutral wind and the electric field for the TEC variations has been studied using a physics-based numerical Ionosphere/Plasmasphere Model (IPM).

In Chapter 2, the study on the global day-to-day ionospheric TEC variability during geomagnetically quiet period has been presented. GPS TEC measurements on a global scale from more than 1000 GPS ground receivers were used to study the local and spatial morphology of day-to-day ionospheric variability. The data used in the study cover four different seasons in 2004, and each season data cover 30 days.

First, the changes in TEC from one day to the next were calculated by differencing the individual GPS/TEC observations obtained at the same location on consecutive days using all available GPS ground stations, which resulted in more than 150 million values of day-to-day change in TEC (ΔTEC). Next, the local standard deviation of the resulting TEC changes were determined to describe the local variability in TEC for each season. Finally, the spatial correlation coefficients were obtained to measure statistical correlations between TEC changes at different locations on the globe.

The largest local TEC variability indicated by the standard deviation occurs around the equatorial anomaly regions with maximum values appearing in the afternoon sector between about 1500-1700 MLT. At both low and middle latitudes, the variability is found to be nearly symmetric about the magnetic equator during equinoxes, while the variability exhibits asymmetries during the solstices. Our results indicate that during the solstices the seasonal asymmetry in the day-to-day TEC variability, with larger variability in the summer hemisphere than in the winter hemisphere during daytime, is in contrast to the well-known seasonal anomaly in the peak F region densities (N_mF_2). On the other hand, the well-known annual anomaly is observed in the TEC variability with a reduction of about 50% in the standard deviation from December to June solstice.

Our study of the spatial correlation indicates that seasonally and local time averaged correlation lengths at middle latitudes are larger than (about twice as big as) those at at low and high latitudes in both meridional and zonal directions. The daytime zonal and meridional correlation lengths are both found to be larger than their corresponding nighttime values. Furthermore, the correlation lengths, as well as the correlation values, hardly differ between the different seasons at all latitudes.

It should be noted that there are strong correlations between geomagnetic con-

jugate points, which are are strongest at low latitudes with correlation coefficients of about 0.8 ($r \approx 0.8$) during both daytime and nighttime. At middle latitudes, the conjugate correlation coefficients are smaller during daytime and are not observed during the night. There are several potential causes of strong correlations between conjugate points, such as solar illumination, neutral meridional winds, and electric fields. It is interesting to note that the TEC changes over most parts of the illuminated disk are largely uncorrelated, indicating that day-to-day changes in the solar illumination only add a statistically insignificant contribution to the day-to-day changes in TEC. However, the most promising candidate to explain the observed conjugate correlations are electric fields since electric fields can be locally generated through neutral wind dynamo action in one hemisphere and then map along magnetic field lines to the conjugate point located in the opposite hemisphere. The resulting transport of the ionization due to the presence of these electric fields in the two hemispheres would lead to a correlated response in TEC at the two conjugate points. The significantly larger correlation coefficient of 0.8 between conjugate points at low latitudes indicates that more than 50% of the observed variability is related to changes in the electric field forcing. The fact that at middle latitudes the conjugate correlations are only observed during daytime indicates that during the night the electric field variations are either small or washed out by other local processes.

In Chapter 3, relative importance of the neutral wind and the electric field for the TEC variations has been studied to better understand the observed TEC variability and its cause using a physics-based numerical Ionosphere/Plasmasphere Model (IPM). IPM requires several inputs including thermospheric neutral wind and the low-latitude electric field provided by existing empirical model. To study the relative importance of the neutral wind and the electric field for the TEC variations,

we took advantage of the fact that these two model inputs can be externally modified. This study focuses on nighttime TEC for spring equinox (DOY 080), medium solar activity (F10.7 = 150) and low geomagnetic activity (Kp = 2).

Nine case studies were performed to find out the impact of the neutral wind on TEC (three kinds of wind perturbations × three different perturbation starting times). Poleward, equatorward and northward winds were superimposed on the default values of the geographic meridional wind obtained from the HWM93. Individual perturbations were superimposed at each of the three different local times (1200, 1500, and 1800 LT) in order to study the effects on TEC in the afternoon and post-sunset due to the variation in perturbation starting time.

In order to investigate the vertical drift effect, six cases were studied (two kinds of $\mathbf{E} \times \mathbf{B}$ vertical drift perturbations × three different perturbation starting times). Downward and upward vertical drift perturbations were superimposed on drift values obtained from the Scherliess and Fejer equatorial vertical drift model at the same three local times as in the case of neutral wind perturbations.

Moreover, to study the longitudinal dependence of changes in TEC change, three different longitude sectors (78°, 273° and 318°E) were chosen that are distinguished by the offset between the geomagnetic and geographic equators.

The poleward and equatorward wind perturbations produce similar ΔTEC responses but opposite in sign throughout the afternoon and evening hours. At middle latitude, the northward and poleward wind perturbations make similar TEC decreases in the northern hemisphere, while the northward and poleward wind perturbations make similar TEC increases in the southern hemisphere. However, at low latitudes the similarity disappears due to an interhemispheric plasma flow associated with the northward wind perturbation.

Imposed upward and downward drift perturbations result in the same magnitude of ΔTEC responses but opposite direction. Near the magnetic equator, significant differences are seen associated with the local time of the imposed drift perturbation. While a downward/upward drift perturbation imposed at 1500 LT results in a decrease/increase in the equatorial TEC, the same perturbation imposed 3 hours later at 1800 LT results in the opposite response.

At middle latitudes, the vertical drift perturbations hardly produce changes in TEC while the wind perturbations make non zero ΔTEC. This is because the vertical drift decreases with latitude, on the contrary, the wind perturbation increases with latitude. At low latitudes, the ΔTEC variations caused by the vertical drift and wind perturbations are almost identical. Therefore, our study suggest that in order to differentiate TEC variations at 2100 LT due to wind perturbation from those caused by vertical drift, other ionospheric parameters such as h_mF_2 and N_mF_2 should be considered.

The TEC responses after an imposed drift or wind perturbation often exhibit a complex nonlinear temporal evolution throughout the afternoon and evening hours. For example, an initially hemispheric asymmetric response in TEC develops for case N15 that over the course at the next few hours develops into a symmetric response. Furthermore, large longitudinal differences are found for the TEC response for the same imposed wind or drift perturbations.

Our results show that the wind and vertical drift perturbation effects on the TEC at 2100 LT vary nonlinearly with elapsed time after the perturbations are added. This nonlinearity is more apparent at low latitudes ($< 30°$) than at middle latitudes ($> 30°$). These results indicate the complex interplay between production, loss, and transport processes.

4.2 Limitations and Suggestions for Future Research

In our spatial correlation study, relatively large spatial bins ($5° \times 15°$) were used in order to acquire a sufficient amount of data in each bin in both hemispheres. This was necessary due to the uneven distribution of our data with a significantly denser data distribution in the northern hemisphere when compared to both the southern hemisphere and the equatorial region. However, the asymmetry in GPS TEC data coverage between two hemispheres could possibly affect our results. For example, our results indicate that seasonal anomaly is also absent or opposite in the day-to-day TEC changes.

Although our study has revealed many of the scale-sizes of day-to-day TEC variability, questions about the physical mechanisms that are responsible for the observed variations remain. For example, it remains unclear how much of the observed variability is due to inherent variations in the ionosphere-thermosphere system, and how much can be attributed to effects due to magnetospheric and mesospheric processes. Clearly, further studies are needed. Furthermore, information about the spatial and temporal correlation of day-to-day variations of other ionospheric parameters (e.g. N_mF_2, h_mF_2, topside scale height) on a global scale is limited.

In addition, Our study was based on TEC observations obtained during mostly geomagnetically quiet and medium solar flux conditions. The dependence of the spatial correlation coefficients on the phase of the solar cycle and on the geomagnetic activity needs to be addressed in future studies.

The study of physical drivers effects on TEC variations was performed using model simulations for equinox, medium solar activity, and geomagnetically quiet conditions. With modification of the input parameters, this study can be easily extended to cover disturbed periods, different seasons and different solar flux conditions. It

would be useful to study the effects of the upper atmospheric and ionospheric physical drivers on the ionosphere and their relative importance during disturbed periods, which could be different from the quiet periods.

Finally, our study indicates that often changes in the meridional wind and plasma drift can lead to basically the same TEC changes. Consequently, the physical causes of observed changes in TEC often cannot be uniquely determined without considering additional information. Therefore, further studies are needed.

APPENDIX

Figure 1.5 is copyrighted by the American Geophysical Union and used with permission.

Permission Letter

Dear Dr. Shim

Shim J. S., L. Scherliess, R.W. Schunk, and D. C. Thompson, Spatial Correlations of Day-to-Day Ionospheric Total Electron Content Variability Obtained from Ground-Based GPS, *J. Geophys. Res., 113*, A09309, doi:10.1029/2007JA012635, 2008.

We are pleased to grant permission for the use of the material requested for inclusion in your thesis. The following non-exclusive rights are granted to AGU authors:

o All proprietary rights other than copyright (such as patent rights).
o The right to present the material orally.
o The right to reproduce figures, tables, and extracts, appropriately cited.
o The right to make hard paper copies of all or part of the paper for classroom use.
o The right to deny subsequent commercial use of the paper.

Further reproduction or distribution is not permitted beyond that stipulated. The copyright credit line should appear on the first page of the article or book chapter. The following must also be included, "Reproduced by permission of American Geophysical Union." To ensure that credit is given to the original source(s) and that authors receive full credit through appropriate citation to their papers, we recommend that the full bibliographic reference be cited in the reference list. The standard credit line for journal articles is:
"Author(s), title of work, publication title, volume number, issue number, citation number (or page number(s) prior to 2002), year. Copyright [year] American Geophysical Union."

If an article was placed in the public domain, in which case the words "Not subject to U.S. copyright" appear on the bottom of the first page or screen of the article, please substitute "published" for the word "copyright" in the credit line mentioned above.

Copyright information is provided on the inside cover of our journals. For permission for any other use, please contact the AGU Publications Office at AGU, 2000 Florida Ave., N.W., Washington, DC 20009.

Michael Connolly
Journals Publications Specialist

UtahState
UNIVERSITY

CENTER FOR ATMOSPHERIC AND SPACE SCIENCES
4405 Old Main Hill
SER Bldg. Room 246
Logan UT 84322-4405

June 3, 2009

Ja Soon Shim
Center for Atmospheric and Space Sciences
Utah State University
4405 Old Main Hill
Logan, UT 84322-4405

Dear Ja Soon,

I am pleased to grant you permission to use the two papers that I co-authored with you in your dissertation. The two papers are:

"Spatial Correlations of Day-to-Day Ionospheric Total Electron Content Variability Obtained from Ground-Based GPS"

"Neutral Wind and Plasma Drift Effects on Low- and Mid-Latitude TEC"

Sincerely,

Robert W. Schunk
Director, Center for
  Atmospheric and Space Sciences

RWS/sj

UtahStateUniversity

June 3, 2009

Ja Soon Shim
Center for Atmospheric and Space Sciences
Utah State University
4405 Old Main Hill
Logan, UT 84322-4405

Dear Ja Soon,

I am pleased to grant you permission to use the two papers that I co-authored with you in your dissertation. The two papers are:

Spatial Correlations of Day-to-Day Ionospheric Total Electron Content Variability Obtained from Ground-Based GPS.

Neutral Wind and Plasma Drift Effects on Low- and Mid-Latitude TEC.

Yours sincerely,

Donald C. Thompson
Res. Assoc. Professor

CURRICULUM VITAE

Ja Soon Shim

Center for Atmospheric and Space Sciences
Utah State University
Logan, UT 84322-4405

EDUCATION

Ph.D., Physics, Utah State University, Logan, Utah, 2009
Ph.D., Physics, Seoul National University, Seoul, Korea, 1993
      Dissertation: "Polarization Effects in Physical Processes of
      High-Spin Particles"
M.S., Physics, Seoul National University, Seoul, Korea, 1989
B.S., Physics Education, Seoul National University, Seoul, Korea, 1987

TEACHING EXPERIENCE

2004-2006 Teaching Assistant, Utah State University, Logan, Utah
1999-2003 Lecturer, Sogang University, Seoul, Korea
1996-1999 Instructor, Myongji University, Seoul, Korea

RESEARCH EXPERIENCE

2007-2009 Research Assistant, Utah State University, Logan, Utah
1995-1996 Post. Doc., Kyunghee University, Seoul, Korea
1994-1995 Post. Doc., Hanyang University, Seoul, Korea
1989-1993 Research Assistant, Seoul National University, Seoul, Korea

PROFESSIONAL MEMBERSHIPS

American Geophysical Union
American Physical Society

PUBLICATIONS

J. S. Shim, L. Scherliess, R.W. Schunk, and D. C. Thompson, Spatial
    Correlations of Day-to-Day Ionospheric Total Electron Content Variability Obtained from Ground-Based GPS, J. Geophys. Res., 113,
    A09309, doi:10.1029/2007JA012635, 2008.

S.Y. Choi, J. S. Shim, H.S. Song, and W.Y. Song, Impacts of the CP-odd phase of the chargino mass matrix in light chargino pair production at LEP II, Phys. Lett. B 449, 207, 1999.

S.Y. Choi, J. S. Shim, H.S. Song, J. Song, C. Yu, Single-photon events in $e^+ e^-$ collisions, Phys. Rev. D 60, 013007, 1999.

J. S. Shim, H. S. Song, Factorization in Process of a Graviton Scattering off and electron for Z and W Production, Phys. Rev. D 53, 1005, 1996.

J. S. Shim, S. Baek , H. S. Song, Polarization Effects in Electroweak Vector Boson Production, J. Korean Phys. Soc. 29, 293, 1996.

S. Y. Choi, J. S. Shim, H. S. Song, Factorization and polarization Effects in Linearized Gravity, Phys. Rev. D 51, 2751, 1995.

S. Y. Choi, J. S. Shim, H. S. Song, Factorization in Graviton Interaction, Phys. Rev. D 48, R5465, 1993.

S. Y. Choi, J. S. Shim, H. S. Song, Factorization of Gravitational Compton Scattering Amplitude in the Linearized Version of General Relativity, Phys. Rev. D 48, 2953, 1993.

S. Y. Choi, Juungil Lee, J. S. Shim, H. S. Song, Lowest-order gravitation Interactions with a Charged Fermion and a Photon, Phys. Rev. D 48, 769, 1993.

S. Y. Choi, Jungil Lee, J. S. Shim, H. S. Song , Spin-2 Particle Polarization, J. Korean Phys. Soc. 25, 576, 1992.

PRESENTATIONS AT PROFESSIONAL MEETINGS

"Spatial Correlations of Day-to-Day Ionospheric Total Electron Content Variability Obtained from Ground-Based GPS", J. S. Shim, L. Scherliess, R.W. Schunk, and D. C. Thompson, Fall Meeting of the American Geophysical Union, San Francisco, CA; December 11-15, 2006.

"Spatial Correlations of Day-to-Day Ionospheric Total Electron Content Variability Obtained from Ground-Based GPS", J. S. Shim, L. Scherliess, R.W. Schunk, and D. C. Thompson, Cedar Workshop, Santa Fe, New Mexico; June 24-29, 2007.

"Neutral Wind and Plasma Drift Effects on the Nighttime TEC Variability", J. S. Shim, L. Scherliess, R.W. Schunk, and D. C. Thompson, Fall Meeting of the American Geophysical Union, San Francisco, CA; December 15-19, 2008.